

University of Verona

DEPARTMENT OF COMPUTER SCIENCE
Master's Degree in Computer Science and Engineering

MASTER'S DEGREE THESIS

Analysis of a Single Actuator Exoskeleton

Candidate:
Davide Costanzi
VR377120

Supervisor:
Prof. Paolo Fiorini, PhD

Co-Supervisor:
PhD Andrea Calanca

Academic Year 2014–2015

Contents

| | |
|---|------------|
| Abstract | vii |
| Sommario | ix |
| 1 Introduction | 1 |
| 2 Related works | 5 |
| 2.1 Introduction | 5 |
| 2.2 Effectiveness of rehabilitation robots | 6 |
| 2.3 Rehabilitation robots background | 6 |
| 2.4 Orthoses for the lower limbs | 7 |
| 2.5 Actuation technologies and limitations | 9 |
| 2.5.1 Traditional actuators | 9 |
| 2.5.2 Compliant actuators | 10 |
| 2.5.3 Limitations and future actuators | 11 |
| 2.6 Conclusion | 12 |
| 3 The single actuator concept | 13 |
| 3.1 Introduction | 13 |
| 3.2 Objectives of the design | 14 |
| 3.3 Description | 14 |
| 3.3.1 Linear model | 15 |
| 3.3.2 Angular model | 19 |
| 3.3.3 Differences between <i>angular</i> and <i>linear</i> models | 24 |
| 3.4 Extensions | 24 |
| 3.5 Conclusion | 28 |
| 4 Validation method | 29 |
| 4.1 Introduction | 29 |
| 4.2 The biomechanical simulator: OPENSIM | 29 |
| 4.2.1 Framework architecture | 30 |
| 4.2.2 Inverse Kinematics | 31 |
| 4.2.3 Inverse Dynamics | 32 |

| | | |
|----------|--|-----------|
| 4.2.4 | Computed Muscle Control | 32 |
| 4.3 | Implementation and integration of the actuator model | 34 |
| 4.3.1 | OPENSIM model | 35 |
| 4.3.2 | Command computation | 35 |
| 4.3.3 | Extensions | 36 |
| 4.4 | Simulation workflow | 37 |
| 4.5 | Conclusion | 37 |
| 5 | Results | 39 |
| 5.1 | Introduction | 39 |
| 5.2 | Test cases evaluation | 39 |
| 5.2.1 | Evaluation method | 40 |
| 5.3 | Simulation results | 41 |
| 5.3.1 | The <i>angular</i> model | 41 |
| 5.3.2 | The <i>extended</i> angular model | 56 |
| 5.4 | Discussion | 83 |
| 5.4.1 | Discussion of the <i>angular</i> model validation | 83 |
| 5.4.2 | Discussion of the <i>extended</i> angular model validation | 83 |
| 5.5 | Conclusion | 85 |
| 6 | Conclusions and future work | 89 |
| | Bibliography | 91 |

List of Figures

| | | |
|------|--|----|
| 3.1 | The linear model | 16 |
| 3.2 | The angular model | 20 |
| 3.3 | The <i>extended</i> angular model | 26 |
| 4.1 | The OPENSIM logo | 30 |
| 4.2 | Schematic of the Computed Muscle Control Algorithm | 33 |
| 5.1 | Case 1 – Results | 43 |
| 5.2 | Case 1 – Generated power (positive torque) | 44 |
| 5.3 | Case 2 – Results | 45 |
| 5.4 | Case 2 – Generated power (positive torque) | 46 |
| 5.5 | Case 3 – Results | 47 |
| 5.6 | Case 3 – Generated power (positive torque) | 48 |
| 5.7 | Case 4 – Results | 49 |
| 5.8 | Case 4 – Generated power (positive torque) | 50 |
| 5.9 | Case 5 – Results | 51 |
| 5.10 | Case 5 – Generated power (positive torque) | 52 |
| 5.11 | Case 6 – Results | 53 |
| 5.12 | Case 6 – Generated power (positive torque) | 54 |
| 5.13 | Case 1 <i>a</i> – Results | 59 |
| 5.14 | Case 1 <i>a</i> – Generated power | 60 |
| 5.15 | Case 1 <i>b</i> – Results | 61 |
| 5.16 | Case 1 <i>b</i> – Generated power | 62 |
| 5.17 | Case 2 <i>a</i> – Results | 63 |
| 5.18 | Case 2 <i>a</i> – Generated power | 64 |
| 5.19 | Case 2 <i>b</i> – Results | 65 |
| 5.20 | Case 2 <i>b</i> – Generated power | 66 |
| 5.21 | Case 3 <i>a</i> – Results | 67 |
| 5.22 | Case 3 <i>a</i> – Generated power | 68 |
| 5.23 | Case 3 <i>b</i> – Results | 69 |
| 5.24 | Case 3 <i>b</i> – Generated power | 70 |
| 5.25 | Case 4 <i>a</i> – Results | 71 |
| 5.26 | Case 4 <i>a</i> – Generated power | 72 |

| | | |
|------|---|----|
| 5.27 | Case 4 <i>b</i> – Results | 73 |
| 5.28 | Case 4 <i>b</i> – Generated power | 74 |
| 5.29 | Case 5 <i>a</i> – Results | 75 |
| 5.30 | Case 5 <i>a</i> – Generated power | 76 |
| 5.31 | Case 5 <i>b</i> – Results | 77 |
| 5.32 | Case 5 <i>b</i> – Generated power | 78 |
| 5.33 | Case 6 <i>a</i> – Results | 79 |
| 5.34 | Case 6 <i>a</i> – Generated power | 80 |
| 5.35 | Case 6 <i>b</i> – Results | 81 |
| 5.36 | Case 6 <i>b</i> – Generated power | 82 |
| 5.37 | Summary results – <i>angular</i> model | 84 |
| 5.38 | Summary results (flexion) – <i>extended</i> angular model | 86 |
| 5.39 | Summary results (extension) – <i>extended</i> angular model | 87 |

List of Tables

| | | |
|-----|--|----|
| 5.1 | Test cases for the <i>angular</i> model | 42 |
| 5.2 | Test cases evaluation for the <i>angular</i> model | 55 |
| 5.3 | ID execution time for the <i>angular</i> model | 55 |
| 5.4 | Test cases for the <i>extended</i> angular model | 56 |
| 5.5 | Test cases evaluation for the <i>extended</i> angular model (positive torques) | 57 |
| 5.6 | Test cases evaluation for the <i>extended</i> angular model (negative torques) | 58 |
| 5.7 | ID execution time for the <i>extended</i> angular model | 58 |

Abstract

The purpose of this thesis is to show that it is possible to design a mechanical structure that is able to actuate the hip of an exoskeleton, only using a *single* rotational electric motor, connecting the two joints by means of elastic bands.

The use of a single actuator could clearly reduce the weight, the energy consumption and the economical cost of the device. Indeed, the development of a *low cost exoskeleton* would improve technology spreading and would encourage the use of the exoskeletons as domestic equipments.

In this project we are only interested in the design and validation of a model of an hip exoskeleton that could be controlled by means of a single actuator. The proposed actuation system receives the torque command from the control layer and then it *computes* the reference position for the single actuator to provide the desired torques to both the hip joints.

The proposed single actuator exoskeleton has been implemented within the OPENSIM simulator and validated. This framework has been used to simulate the exoskeleton coupled with the model of the lower limbs of the human body for a walking task, using a movement based on real data of a normal gait. Then, using an inverse dynamics analysis, we compared the forces generated by the muscles with and without the contribution of the exoskeleton. The results showed that the energy generated by the muscles with the enabled exoskeleton, was less than the one without external help: this makes us confident of the effectiveness of the solution.

The future prospective of this work is further validation using a real world exoskeleton. Also, we want to extend the principle of using a single actuator to control several joints.

Sommario

Lo scopo di questa tesi è mostrare che è possibile progettare una struttura meccanica in grado di attuare i giunti delle anche di un esoscheletro, usando un *solo* motore elettrico rotazionale, collegato ai due giunti tramite degli elastici.

L'uso di un singolo attuatore può diminuire il peso, il consumo energetico e soprattutto il costo del dispositivo. Inoltre, lo sviluppo di un *esoscheletro a basso costo* permetterebbe a questa tecnologia di diffondersi maggiormente ed incoraggerebbe l'uso degli esoscheletri come strumenti domestici.

In questo lavoro l'interesse si concentra sul progetto e la validazione del modello di un esoscheletro per le anche, che possa essere controllato per mezzo di un singolo attuatore. Il sistema di attuazione proposto riceve il comando di coppia dallo strato di controllo e quindi calcola il riferimento di posizione per il singolo attuatore, in modo che fornisca le coppie desiderate ad entrambi i giunti delle anche.

L'esoscheletro a singolo attuatore qui proposto è stato implementato all'interno di OPENSIM e validato tramite alcune simulazioni. Questo sistema è stato usato per testare l'esoscheletro accoppiato al modello degli arti inferiori del corpo umano, in una prova di cammino; il movimento riprodotto è stato ricavato da dati reali di una camminata normale. Usando quindi un'analisi della dinamica inversa, abbiamo confrontato le forze generate dai muscoli con e senza l'aiuto dell'esoscheletro. I risultati hanno mostrato che l'energia generata dai muscoli con l'esoscheletro attivo, era inferiore a quella generata senza l'aiuto esterno: questo ripone una certa fiducia nell'efficacia della soluzione.

La prospettiva futura di questo lavoro è la sua applicazione a qualche esoscheletro reale e, successivamente, provare ad estendere il principio di usare di un singolo attuatore per riuscire a controllare più giunti, come quelli delle ginocchia o delle caviglie.

Introduction

Assistive and rehabilitation robotics is the new frontier of robots development. In the past decades, the research and the investments in the robotic field were mainly addressed to the development of industrial automation technologies, where the interaction with humans was a marginal issue. In the near future, the need of robotic devices that must closely interact with humans and with disabled and elderly people will surely increase. In the 1950s, only 4.9% of the world's population was over the age of 65. Today, almost 20% is over 65 and realistic estimations forecast that this percentage will exceed 35% by 2050 [16]. Such a demographic shift in world population is going to impose a large burden of care to treat the health risks associated with ageing. Robotic solutions can help to tackle these issues and to enable the elderly regaining their independence and maintain an enriching, fulfilling lifestyle. A proof of this new interest can be the investments planned within the *Horizon2020* programme [64]. Or in human-mobility technology, the research investment shift of large automobile companies, such as Honda and Toyota, from wheeled devices to anthropomorphic exoskeletal technologies that allow humans to move bipedally at enhanced speeds. Perhaps in the latter half of this century, exoskeletons and orthoses will be as pervasive in society as wheeled vehicles are today [27].

Focusing on rehabilitation robotics, the exoskeletons are promising devices but still too expensive to be the state-of-the-practise for the treatment of disabling diseases where they are yet showed their potentials, like stroke, cerebral palsy and spinal cord injury. Further development of this technology needs safe and natural human-robot interaction, affecting how the exoskeletons are actuated. Traditional actuator technology adopted “the stiffer the better” paradigm and is unsuitable for fulfilling these requirements, we need “soft” actuators that exploit elasticity. As nature teaches us, animal muscles provide intrinsic elasticity leading important advantages in terms of stability, efficiency and force

accuracy [56], characteristics desirable also in robots interacting with humans. We too want to benefit from elasticity. Indeed elastic actuators are nowadays wide adopted, for their intrinsic safety, efficiency and ability to apply forces in a more accurate way than other actuators. Future exoskeletons need to be wearable devices. The enabling technologies for these kind exoskeletons must be lightweight and energy efficient because of portability requirements.

In this thesis to tackle this needs, we propose the new concept of a *single actuator exoskeleton* applied to an hip assistance device. Using a position control and under some assumption that we will give later, we will be able to apply torque profiles to both the hips. Our purpose is to show that it is possible to design a mechanical structure that using a *single* rotational electric motor can reach the aim. The transmission between the single actuator and the joint is provided by means of elastic bands so that we can have a compliant interaction with the user and the exoskeleton. To this purpose, we first provide a theoretical rationale and then we validate it within a simulation environment.

The use of a single actuator could clearly reduce the weight, the energy consumption and the economical cost of the device. The possible development of a *low cost exoskeleton* would improve technology spreading and would encourage the use of the exoskeletons as domestic equipments.

The starting assumptions for this project were:

- in most cases it is sufficient to help one movement of the hips between the *flexion* and the *extension*;
- while walking, it is never necessary to provide torque for flexion (or extension) to both the hips at the same time;
- the gait movement is highly periodic.

In this project we proposed a theoretical rationale to provide kinematic and dynamic constraints for a model of an hip exoskeleton that could be controlled by means of a single actuator. The proposed actuation system, given a desired torque command and knowing the positions of the controlled joints, *computes* the reference position for the single actuator to provide the desired torques to both the hip joints. As it will be described in chapter 3, we decided to initially developed a model addressed to give torques only for the flexion. Then, we studied a possible extension of the model that tries to give both extension and flexion torques. Upon these models, it will also be discussed the constraints on the input torque commands needed to ensure that the actuator can correctly apply them.

The proposed single actuator exoskeleton has been implemented within the OPENSIM simulator [66] and validated. This framework is a biomechanical simulator developed at the Stanford University that allows to simulate a complex body model. This simulator provides two main analysis: the first one is a forward dynamics analysis, that given the muscle excitation commands, returns the resulting generalized force at the joints in each time frame, from which it is possible to compute the resulting movement. The second is an inverse dynamics analysis, that given the joints' positions in each frame, returns the generalized forces generated at each joint by the muscles needed to produce the movement, also taking into account the presence of external forces, if any. The exoskeleton has been simulated coupled with the model of the lower limbs of the human

body for a walking task, using a movement based on real data of a normal gait. Then, using an inverse dynamics analysis, the forces generated by the muscles with and without the contribution of the exoskeleton will be compared. The results will show that the energy generated by the muscles with the enabled exoskeleton, was less than the one without external help: this would make us confident of the effectiveness of the solution. Moreover, this result can indicate that the exoskeleton supports the movement and it does not counteract.

The future prospective of this work is to apply it to some real exoskeletons, such as the one developed in [11]. This exoskeleton has the aim to help spastic people to better coordinate their gait, and the proposed single actuator would substitute the two pneumatic muscles currently used to actuate the hip. Nevertheless, the principle of this work could be applied to a large variety of exoskeletons and it could probably be extended in order to control with a single actuator not only the two hip joints, but several joints, like the knee or ankle ones.

This document is structured as follows: chapter 2 will discuss the literature related with exoskeletons, their applications to rehabilitation and eventually an overview of the mainly used actuation methods, focusing on the elastic actuators; chapter 3 will present the mechanical model of the developed actuator. The validation method will be described in chapter 4, providing also an overview of OPENSIM[66] and the implementation of the proposed actuator into the simulation environment. The chapter 5 will present the results of the simulations and how well these respond to the objectives. Then eventually, there will be the conclusions in chapter 6.

Related works

2.1 Introduction

This chapter will present an overview of the literature about the exoskeleton technology and in details its use in the field of *rehabilitation robotics*. Thus, it will be described the available techniques for the actuation of these equipments.

The aim in developing robots that closely interacts with human beings can be efficiently summarized by this quote:

It's not well appreciated, but over half of the world's population suffers from some form of cognitive, emotional, sensory or motor condition, and because of poor technology, too often, conditions result in disability and a poorer quality of life. Basic levels of physiological function should be a part of our human rights. Every person should have the right to live life without disability if they so choose – the right to live life without severe depression; the right to see a loved one, in the case of seeing-impaired; or the right to walk or to dance, in the case of limb paralysis or limb amputation.

As a society, we can achieve these human rights, if we accept the proposition that humans are not disabled. A person can never be broken. Our built environment, our technologies, are broken and disabled. We the people need not accept our limitations, but can transcend disability through technological innovation. Indeed, through fundamental advances in bionics in this century, we will set the technological foundation for an enhanced human experience, and we will end disability.

*Hugh Herr
Bionics designer, MIT professor – TED2014
Vancouver, Canada, March 17-21*

This chapter is organized as follows: section 2.2 explains some clinical studies on the use of robot based therapy. Section 2.3 provides a background knowledge about different approaches to rehabilitation robotics. Section 2.4 describes some prototypes and commercial products that represents the state of the art of the robots for the lower limbs. In section 2.5, we presented the today technologies used for the actuation of these equipments, the their limitations and possible future developments. Then, section 2.6 is the conclusion of the chapter.

2.2 Effectiveness of rehabilitation robots

At the moment there is a general lack of important clinical studies on the effectiveness of rehabilitation robotics, although many researchers are confident that robotic rehabilitation could have an effectiveness similar (or even better) to the traditional motor learning therapy. A study has been presented where more than one hundred stroke patients were treated with robotic machinery [34]. The result report that «In patients with long-term upper-limb deficits after stroke, robot-assisted therapy did not significantly improve motor function at 12 weeks, as compared with usual care or intensive therapy. In secondary analyses, robot-assisted therapy improved outcomes over 36 weeks as compared with usual care but not with intensive therapy». This means that robots can give the same benefits of treatments with expert therapists. However this result is not considered fully positive by some part of robotics community because there were expectations for even better outcomes. Some scientists are in fact convinced that this is mainly due to the not yet mature technology. Moreover there is a lack of knowledge about clinical outcomes with young patients and more complex pathologies such as cerebral palsy (CP) where lesion is not as specific as in stroke or spinal cord injury (SCI).

Similar results can be found in other literature works. In [5, 52] a systematic review confirms the potential for robotic assisted devices to improve motor functions of stroke in upper limbs. In [35] a review of recent developments for upper limb exoskeletons in patients with neuromuscular disorders is presented, with a discussion of potential areas for future researches where robots could be more effective and less expensive than traditional rehabilitation. In [45] authors found that training with passive devices in a gravity-reduced environment can provide comparable results to those achieved with robotic assisted rehabilitation. Also, there is evidence that training performed in virtual reality environment can induce cortical reorganization and associated recovery in stroke [62].

2.3 Rehabilitation robots background

Rehabilitation robots can be used with gain two distinct purposes: to improve motion performance or to learn new motor abilities. For instance, in stroke rehabilitation it was shown that an augmentation of errors can accelerate the learning process [21] because the mental representation of a given task is built in an adaptive error driven process ([47, 51]). So, in this case the focus is on learning (by means of brain plasticity) and usually the motion performance is downgraded. On the other hand robots that have the aim of improving performance are designed to augment human capabilities, such as force and

endurance. These can often have also a positive effect on learning because enhancements of movements create more afferent feedback to the user.

The rehabilitation robots can be classified in two main categories, based on the mechanical interaction they have with the patients: prostheses, devices applied in series with human body to substitute some missing or damaged parts, and orthoses, working in parallel with human limbs and usually presenting a coordinated control between robot and human. Particular orthoses, where kinematic chain follows the human anatomy, are called exoskeletons since they usually provide an external shell that remembers the insect's one. Dealing with human anatomy, peculiar aspects of exoskeleton are ergonomic design and complex kinematic compatibility. In fact joint misalignment can cause undesirable interaction forces and pain. Otherwise, when the orthoses have a different kinematic from human's, we have end-effector based orthoses (or peripheral actuated orthoses) in which the interaction with humans considers a single kinematic link. For these devices, the mechanical design can be simpler but there is only partial control of user movements [41]. Prosthesis and portable exoskeleton, grounded or not, are also called wearable robots. Non wearable robots are fixed to the ground, like most of the commercial rehabilitation systems, or mobile with moving base or appendix that are usually suited to carry the power source and other high weight parts [10, 32].

Interaction between a human and a robot device can be achieved through internal or external force systems. In external force systems the interaction forces are transmitted to an external base that can be fixed or mobile with the user. This principle is typical of empowering or load carrying exoskeletons and leads to high force transmission. A class of such robots aims to simply transfer human load to the ground relieving the user from gravity. On the other hand internal force systems transmit power between segments of human limb, usually to complement or replace weak or lost functions of human musculoskeletal system. The forces generated by such a system are more complicated because they concern two, or more, human segment at once as they act "between" them. Preferred control strategies in this case are impedance and stiffness control, while force control is more suitable when the device is an external one.

An intrinsic characteristic of rehabilitation robots is the dual cognitive and physical interaction with humans. The physical human-robot interaction (pHRI) is due to the generation of supplementary forces by the robotic system, to empower or overcome human limits. On the other hand human motor control implies a cognition process which is influenced when dealing with "augmented" body capability. Moreover the cognitive human-robot interface (cHRI) can be empowered by means of bioelectrical variables that bridge nerves information directly on the robots and even on the inverse pathway that is stimulating nerves to produce feedback information to the brain [59].

2.4 Orthoses for the lower limbs

Focusing on lower limb orthoses, many devices have been developed so far for gait assistance/training. Some devices only apply mechanical restrictions to user gait to correct for kinematic pathological misplacements. Other ones integrate actuators to one or more joints to act also on gait dynamics. The latter can be used to improve the patient gait efficiency or to replace a missing motor function.

An intermediate approach to orthotic design is to deploy passive elements that generate forces, i.e. springs, damper, brakes etc. This strategy allows to increase energy efficiency of the device without adding a power source that increases the weight of the device, especially if it is to be carried on mobile orthoses.

At present, commercial active orthoses are quite common. As mentioned before they can be classified in external and peripheral actuated. The first ones are more sophisticated and versatile; they use actuators for every moving joint of the kinematic chain of interest. On the other hand, peripheral actuation attempts to carry only the extremities or the single joint without considering the entire leg kinematics. Examples of commercial ergonomic, external actuated, orthosis are Lokomat® and ReWalk™ while Gangtrainer™ and Innowalk® are peripheral actuated. Unfortunately most of these commercial orthoses are not mobile because of their mass and power need. Some of them overcome this limitation by deploying a virtual reality environment to augment patient motivation.

Maybe the most famous example of not mobile external actuated orthosis is Lokomat® a commercial product from Hocoma which is an eight degree of freedom orthosis that is used in many rehabilitation centers. However at the moment this system is suited for therapy where the patient is almost passive, while is proven that an active role of patient is a favorable condition in rehabilitation [55]. From research side a similar comprehensive system is developed at the University of Twente with some major improvement. This system is called Lopes [20, 58] and is based on series elastic actuators. Many rehabilitation strategies have been tested on it using new paradigms e.g. patient centered control [54].

In the last few years some examples of commercial mobile actuated orthoses have also become available, in particular for SCI patients with the dual purpose of rehabilitation and regaining (quite) autonomous walking and helping the user in common daily movements like doing steps, standing and sitting. Most of these devices requires the capacity of the user to keep balance at least for the trunk, by using external supports like crutches or rolling walkers: for sake of example we have the previously cited ReWalk™ [44, 2], the eLegs at Berkley Bionics™ [6], the Mina prototype at IHMC insitute (FL, USA) [52] or the WPAL developed at Nagoya University [30], the recent Ekso™ [7] or recent applications of the Japanese HAL for intention based walking [49]. There is also an example of commercial exoskeleton that is able of self-equilibrium and self-sustaining, the REX™ [8]. Although, this capacity is achieved at the cost of having a big and heavy machinery and loosing intention based control: in fact, the user must be completely passive in the lower limbs and it is controlled by a joystick as if were an electric wheelchair. This compromise, though, allows this exoskeleton to be used by people with an almost complete SCI up to the C4/5 level. The control of these devices and the self-equilibrium are the main still opened issues that slow down the marketing of them [19, 27]. A real intention based control has still to come, because an exoskeleton should be able to accomplish many different tasks that imply different operating modes and, if it is able to effort more than one task, at least the switching must be done by giving an explicit command to the device, e.g. pushing a button.

On the research side the field of active orthosis is very ample. It starts on the previous half century with purely mechanical orthosis, reaching the first computer based orthosis on the 70s years. For a detailed historical background

and state of the art of active orthoses see [19]. Examples of these research devices are the Vanderbilt University’s lower limb exoskeleton [22] and numerous “soft” exoskeleton called exosuit that can actuate only the hips [4, 26, 39] or the whole leg [60, 3, 18] but for their intrinsic compliancy are only suitable for people with limited gait difficulties of to increase the efficiency of the walking.

Different kind of active Ankle-Foot orthoses have been developed by MIT Biomechatronics Lab [9] and [37] that one of the few active orthoses with a study that shows it can reduce the metabolic cost of human walking. These kind of orthoses have also been studied by Dan Ferris’s Lab at Michigan University [23, 46], by Agrawal’s Lab at University of Delaware [1] and by the Arizona states University [28] using the jack-springTM actuator. These devices are used for example to assists the drop-foot gait by modulating the impedance of the orthotic joint throughout the walking cycle, or coupled with surface EMG sensor for enhance muscle strength.

Knee orthoses have been developed at the Northeastern University [61] and at Berlin University of Technology [25, 24], basing on dissipative and brake principles, EMG, ground reaction forces and inter joint couplings; all the mentioned orthoses miss full leg support.

2.5 Actuation technologies and limitations

This section reports a brief description of the electromagnetic and hydraulic actuators that are the most traditional actuators in today robotics. Then, there will be an excursus on pneumatic artificial muscles and series elastic actuators that represent the basis of the development of compliant actuators. The last subsection is dedicated to exploit the limitation of these technologies when applied to rehabilitation robotics.

2.5.1 Traditional actuators

A wide range of application uses commonly electric motors; they convert the electrical energy into mechanical movement, by means of known electromagnetic phenomena, like Lorentz force or Faraday induction. Theoretically they can be considered a good approximation of force source but the unavoidable presence of a motor gear introduces significant frictions, dissipations and increases the reflected inertia at the output of gear box. Moreover the power needing can significantly influence on the weight of actuator. Electric motors can reach a very high level of accuracy and stability on position control even using simple linear algorithms. On the other side force and impedance control needs the presence of a force feedback signal and robust control algorithms, especially in case of intermittent contact with hard surfaces. The most used force/torque sensors are load cells and, depending on the target precision, they can be very expensive. Another drawback is that a stiff actuator inertia cannot be fully masked by any causal controller as showed in [13] and this inertia can lead to undesired interaction force in human-robot interaction.

Hydraulic motors, instead, convert hydraulic energy into mechanical energy. Hydraulic systems typically use pumps in conjunction with valves and piping to form a hydraulic powered transmission. Usually, a carrier line connect a pump to a motor, which then draws fluid from a reservoir and forces it into the motor.

The fluid forces the movable components of the motor into motion, which in turn rotates the attached shaft. The shaft, which is mechanically linked to the work load, provides rotary mechanical motion. Finally, the fluid is discharged at low pressure and transferred back to the pump. A famous example of hydraulic actuated exoskeleton is the BLEEX, now developed into eLegs and HULC, at Berkley University [63, 31].

In portable robotics, the typical power supplies for electric and hydraulic motors are rechargeable batteries. Nowadays batteries are also not lightweight but with a positive trend during last decades and have a power to weight ratio better than other technologies (e.g. compressed air bottle).

2.5.2 Compliant actuators

A compliant mechanism is a flexible body that transfers an input force or a displacement between two points through its elastic deformation. Compliant actuators are power device that integrate such compliant elements providing an intrinsic passive elasticity. The advantages of compliancy are numerous. First they minimize impact force due to shocks, leading the actuator to stably interact also with discontinue forces. Second they are intrinsically safe for human robot interaction due to the elastic decoupling. Third they can provide more accuracy in force control. Also they can store and release energy in passive elastic elements leading to more efficiency in harmonic task. For example compliant actuated legged robots are proven to be from ten to hundred times more efficient in comparison with their stiff counterpart [14]. Other reasons to choose compliancy are dependent from the specific realization.

It is possible to observe from literature that compliancy can be reached in two main ways. First simply by the union of a stiff active part (like a motor) and passive elastic element (like a spring) coupled together by a mechanical system, and second by a unique elements that is at the same time active and (passively) elastic. Just to give an example, the so called pneumatic artificial muscles (PAM) use the latter concept while series elastic actuators (SEA) are instances of the first one. Starting from these two first proposals of compliant actuators many other were developed since nowadays. Some of them are based on an antagonistic setup of PAM or SEA, others are based on more complex design combining lever, cams, springs and motors [57].

The pneumatic actuators are probably the first compliant actuator ever developed. The first prototype of pneumatic artificial muscle (PAM) dates the late 1950's and since then many variants were proposed [15]. Generally, their structure is composed by a rubber tube and an external braid of fiber that transforms the air radial expansion in axial contraction. Their compliance is due to the compressibility of actuator fluid that is contained in the inner tube. The actuator dynamics is highly non-linear and the mathematical model, firstly studied by Chou and Hannaford [12], then improved in [48, 53], is very complex. One of the main advantages of PAM is the very high power to weight ratio which is combined with high forces and high reliability, a characteristic that today is hardly achievable with other technologies. However this benefit is completely invalidated by the power source drawback, as they work with compressed air: at present time it is not possible to reach a power density favorable for portability. Despite this problem and the difficulties in control, PAM are appreciated for other reasons, e.g. they don't need a gearbox, they are backdrivable, they can

be compared to human muscles and they are extremely lightweight if the power is carried externally.

The so called “Series Elastic Actuator” (SEA) were firstly introduced in 1994 at MIT laboratory, starting from the simple idea of applying a linear spring in series with traditional motors, proving relevant benefit [42]. Authors propose to measure spring position at both edges, the one attached to the motor and the other to the load. In this way is possible to measure the force through spring deformation. The advantages of using SEA are, for example, low output impedance and backdriveability thus performing a safer interaction with humans, force control accuracy and stability are improved providing also shock tolerance. Moreover they exhibit reduced motor requirements on force transmission, high force fidelity and possibly high efficiency in harmonic application by storing and releasing energy in and from the spring. Because of the low pass behaviour of mass-spring systems, generally bandwidth and maximum forces are reduced and thus high power motors are required. However, authors show that in some condition the maximum force is augmented and even that bandwidth is improved in load motion task [43].

2.5.3 Limitations and future actuators

The need for a safe and natural human-robot interaction leads actuator technology to be safe and “soft”. This scenario is very different from “the stiffer the better” paradigm that is prevailing in the industrial robotics. As we learn from nature animal muscle provide intrinsic elasticity thus leading to some unquestionable advantage in terms of stability, efficiency and force accuracy [56]. Of course these characteristics are desirable also in robots that interact with humans.

Even through elastic elements can provide an augmented efficiency of orthotic systems, the enabling technology for building a light weight device has still to come, because of the low power density of today motors and relative power supply. This is a very limiting factor for mobility that was already outlined at the very beginning of this research field (around 1960s) and despite several improvement of the art it is still valid nowadays. For grounded orthoses this problem can be easily dressed out and in some severe pathology a compromise of wearability can be found as for example in [10].

A possible solution is to use as less as possible active elements in the design of the orthoses, because each active joint means a motor, a power supply and then weight. We have examples of walking robots that are designed to have a mechanical structure that exploit the gravitational potential energy and elasticity to reduce the power needs: the passive walkers have no actuated joints at all, but they can only work on inclined planes [36]. However their principle can be used to obtain an active walker by adding only a single motor, as stated by the thesis of Nicola Piccinelli [40]. In this work he actuated, via a simulation, a compass walker with a single motor at the top of it, using an energetic control strategy, and at a very low expense of energy. There is also the possibility to help the human walking by means of a completely passive elastic orthosis, only composed by pulleys and elastic bands called “exotendons”, as studied by Van Den Bogert [56]. However, the under-actuated nature of the exoskeleton so built can really modify the human dynamics putting the wearer in a sort of unnatural force field, so that his own motor control need to adapt.

Another possibility is to develop new kind of actuators, more similar to the examples given to us by the nature, as tried with the previously described PAM. The Dielectric Elastomer Actuators (DEAs) are a promising technology that take inspiration from the biological structure of the muscles. The DEAs are novel, muscle-like actuators that operate on the electromechanical response of a polymeric material to the application of an electric field [33]. As depicted in [38], DEAs are compliant viscoelastic actuators that provide a linear contractile force and are capable of both isometric and eccentric actuation and also multidirectional actuation. So, for their similarities with natural muscle can have promising applications for bionics applications. However, this technology is relatively young and research must still be done to reach a development sufficient to apply them to a commercial device.

2.6 Conclusion

This chapter presented an overview of the literature about the exoskeleton technology and their use as rehabilitation devices. We also described the actuation techniques applied to these equipments. Section 2.2 explained some clinical studies that show the effectiveness of robot based rehabilitation. Section 2.3 provided a background knowledge about different approaches to rehabilitation robotics. Section 2.4 described some prototypes and commercial products that represents the state of the art of the robots for the lower limbs. In section 2.5, we presented the today technologies used for the actuation of these equipments, the their limitations and possible future developments.

The single actuator concept

Modelling and theoretical analysis

3.1 Introduction

This chapter describes the single actuator design and its analysis. The starting idea was to actuate an exoskeleton attaching at the back of the user a single motor connected to the hip joints by means of elastic links, instead of using two motors, one for each joint. This configuration can replace, for example, the two pneumatic actuators used in [11], an exoskeleton previously described, or actuate a similar structure. In order to exploit this idea, the work has been divided into two phases: first, we aimed to achieve a simplified goal by abstracting and facing the problem in as general as possible manner; second, we wanted to further develop the model achieved in the first phase to apply it to the target exoskeleton.

The first step led to the definition of the *linear* problem (page 15) which is substantially obtained by “unrolling” the rotational joints, so it is formulated in terms of forces and linear motion quantities. The objective of this version of the problem was to establish the mathematical foundations of the single actuator concept that has been then enriched by applying it to the more realistic *angular* problem (page 19). In this formulation we had to solve the challenge of giving a desired torque pattern to two independent joints, the hips of the exoskeleton, by using a single motor. We also supposed to know the trajectories that each joint would have to follow. However, in this version there are still some constraints on the allowed torque profiles, but they were useful to simplify the task: in fact, we assumed that we had to apply the torques only in one direction and always in the same, i.e. only flexion torques (positive). In addition, the reference torque

patterns for the two joints had to be such to guarantee a torque equal to zero for at least one of the joints in every instant. Developing this second model, we had also to ensure that, when the torque was to be applied to one of the joints, the other one was subjected to zero torque, independently from its trajectory. We studied then further development to try to relax this assumption, allowing the desired torques to be negative: in section 3.4 we will present a possible extension of the *angular* model to overcome (partially) the issue of not helping the extension movement.

The structure of the chapter is as follows: section 3.2 will make explicit the objectives pursued in modelling the actuator; section 3.3 will describe the *linear* and the *angular* model developed (respectively, in subsection 3.3.1 and 3.3.2). Section 3.4 will describe the *extended* angular model that tries to apply both positive and negative torques to the controlled joints. The last section (3.5) contains the conclusion.

3.2 Objectives of the design

The objectives we pursued in developing three models we are going to present in the following, can be summarized in these steps:

- to mathematically define the problem to which the model is addressed, in an as general as possible way;
- to define a mechanical model able to reach the defined objectives;
- to characterize the torque patterns that the model can apply, if possible.

In the evolution from the *linear* to the *angular* model we also had the additional aim of applying the model to the specific problem of giving torque to the hip joints of an exoskeleton, in order to reach a version that can be simulated.

So in developing the three models, the *linear*, the *angular* and the extension of the latter, we had to find:

- an assignment for the model parameters that allows to apply the desired torques;
- a feasible kinematic law, i.e. a timed function that describes at each instant the desired position of the single actuator so that the model exactly applies the reference torques.

3.3 Description

This section characterizes the problem addressed by the model, how it is solved and the rationale behind the choices:

- subsection 3.3.1 describes the starting problem, for simplicity the linear case;
- subsection 3.3.2 extends the linear problem by considering a realistic torsional motor and angular variables;
- subsection 3.3.3 explains the differences between the two models.

3.3.1 Linear model

The problem addressed in this subsection has this statement:

Problem 1 (Linear version). Given $x_l(t)$ and $x_r(t)$ respectively the left and the right joint positions at time $t > 0$ such that:

$$(A1) \quad |x_l(t)| \leq X_{l,max} \quad \forall t > 0;$$

$$(A2) \quad |x_r(t)| \leq X_{r,max} \quad \forall t > 0.$$

Given $f_l(t)$ and $f_r(t)$ the reference forces to be applied to the left and the right joints such that:

$$(B1) \quad 0 \leq f_l(t) \leq F_{l,max} \quad \forall t > 0;$$

$$(B2) \quad 0 \leq f_r(t) \leq F_{r,max} \quad \forall t > 0;$$

$$(B3) \quad f_l(t) > 0 \Rightarrow f_r(t) = 0 \quad \forall t > 0;$$

$$(B4) \quad f_r(t) > 0 \Rightarrow f_l(t) = 0 \quad \forall t > 0.$$

Given the fixed points O_l , O_r and O_a , respectively the origins of the 1D reference system for the left, the right joint and the actuator such that they are aligned and work on the same axis, we must determine:

(C1) The model parameters:

- K_l and K_r the linear spring constants of the left and the right elastic band, respectively connecting the actuator to the left and the right joint;
- $L_{0,l}$ and $L_{0,r}$ the resting length of the left and the right elastic band.

(C2) A feasible kinematic law, i.e. a function $x_a(t)$ describing the desired position of the actuator at time $t > 0$ so that the model exactly applies the reference forces $f_l(t)$ and $f_r(t)$ to the joints;

(C3) Under which constraints (on the structure or on the reference functions) the model could safely fulfil the given references.

In the following, we also consider that the distances between O_l and O_a , called D_l , and between O_r and O_a , called D_r , are constant.

We took into account the possibility to have some other “feasibility constraints” on the kinematic law that must be provided, ordered by increasing difficulty to be meet:

$$(a) \quad |x_a(t)| \leq X_{a,max} \quad \forall t > 0, \text{ it is an obvious physical constraint;}$$

$$(b) \quad |\dot{x}_a(t)| \leq V_{a,max} \quad \forall t > 0;$$

$$(c) \quad |\ddot{x}_a(t)| \leq A_{a,max} \quad \forall t > 0.$$

We will study under which conditions these other constraints could be meet, starting from (a) (position constraint).

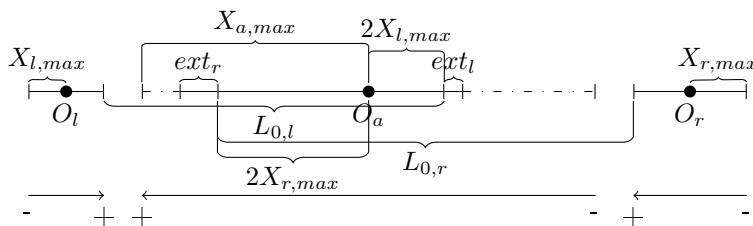


Figure 3.1: The linear model

Model parameters (C1)

In figure 3.1 we can see the schematic description of the linear model. The design principle of the model is that, accordingly to conditions (B3) and (B4), we have two operating modes:

- if $f_l(t) > 0$ then $x_a(t) \leq 0$;
- if $f_r(t) > 0$ then $x_a(t) \geq 0$.

In order to determine the resting length of the two elastic bands, we must ensure that when we have the maximum distance between the position of the motor and the position of the joint not currently controlled, the elastic band for that joint applies zero force. So this is the case when $x_a(t) = 0$ and the joints coordinates are at the minimum (negative):

- $L_{0,l} = D_l + X_{l,max}$;
- $L_{0,r} = D_r + X_{r,max}$.

The values for the linear spring constants are not uniquely determined, but we can state some constraints on them because of (a) (position constraint): indeed, we must be able to extend the elastic band length in order to give the maximum force, within the movement bounds of the actuator.

For example we could consider the extreme case in which we have $f_r(t) = F_{r,max}$ and $x_r(t) = X_{r,max}$. The left elastic band could apply some force if $x_a(t) > 2X_{r,max}$ and if we want to apply a force of $F_{r,max}$, we must extend the elastic band of $ext_r = \frac{F_{r,max}}{K_r}$, so $x_a(t)$ must be $2X_{r,max} + ext_r$. The actuator will be able to apply this command if and only if $x_a(t) \leq X_{a,max}$, so we have:

$$K_r \geq \frac{F_{r,max}}{X_{a,max} - 2X_{r,max}} \quad (3.1)$$

and it is obvious that we must have $X_{a,max} > 2X_{r,max}$, at least.

We can proceed similarly for the other side, where we have the extreme case when $f_l(t) = F_{l,max}$, $x_r(t) = X_{l,max}$ and to apply some force must be $x_a(t) < -2X_{l,max}$. The required extension for the left elastic band is $ext_l = \frac{F_{l,max}}{K_l}$, therefore $x_a(t) = -2X_{l,max} - ext_l$ and we want this value to be greater or equal to $-X_{a,max}$. So we have this condition:

$$K_l \geq \frac{F_{l,max}}{X_{a,max} - 2X_{l,max}} \quad (3.2)$$

and also in this case $X_{a,max} > 2X_{l,max}$.

Summarizing, this is the parameters assignment:

$$L_{0,l} = D_l + X_{l,max}, \quad K_l \geq \frac{F_{l,max}}{X_{a,max} - 2X_{l,max}}, \quad (3.3a)$$

$$L_{0,r} = D_r + X_{r,max}, \quad K_r \geq \frac{F_{r,max}}{X_{a,max} - 2X_{r,max}} \quad (3.3b)$$

Kinematic law (C2)

In order to use this actuator, we must define a kinematic law $x_a(t)$ that, given the joint trajectories $x_l(t)$ and $x_r(t)$, and the desired forces $f_l(t)$ and $f_r(t)$, says the position of the actuator. The input functions must respect the conditions stated in the problem 1.

The kinematic law can be expressed as:

$$x_a(t) := \begin{cases} -X_{l,max} - x_l(t) - \frac{f_l(t)}{K_l}, & \text{if } f_l(t) > 0 \\ X_{r,max} + x_r(t) + \frac{f_r(t)}{K_r}, & \text{if } f_r(t) > 0 \\ 0, & \text{if } f_l(t) = 0 \text{ and } f_r(t) = 0 \end{cases} \quad (3.4)$$

The correctness of this kinematic law is showed in the following, by demonstrating this theorem:

Theorem 1 (Linear kinematic law). *Given the model depicted in figure 3.1 with the parameter assignment of equation 3.3, the joint positions $x_l(t)$ and $x_r(t)$ respecting the assumptions (A1) and (A2) of problem 1 and the reference forces $f_l(t)$ and $f_r(t)$ respecting the assumptions (B1), (B2), (B3) and (B4), if the trajectory of the single actuator $x_a(t)$ is the one defined in 3.4 then the model applies exactly the reference forces $f_l(t)$ and $f_r(t)$ to the left and the right joint respectively.*

Proof. **Case $f_l(t) > 0$:** the length of the left elastic band is $D_l - x_l(t) - x_a(t)$. Substituting $x_a(t)$ and $L_{0,l}$:

$$\begin{aligned} D_l - x_l(t) + X_{l,max} + x_l(t) + \frac{f_l(t)}{K_l} \\ = D_l + X_{l,max} + \frac{f_l(t)}{K_l} \\ = L_{0,l} + \frac{f_l(t)}{K_l} \end{aligned}$$

So the elastic band has exactly the length required to apply a force of intensity $f_l(t)$ to the left joint. Instead, the length of right elastic band is $D_r - x_r(t) + x_a(t)$. Substituting $x_a(t)$, using upper bounds for $-x_l(t)$ and $-x_r(t)$, substituting $L_{0,r}$ and knowing that $\frac{f_l(t)}{K_l}$ is positive:

$$\begin{aligned} D_r - x_r(t) - X_{l,max} - x_l(t) - \frac{f_l(t)}{K_l} &\leq D_r + X_{r,max} - X_{l,max} + X_{l,max} - \frac{f_l(t)}{K_l} \\ &= D_r + X_{r,max} - \frac{f_l(t)}{K_l} = L_{0,r} - \frac{f_l(t)}{K_l} < L_{0,r} \end{aligned}$$

So the elastic band is loose and it applies no force to the right joint.

Case $\mathbf{f}_r(\mathbf{t}) > \mathbf{0}$: it is similar to the previous case, the length of the right elastic band is $D_r - x_r(t) + x_a(t)$. Substituting $x_a(t)$ and $L_{0,r}$:

$$\begin{aligned} D_r - x_r(t) + X_{r,max} + x_r(t) + \frac{f_r(t)}{K_r} \\ = D_l + X_{r,max} + \frac{f_r(t)}{K_r} \\ = L_{0,r} + \frac{f_r(t)}{K_r} \end{aligned}$$

So the elastic band has exactly the length required to apply a force of intensity $f_r(t)$ to the right joint. On the other hand, the length of the left elastic band $D_l - x_l(t) - x_a(t)$ and, in analogous manner of the previous case, we can conclude that it less than the resting length $L_{0,l}$, so it is loose and it applies no force to the left joint.

Case $\mathbf{f}_l(\mathbf{t}) = \mathbf{0}$ and $\mathbf{f}_r(\mathbf{t}) = \mathbf{0}$: in this case we choose to leave the actuator in the neutral position, although this could not be the best choice; positions within the interval $[-X_{l,max} - x_l(t), X_{r,max} + x_r(t)]$ are all available solutions. The elastic bands are both loose and the proof is similar to the two previous cases. \square

Constraints (C3)

In the previous paragraphs we only considered the constraint on the position of the actuator (a) and we found a kinematic law that works with no other constraints on the input forces and joint trajectories except from the hypothesis of the problem 1.

Now we will study under which conditions the other constraints on the actuator movement could be satisfied, such as the one on the maximum velocity (b) and the one on the maximum acceleration (c) of it. In order to achieve this, we will have to add further constraints on the input forces and joint trajectories.

If we consider x_l , x_r , f_l and f_r continuous and derivable functions, the solution is straightforward for the intervals where $f_l(t) > 0$ or $f_r(t) > 0$ (i.e. where also x_a is continuous and derivable):

$$f_l(t) > 0 \Rightarrow \left| \dot{x}_a(t) = -\dot{x}_l - \frac{\dot{f}_l}{K_l} \right| \leq V_{a,max}, \quad \left| \ddot{x}_a(t) = -\ddot{x}_l - \frac{\ddot{f}_l}{K_l} \right| \leq A_{a,max} \quad (3.5a)$$

$$f_r(t) > 0 \Rightarrow \left| \dot{x}_a(t) = \dot{x}_r + \frac{\dot{f}_r}{K_r} \right| \leq V_{a,max}, \quad \left| \ddot{x}_a(t) = \ddot{x}_r + \frac{\ddot{f}_r}{K_r} \right| \leq A_{a,max} \quad (3.5b)$$

On the other hand, in the intervals where both f_l and f_r are zero the function x_a has discontinuities. It is obvious that this case occurs when we have a transition between the two operating modes: for example when moving from $f_l(t_1) > 0$ to $f_r(t_2) > 0$, with $t_1 < t_2$, because of the continuity of f_l and f_r and the constraints (B3) and (B4), we surely have an instant $t_1 < t^* < t_2$, or a neighbourhood of it, where $f_l(t^*) = f_r(t^*) = 0$ and this is where the discontinuity occurs.

Also having the best controller in this interval, it cannot exceed the maximum velocity moving from the last position before entering in the phase where both forces are 0, for example at time t_1 , to the first position where one of the forces is newly greater than 0, for example at time t_2 . So there must enough time between these two instants, $\Delta t = t_2 - t_1$, to allow to move between this two points. Therefore, in order to make the kinematic law feasible, it is a necessary condition that when we have the greater distance between $x_a(t_1)$ and $x_a(t_2)$, the mean velocity stays below $V_{a,max}$: this imposes a lower bound Δt_{min}^v to the temporal interval between the falling of one input force and the rising of the other (if the falling one and the rising one are the same, the maximum distance between the two points is lower, so the minimum temporal interval could be smaller).

So we have:

$$\Delta t_{min}^v = \frac{2(X_{l,max} + X_{r,max})}{V_{a,max}} \quad (3.6)$$

If we also consider the constraint on the acceleration (c), this controller cannot exceed the maximum acceleration too. So there is another necessary condition, the one that when we have the greater difference between $\dot{x}_a(t_1)$ and $\dot{x}_a(t_2)$, the mean acceleration stays below $A_{a,max}$ and this therefore imposes another lower bound Δt_{min}^a to the temporal interval between the starting and the ending of the phase with both the forces at 0.

So we have:

$$\Delta t_{min}^a = \frac{2V_{a,max}}{A_{a,max}} \quad (3.7)$$

3.3.2 Angular model

The statement of the angular version of the problem to which the model is addressed, is as follows:

Problem 2 (Angular version). Given $\theta_l(t)$ and $\theta_r(t)$ respectively the left and the right joint positions at time $t > 0$ such that:

$$(A1) \quad -\beta_l \leq \theta_l(t) \leq \alpha_l \quad \forall t > 0;$$

$$(A2) \quad -\beta_r \leq \theta_r(t) \leq \alpha_r \quad \forall t > 0.$$

Given $\tau_l(t)$ and $\tau_r(t)$ the reference torques to be applied to the left and the right joints such that:

$$(B1) \quad 0 \leq \tau_l(t) \leq T_{l,max} \quad \forall t > 0;$$

$$(B2) \quad 0 \leq \tau_r(t) \leq T_{r,max} \quad \forall t > 0;$$

$$(B3) \quad \tau_l(t) > 0 \Rightarrow \tau_r(t) = 0 \quad \forall t > 0;$$

$$(B4) \quad \tau_r(t) > 0 \Rightarrow \tau_l(t) = 0 \quad \forall t > 0.$$

In addition to these constraints, the application context allows three other assumptions:

$$(B4) \quad \tau_l(t) > 0 \Rightarrow \theta_r(t) > 0 \quad \forall t > 0;$$

$$(B5) \quad \tau_r(t) > 0 \Rightarrow \theta_l(t) > 0 \quad \forall t > 0;$$

$$(B6) \quad \tau_l(t) = 0 \text{ and } \tau_r(t) = 0 \Rightarrow \theta_l(t)R_l + \theta_r(t)R_r \geq 0 \quad \forall t > 0.$$

Given the fixed points O_l , O_r and O_a , respectively the centre of rotation of the left, the right joint and the actuator, we must determine:

(C1) The model parameters:

- K_l and K_r the linear spring constants of the left and the right elastic band, respectively connecting the actuator to the left and the right joint's pulleys;
- $L_{0,l}$ and $L_{0,r}$ the resting length of the left and the right elastic band.

(C2) A feasible kinematic law, i.e. a function $\theta_a(t)$ describing the desired position of the actuator at time $t > 0$ so that the model exactly applies the reference torques $\tau_l(t)$ and $\tau_r(t)$ to the joints.

There are also other three independent parameters, R_l , R_r and R_a that are the lengths of the radii of the pulleys of the left joint, the right joint and the actuator. Their values can be freely chosen independently from the other parameters, although some choices are better with respect to a real implementation.

In the following, we also consider that the distances between O_l and O_a , called D_l , and between O_r and O_a , called D_r , are constant.

For this formulation of the problem, we did not consider the so called “feasibility constrains”, because the analogous angular formulation of these constraints are more difficult to be analysed than the linear ones. On the other hand, a constraint like $|\theta_a(t)| \leq \Theta_{a,max} \quad \forall t > 0$ does not make sense for an angular actuator. The angular versions of the other constraints would be analysed in further developments of the model.

Model parameters (C1)

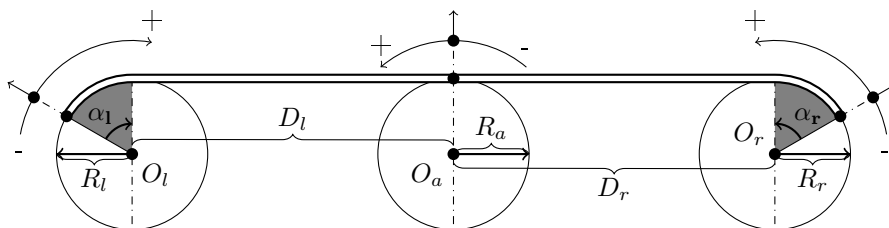


Figure 3.2: The angular model

In figure 3.2 we can see the schematic description of the angular model. The state depicted in the figure represents the 0 coordinate for all the three angular reference system, for the left joint, the right joint and the actuator, and their orientation is indicated by the curved arrows at the top of the figure. The two elastic bands, represented with a line with this style ==, are fixed on the pulleys in correspondence of the nodes represented in this way \bullet and in the picture they are both in resting position.

The design principle of this model is similar to the one of the linear version. Accordingly to conditions (B3) and (B4), we have two operating modes:

- if $\tau_l(t) > 0$ then $\theta_a(t) \leq 0$;
- if $\tau_r(t) > 0$ then $\theta_a(t) \geq 0$.

Considering for an instant the application context of this actuator, the actuation of the hip joints of an exoskeleton, the choice of the reference systems for the joints is straightforward. If we imagine to put the actuator on the back of the user at the hips level, the two side pulleys rigidly connected to the hip joints and an inextensible guide for the elastic bands connecting the actuator to the two joints, then this choice allows to indicate with the value, for example, of $\theta_l(t)$, both the pulley rotation and the angle of the left hip, as commonly measured by physician. This is the angle between the leg and the vertical axis, positive for the flexion and negative for the extension.

In order to determine the resting length of the two elastic bands and their insertion points on the joints' pulleys, we must ensure that, whatever the position of the two joints is, the elastic force that we apply is entirely used as torque. This happens when the force is orthogonal to the radius. So if we advance the insertion point of the elastic bands of an angle of α_l (or α_r), that is the maximum positive displacement, in the worst case the insertion point of the elastic band is at the top of pulley, and also in this position the force is orthogonal to the radius. Now we have to consider the linear distance between the top of the pulley of the actuator and the same point of the pulley of the left or right joint: if $R_l = R_a$ this distance for the left side is exactly D_l , otherwise it is $D_l^* = \sqrt{D_l^2 + (R_l - R_a)^2}$; for the right side, instead, it is $D_r^* = \sqrt{D_r^2 + (R_r - R_a)^2}$.

We would also have to ensure that when we have the maximum distance between the insertion of the elastic band on the actuator pulley and the insertion of the elastic band on the pulley of the joint not currently controlled, the elastic band for that joint is loose. Ignoring for a moment the assumptions (B4) and (B5), this occurs for the left joint when $\theta_a(t) = 0$ and $\theta_l(t) = -\beta_l$, so the left elastic band resting length would have to be $D_l^* + (\alpha_l + \beta_l)R_l$ and for the right elastic band the resting length would have to be $D_r^* + (\alpha_r + \beta_r)R_r$.

Nevertheless, this configuration has a problem, because in the transition between the two operating modes we could have an high angular displacement for the actuator. For example consider this situation: the starting state is $\theta_l(t_1) = 0$ and $\tau_l(t_1) > 0$, so $\theta_a(t_1) < \beta_l \frac{R_l}{R_a}$ and the final state is $\theta_r(t_2) = 0$ and $\tau_r(t_2) > 0$, so $\theta_a(t_2) > \beta_r \frac{R_r}{R_a}$. In the transition between t_1 and t_2 , the actuator has to move for at least $\frac{\beta_l R_l + \beta_r R_r}{R_a}$ degrees.

Therefore, we choose to use some informations from the application context, that are represented by assumptions (B4) and (B5). So the case for which we have the maximum distance between the actuator and the joint not currently controlled, is when $\theta_a(t) = 0$ and the joints coordinates are 0:

$$L_{0,l} = D_l^* + \alpha_l R_l \quad (3.8a)$$

$$L_{0,r} = D_r^* + \alpha_r R_r \quad (3.8b)$$

The values for the linear spring constants are not uniquely determined and having no constraint about the angular position of the actuator (as instead we had for the linear model), they have no model constraints too.

Kinematic law (C2)

In order to use this actuator, we must define a kinematic law $\theta_a(t)$ that, given the joint trajectories $\theta_l(t)$ and $\theta_r(t)$, and the desired torques $\tau_l(t)$ and $\tau_r(t)$, says the angular position of the actuator. The input functions must respect the conditions stated in the problem 2.

The kinematic law can be expressed as:

$$\theta_a(t) := \begin{cases} -\frac{\tau_l(t) + K_l R_l^2 \theta_l(t)}{K_l R_l R_a}, & \text{if } \tau_l(t) > 0 \\ \frac{\tau_r(t) + K_r R_r^2 \theta_r(t)}{K_r R_r R_a}, & \text{if } \tau_r(t) > 0 \\ \frac{\theta_r(t) R_r - \theta_l(t) R_l}{2R_a}, & \text{if } \tau_l(t) = 0 \text{ and } \tau_r(t) = 0 \end{cases} \quad (3.9)$$

The correctness of this kinematic law is showed in the following, by demonstrating this theorem:

Theorem 2 (Angular kinematic law). *Given the model depicted in figure 3.2 with the parameter assignment of equation 3.8, the joint positions $\theta_l(t)$ and $\theta_r(t)$ respecting the assumptions (A1) and (A2) of problem 2 and the reference torques $\tau_l(t)$ and $\tau_r(t)$ respecting the assumptions (B1), (B2), (B3), (B4), (B4), (B5) and (B6), if the trajectory of the single actuator $\theta_a(t)$ is the one defined in 3.9 then the model applies exactly the reference torques $\tau_l(t)$ and $\tau_r(t)$ to the left and the right joint respectively.*

Proof. Case $\tau_l(t) > 0$: the length of the left elastic band is $D_l^* + (\alpha_l - \theta_l(t))R_l - \theta_a(t)R_a$. Substituting $\theta_a(t)$ and $L_{0,l}$:

$$\begin{aligned} D_l^* + \alpha_l R_l - \theta_l(t) R_l + \frac{\tau_l(t) + K_l R_l^2 \theta_l(t)}{K_l R_l} \\ = D_l^* + \alpha_l R_l + \frac{\tau_l(t)}{K_l R_l} \\ = L_{0,l} + \frac{\tau_l(t)}{K_l R_l} \end{aligned}$$

So the elastic band applies a force of intensity $\frac{\tau_l(t)}{R_l}$ to the left joint and given that it is orthogonal to the radius of the pulley, we have a torque of the required intensity $\frac{\tau_l(t)}{R_l} R_l = \tau_l(t)$. Instead, the length of right elastic band is $D_r^* + (\alpha_r - \theta_r(t))R_r + \theta_a(t)R_a$. Substituting $\theta_a(t)$, using the constraints (B4) and (B5) in order to have 0 as upper bound for $-\theta_l(t)$ and $-\theta_r(t)$, substituting $L_{0,r}$ and knowing that $\frac{\tau_l(t)}{K_l R_l}$ is positive:

$$\begin{aligned} D_r^* + \alpha_r R_r - \theta_r(t) R_r - \frac{\tau_l(t) + K_l R_l^2 \theta_l(t)}{K_l R_l} \leq D_r^* + \alpha_r R_r - \frac{\tau_l(t)}{K_l R_l} \\ = L_{0,r} - \frac{\tau_l(t)}{K_l R_l} < L_{0,r} \end{aligned}$$

So the elastic band is loose and it applies no force to the right joint.

Case $\tau_r(\mathbf{t}) > \mathbf{0}$: it is similar to the previous case, the length of the right elastic band is $D_r^* + (\alpha_r - \theta_r(t))R_r + \theta_a(t)R_a$. Substituting $\theta_a(t)$ and $L_{0,r}$:

$$\begin{aligned} & D_r^* + \alpha_r R_r - \theta_r R_r + \frac{\tau_r(t) + K_r R_r^2 \theta_r(t)}{K_r R_r} \\ &= D_r^* + \alpha_r R_r + \frac{\tau_r(t)}{K_r R_r} \\ &= L_{0,r} + \frac{\tau_r(t)}{K_r R_r} \end{aligned}$$

So the elastic band applies a force of intensity $\frac{\tau_r(t)}{R_r}$ to the right joint and given that it is orthogonal to the radius of the pulley, we have a torque of the required intensity $\frac{\tau_r(t)}{R_r} R_r = \tau_r(t)$. On the other hand, the length of the left elastic band $D_l^* + (\alpha_l - \theta_l(t))R_l - \theta_a(t)R_a$ and, in analogous manner of the previous case, we can conclude that it less then the resting length $L_{0,r}$, so it is loose and it applies no force to the left joint.

Case $\tau_l(\mathbf{t}) = \mathbf{0}$ and $\tau_r(\mathbf{t}) = \mathbf{0}$: in this case we choose to leave the actuator in the average position of the two bounds, although this could not be the best choice; every position within the interval $\left[-\theta_l(t)\frac{R_l}{R_a}, \theta_r(t)\frac{R_r}{R_a}\right]$ is an available solution. The elastic bands are both loose and the proof uses the constraint (B6).

Consider $\hat{\theta}_a \in \left[-\theta_l(t)\frac{R_l}{R_a}, \theta_r(t)\frac{R_r}{R_a}\right]$; the length of the left elastic band is:

$$L_l^{\hat{\theta}_a} = D_l^* + (\alpha_l - \theta_l(t))R_l - \hat{\theta}_a R_a$$

and the length of the right elastic band is:

$$L_r^{\hat{\theta}_a} = D_r^* + (\alpha_r - \theta_r(t))R_r + \hat{\theta}_a R_a$$

The left elastic band has the maximum length when $\hat{\theta}_a = -\theta_l(t)\frac{R_l}{R_a} = \hat{\theta}_{a,min}$, so:

$$L_l^{\hat{\theta}_{a,min}} = D_l^* + \alpha_l R_l - \theta_l(t)R_l + \theta_l R_a = L_{0,l}$$

and it is loose; when this occurs the length of the right elastic band is:

$$L_r^{\hat{\theta}_{a,min}} = D_r^* + \alpha_r R_r - (\theta_r(t)R_r + \theta_l(t)R_l) \leq L_{0,r}$$

where in the last step we used the constraint (B6) to obtain 0 as lower bound for $\theta_r(t)R_r + \theta_l(t)R_l$, so we can conclude that also the right elastic band is loose.

Conversely, the right elastic band has the maximum length when $\hat{\theta}_a = \theta_r(t)\frac{R_r}{R_a} = \hat{\theta}_{a,max}$ and proceeding in a manner similar to before we can conclude that it is loose and, using the constraint (B6), that also the left elastic band is loose. \square

Implementation advices

This paragraph will present some advices about the choice of the independent parameters K_l and K_r and the radii of the pulleys.

A real implementation of this actuator should take into account that the torques we must generate at the joints are big, with respect to the ones that a motor could generate at the actuator pulley. So it is advisable to put a reduction ratio between the two pulleys, choosing $R_r \gg R_a$ and $R_l \gg R_a$: this will cause the actuator to move faster than the two joints, but this should not be an issue because the movement of these is slow with respect to the velocity that a motor could reach.

3.3.3 Differences between *angular* and *linear* models

The models presented in the previous subsections, the *linear* in 3.3.1 and the *angular* in 3.3.2, have some differences that justify the passage from the first to the latter: this subsection makes these differences explicit. The main difference is in the type of the physical quantities used to describe them: the first uses forces and linear motion quantities, the latter torques and angular motion quantities. The other important differences are:

- *Constraints on joints coordinates*: the linear model has symmetrical constraints to both the left and right joints and also on the actuator coordinates; the angular has no constraints at all on the coordinates of the actuator and the constraints on the joints are not required to be symmetrical.
- *Additional constraints on the torque references*: the angular model requires additional constraints on the input reference torque functions, the ones from (B4) to (B6), but this allows to have shorter elastic bands and so less angular distance to traverse when switching between the two operating modes.
- *Unconstrained linear spring constants*: the angular model has no constraints on the linear spring constant of the elastic bands; the linear model has this type of constraints only because of the coordinates constraints on the actuator, that as stated before the angular does not have.
- *Independent model parameters*: the angular model has additional independent parameters such as the radii of the pulleys, that are not present in the linear model.

3.4 Extensions

In this section we analyse the possibility to give some negative torque to the two joints. We started from the assumption that when we have to apply positive torque to a joint, we probably have to give negative torque to the other. So we developed a model that could work if we have some kind of symmetry in the movements and in the reference torque of the two joints. It is not as mathematically founded or analysed as the previous two models, but it could be developed further in future works.

The statement of the extended angular version of the problem, is as follows:

Problem 3 (Extended angular version). Given $\theta_l(t)$ and $\theta_r(t)$ respectively the left and the right joint positions at time $t > 0$ such that:

$$(A1) \quad -\beta_l \leq \theta_l(t) \leq \alpha_l \quad \forall t > 0;$$

$$(A2) \quad -\beta_r \leq \theta_r(t) \leq \alpha_r \quad \forall t > 0.$$

Given $\tau_l(t)$ and $\tau_r(t)$ the reference torques to be applied to the left and the right joints such that:

$$(B1) \quad T_{l,min} \leq \tau_l(t) \leq T_{l,max} \quad \forall t > 0;$$

$$(B2) \quad T_{r,min} \leq \tau_r(t) \leq T_{r,max} \quad \forall t > 0;$$

$$(B3) \quad \tau_l(t) > 0 \Leftrightarrow \tau_r(t) < 0 \quad \forall t > 0;$$

$$(B4) \quad \tau_r(t) > 0 \Leftrightarrow \tau_l(t) < 0 \quad \forall t > 0.$$

Given the fixed points O_l , O_r and O_a , respectively the centre of rotation of the left, the right joint and the actuator, we must determine:

(C1) The model parameters:

- K_l and K_r the linear spring constants of the *upper* left and right elastic band, respectively connecting the actuator to the left and the right joint's pulleys;
- K_l^I and K_r^I the linear spring constants of the *lower* left and right elastic band, respectively connecting the actuator to the left and the right joint's lower pulleys;
- $L_{0,l}$ and $L_{0,r}$ the resting length of the *upper* left and right elastic band.
- $L_{0,l}^I$ and $L_{0,r}^I$ the resting length of the *lower* left and right elastic band.

(C2) A feasible kinematic law, i.e. a function $\theta_a(t)$ describing the desired position of the actuator at time $t > 0$ so that the model exactly applies the reference torques $\tau_l(t)$ and $\tau_r(t)$ to the joints.

We did not consider assumptions from the application context, as we did for the angular version (problem 2), because we will not demonstrate the formal correctness of the kinematic law. Nevertheless, we suppose that it is useful to make these assumptions when applying positive torques:

$$(B5) \quad \tau_l(t) > 0 \Rightarrow \theta_r(t) > 0 \quad \forall t > 0;$$

$$(B6) \quad \tau_r(t) > 0 \Rightarrow \theta_l(t) > 0 \quad \forall t > 0.$$

And similar assumptions could have been done (or derived) while applying negative torques. But for now this goes out the scope of this work.

There are also other three independent parameters, R_l and R_l^I , R_r and R_r^I and R_a that are the lengths of the radii of the pulleys (for the *upper* and the *lower* elastic band) of the left joint, the right joint and the actuator. Their values can be freely chosen independently from the other parameters, although some choices are better with respect to a real implementation.

In the following, we also consider that the distances between O_l and O_a , called D_l , and between O_r and O_a , called D_r , are constant.

For this formulation of the problem, we did not consider the so called "feasibility constraints", for the same motivations we did not for the angular model (see 3.3.2).

Model parameters (C1)

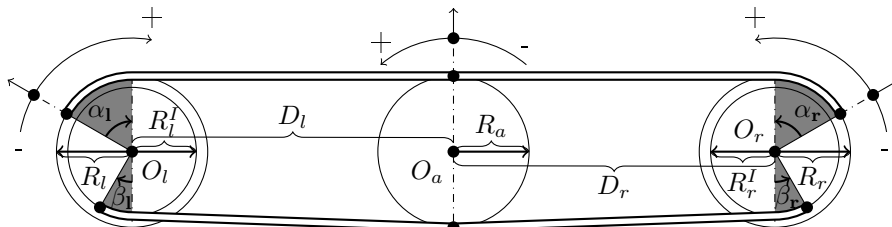


Figure 3.3: The *extended* angular model

In figure 3.3 we can see the schematic description of the *extended* angular model. The state depicted in the figure represents the 0 coordinate for all the three angular reference system, for the left joint, the right joint and the actuator, and their orientation is indicated by the curved arrows at the top of the figure. The four elastic bands (two upper and two lower), represented with a line with this style \equiv , are fixed on the pulleys in correspondence of the nodes represented in this way \bullet and in the picture they are all in resting position.

The design principle of this model is the same as the angular version. Accordingly to conditions (B3) and (B4), we have two operating modes:

- if $\tau_l(t) > 0$ (and $\tau_r(t) < 0$) then $\theta_a(t) \leq 0$;
- if $\tau_r(t) > 0$ (and $\tau_l(t) < 0$) then $\theta_a(t) \geq 0$.

The choice of the reference systems for the joints follows from the application context, as we stated before at page 20.

Below, we explain some important differences with respect to the figure 3.2 representing the model resolving the simple angular version of the problem.

First of all we can see that the extended angular model has an additional pulley for each joint, rigidly connected to the old one but slightly rotated with respect to this and with a possibly different radius: it is addressed to giving negative torque to the joint while the joint of the other side is actuated in order to give positive torque to that joint. The two elastic bands in the lower part of the figure have the same purpose.

The resting length of the two elastic bands that are inherited from the previous angular model and their insertion points are the same for the identical reason, as defined in equation 3.8. So they are:

- $L_{0,l} = D_l^* + \alpha_l R_l$;
- $L_{0,r} = D_r^* + \alpha_r R_r$.

with $D_l^* = \sqrt{D_l^2 + (R_l - R_a)^2}$ and $D_r^* = \sqrt{D_r^2 + (R_r - R_a)^2}$.

In order to determine the resting length of the two *lower* elastic bands and their insertion points on the joints' pulleys, we must ensure that, like for the upper elastic bands, whatever the position of the two joints is, the elastic force that we apply is entirely used as torque. This happens when the force is orthogonal to the radius. So we must advance the insertion point of the elastic bands of an angle of β_l (or β_r), that is the maximum negative displacement. Doing

this in the worst case the insertion point of the elastic band is at the bottom of pulley, and also in this position the force is orthogonal to the radius. Now we have to consider the linear distance between the bottom of the pulley of the actuator and the same point of the pulley of the left or right joint: if $R_l^I = R_a$ this distance for the left side is exactly D_l , otherwise it is $D_l^{I*} = \sqrt{D_l^2 + (R_l^I - R_a)^2}$; for the right side, instead, it is $D_r^{I*} = \sqrt{D_r^2 + (R_r^I - R_a)^2}$.

We chose a resting length for the lower elastic bands such that they are loose when the corresponding upper elastic band is tight. So when $\theta_a(t) = 0$ and the joints coordinates are 0, the distances are:

$$L_{0,l}^I = D_l^{I*} + \beta_l R_l^I \quad (3.10a)$$

$$L_{0,r}^I = D_r^{I*} + \beta_r R_r^I \quad (3.10b)$$

The values for the linear spring constants are not uniquely determined, both the upper and the lower ones, and having also for this version of the problem no constraint about the angular position of the actuator, the linear spring constants have no model constraints too.

Kinematic law (C2)

The kinematic law for this version of the model is substantially the same of the simple angular model, stated in 3.9, taking into account the possibility of negative torque references:

$$\theta_a(t) := \begin{cases} -\frac{\tau_l(t) + K_l R_l^2 \theta_l(t)}{K_l R_l R_a}, & \text{if } \tau_l(t) > 0 \\ \frac{\tau_r(t) + K_r R_r^2 \theta_r(t)}{K_r R_r R_a}, & \text{if } \tau_r(t) > 0 \\ \frac{\theta_r(t) R_r - \theta_l(t) R_l}{2R_a}, & \text{if } \tau_l(t) \leq 0 \text{ and } \tau_r(t) \leq 0 \end{cases} \quad (3.11)$$

The law is targeted to follow the torque profile of the joint to which we have to apply a positive torque, while trying to give some negative torque to the opposite joint. This choice tries to exploit the periodicity and, possibly, the symmetry of the gait movement.

So our attempt is to apply some negative torques while not affecting the positive torques application. Thus, below we will state which are the torques applied by the lower elastic bands, given the actuator position.

For the left side we have that the length of the lower elastic band is $l_l^I(t) = D_l^{I*} + (\beta_l + \theta_l(t))R_l^I + \theta_a(t)R_a$, so the applied torque is $\tau_l^-(t) = -K_l^I(l_l^I(t) - L_{0,l}^I)R_l^I$ when $l_l^I(t) - L_{0,l}^I > 0$, otherwise it is 0. So simplifying we have:

$$\tau_l^-(t) = \begin{cases} -K_l^I(\theta_l(t)R_l^I + \theta_a(t)R_a)R_l^I, & \text{if } \theta_l(t)R_l^I + \theta_a(t)R_a > 0 \\ 0, & \text{otherwise} \end{cases} \quad (3.12)$$

and this is the only torque applied when $\theta_a(t) > 0$, so when $\tau_r(t) > 0$.

For the right side we have that the length of the lower elastic band is $l_r^I(t) = D_r^{I*} + (\beta_r + \theta_r(t))R_r^I - \theta_a(t)R_a$, so the applied torque is $\tau_r^-(t) = -K_r^I(l_r^I(t) -$

$L_{0,r}^I R_r^I$ when $l_r^I(t) - L_{0,r}^I$, otherwise it is 0. So simplifying we have:

$$\tau_r^-(t) = \begin{cases} -K_r^I(\theta_r(t)R_r^I - \theta_a(t)R_a)R_r^I, & \text{if } \theta_r(t)R_r^I - \theta_a(t)R_a > 0 \\ 0, & \text{otherwise} \end{cases} \quad (3.13)$$

and this is the only torque applied when $\theta_a(t) < 0$, so when $\tau_l(t) > 0$.

3.5 Conclusion

This chapter described the models at the basis of the proposed single actuator for the hip joints of an exoskeleton and the objectives that guided its development.

Section 3.2 stated the objectives and the content of the chapter. In section 3.3, there was the description of two models:

- a simplified *linear* version addressed to solve the problem 1, used as starting point to face the issues in an easier context;
- an *angular* version addressed to solve the problem 2, that is the main model used in the simulated implementation.

Section 3.4 described an *extended* angular model, addressed to solve the problem 3. This model tries to overcome the issue that the simpler base angular model can apply only positive torques to the controlled joints.

The objectives that we accomplished in developing these models were to find:

- an assignment for the model parameters that allows to apply the desired torques;
- a feasible kinematic law, i.e. a timed function that describes at each instant the desired position of the single actuator so that the model exactly applies the reference torques.

For the *linear* model the parameter assignment is described in equations 3.3 and the kinematic law is defined in equation 3.4. For the *angular* model the parameter assignment is described in equations 3.8 and the kinematic law is defined in equation 3.9. The parameter assignment for the *extended* angular model for the common parts, i.e. the upper elastic bands, is the same of the *angular* model, while for the other it is defined in equation 3.10. The kinematic law for this last model is substantially the same of the *angular* model and is defined in equation 3.11.

The next chapter will present the validation method of the proposed angular models parameters and kinematic laws.

Validation method

4.1 Introduction

The objective of this chapter is to describe the validation method proposed for the single actuator. The model of the actuator will be implemented within the OPENSIM simulator to be validated with respect to a normal gait task. So there will be a brief presentation of the simulator, its capabilities and the tools that has been used. Then it will be explained the steps accomplished, by means of external MatLab® scripts, and the workflow that has been developed. So the validation will be by means of a simulation.

The chapter is structured as follows: section 4.2 will describe the OPENSIM framework and the tools used in this thesis; section 4.3 will be dedicated to the integration of the exoskeleton in the gait model that has been done to validate the proposed actuator; section 4.4 will be a summary of the workflow used for the simulation. Then there will be the conclusion of this chapter in section 4.5.

4.2 The biomechanical simulator: OPENSIM

This section will present OPENSIM[66], the simulation framework used to validate the *angular* model developed in the previous chapter (see section 3.3). OPENSIM is an open source and extensible project developed at NIH National Center for Physics-Based Simulation of Biological Structures at Stanford University. It is funded by NIH Roadmap grant U54 GM072970, the NIH research infrastructure grant R24 HD065690 and the DARPA Warrior Web Program. The reference article for this project is [17]. It is also supported by the National Center for Simulation in Rehabilitation Research (NCSRR), a National Center

for Medical Rehabilitation Research (NCMRR).¹

OPENSIM is a software platform for modelling biological structures, like humans or animals, and also robots and their environment, simulating their interaction and movement. OPENSIM has a graphical user interface (GUI) for the visualization of the models and generating and analysing simulations. It also includes an application programming interface (API) that can be used by developers to extend the software.

The informations contained in this section are partially taken from the documentation of the 3.x version of the software, available on line at [65].

4.2.1 Framework architecture

The OPENSIM software is a powerful framework that can be used for analysis and simulation of complex dynamic models, such as biological structures. This subsection contains an overview of this software and its capabilities. These are the main functionalities that it has:

- **Create and edit models:** it allows to build models of a variety of musculoskeletal structures and other complex mechanisms. Models can consist of rigid bodies, simple and complex joints, constraints, springs, dampers, contacts, controllers, muscles and other actuators. The GUI allows to load and visualise models and edit their properties. The muscle models are based on well known muscle-tendon dynamics models. There is also a wide library of musculoskeletal models of upper and lower limbs, with different levels of detail.
- **Analyse and simulate models and motions:** there are tools to import and visualise experimental data such as markers, joint kinematics and external forces. Using the *Scale tool* it is possible to create subject-specific instances of the model; there are also fast and robust tools to perform *Inverse Kinematics*, *Inverse Dynamics* and generate a *Forward simulation* of the movement. The *Computed Muscle Control* tool can be used to generate muscle-driven simulations. The *Analysis* and *Probe* tools allow to study virtually any quantity, such as muscle work, center of mass trajectories and others, and the GUI can be used to create plots of these.
- **Customize workflows and extend the software:** the OPENSIM library of models and tool are all available via MatLab® scripting and the GUI itself has scripting capabilities. This allows to set up batch processing routines or to extend the software functionalities. There is also an extensible *Application Programming Interface* (API) that can be used by C++ programs or for writing new plug-ins. Existing functionalities could be combined in new ways and new model components and analysis can be developed. The new plug-ins are then easily accessible through the graphical interface.



Figure 4.1: The OPENSIM logo - Copyright (c) 2009-2012 Stanford University

¹See <http://opensim.stanford.edu/about/index.html> for the NCSRR and <http://ncmrr.org> for the NCMRR.

- **Open source platform:** OPENSIM is free and available to anyone, open to both academic research and commercial applications. Models and simulations developed on the OPENSIM platform can be freely shared, reproduced and used by others. There is a wide community of experts using this software.

Summarizing, OPENSIM gives a library of biomechanical models that can be modified or written from scratch using the available components or user defined ones. Starting from these models it is possible to simulate them, using movements taken by real data or synthesized from control signals, and to analyse their behaviour with the tools made available from the framework. The remaining subsections will describe the tools used in this thesis.

4.2.2 Inverse Kinematics

The *Inverse Kinematics* (IK) Tool allows to map the real sensor data of a movement to the simulated model, in order to perform the required analysis on the motion. It is a fundamental step for many other tools, such as *Inverse Dynamics* (subsection 4.2.3) and *Computed Muscle Control* (subsection 4.2.4).

The tool steps through each time frame of the experimental data and sets the joint coordinates of the model in a pose that “best matches” the experimental marker and coordinate data for that time frame. A “best match” is a pose that minimises a sum of weighted squared errors of markers and/or coordinates. The *marker error* is the distance between an experimental marker and the corresponding marker on the model when its generalized coordinates are the ones computed by the tool. The *coordinate error* is the difference between an experimental coordinate value and the coordinate value computed by the tool; the “experimental coordinate values” can be the joint angles obtained directly from the motion capture system, or from an external specialized algorithm or from other measuring devices, such as a goniometer. It can also be a fixed desired value for a coordinate, for some user’s purpose. Moreover, the tool allows a distinction between *prescribed* and *unprescribed coordinates*: the first are coordinates whose trajectories are known and which do not need to be computed by the tool; the latter, on the other hand, are coordinates whose value is computed using the tool. Each unprescribed coordinate and each marker has an associated weight, specifying how strongly its error should be minimized.

Mathematically, the IK tool solves the weighted least squares problem stated as follows:

$$\min_{\mathbf{q}} \left[\sum_{i \in \{\text{markers}\}} w_i \|\mathbf{x}_i^{\text{exp}} - \mathbf{x}_i(\mathbf{q})\|^2 + \sum_{j \in \{\text{unprescribed coordinates}\}} \omega_j |q_j^{\text{exp}} - q_j|^2 \right] \quad (4.1)$$

having $q_j = q_j^{\text{exp}}$ for each prescribed coordinate j . The tool finds for each time frame the generalized coordinates vector \mathbf{q} that minimizes the cost equation, where $\mathbf{x}_i^{\text{exp}}$ is the experimental position of the marker i , $\mathbf{x}_i(\mathbf{q})$ is the position of the corresponding marker on the model, function of the generalized coordinate values, and q_j^{exp} is the experimental value for the coordinate j . All the prescribed coordinates are set to their experimental values. The marker weights (w_i) and the coordinate weights (ω_j) are specified respectively by the <IKMarkerTask> and <IKCoordinateTask> tags of the XML settings file of the

tool. The least squares problem is then solved using a general quadratic solver, with a convergence criterion of 0.0001 and a limit of 1000 iterations.

For more informations about this tool, visit the *User's Guide* documentation at this link <http://simtk-confluence.stanford.edu:8080/display/OpenSim/Inverse+Dynamics>.

4.2.3 Inverse Dynamics

The *Inverse Dynamics* (ID) Tool determines the generalized forces at each joint responsible for a given movement of the model. Given the kinematics (i.e. states or motion) describing the model's movement and perhaps a portion of the kinetics (i.e. external loads) applied to the model, the ID Tool computes the internal forces (or torques) generated. For a musculoskeletal model these are the forces caused by the muscles. In classical mechanics the relationship between force and acceleration, the 2nd Newton's law $\mathbf{F} = m\mathbf{a}$, is expressed by means of equations of motion. The ID Tool solves these equations to yield the net forces and torques at each joint which produce the movement. As kinematic data can be used the ones generated by the Inverse Kinematics Tool or in other manners.

The classical equations of motion can be expressed in this form:

$$\tau = M(\mathbf{q})\ddot{\mathbf{q}} - \mathbf{G}(\mathbf{q}) - \mathbf{C}(\mathbf{q}, \dot{\mathbf{q}}) - \mathbf{A}(\mathbf{q}, \dot{\mathbf{q}}, \mathbf{x}, t) \quad (4.2)$$

where, for a model with N degrees of freedom, \mathbf{q} , $\dot{\mathbf{q}}$ and $\ddot{\mathbf{q}} \in \mathcal{R}^N$ are the vectors of generalized positions, velocities and accelerations, $M(\mathbf{q}) \in \mathcal{R}^{N \times N}$ is system mass matrix that depends on the model configuration, $\mathbf{C}(\mathbf{q}, \dot{\mathbf{q}}) \in \mathcal{R}^N$ is the vector of Coriolis and centrifugal forces, $\mathbf{G}(\mathbf{q}) \in \mathcal{R}^N$ is the vector of gravitational forces and $\mathbf{A}(\mathbf{q}, \dot{\mathbf{q}}, \mathbf{x}, t) \in \mathcal{R}^N$ is the vector of applied loads, that are the external forces applied to the model, such as the ground reaction, passive bodies or active components and it can explicitly depend on time t and the input controls to the actuators. The resulting generalized forces $\tau \in \mathcal{R}^N$ are what the tool computes.

For more informations about this tool, visit the *User's Guide* documentation at this link <http://simtk-confluence.stanford.edu:8080/display/OpenSim/Inverse+Kinematics>.

4.2.4 Computed Muscle Control

The *Computed Muscle Control* (CMC) Tool has the purpose of computing a set of muscle excitations (or, more generally, actuator controls) that will drive a dynamic musculoskeletal model, trying to track as good as possible a set of desired kinematics in the presence of applied external forces (if any). It uses as input data the ground reaction forces and the output kinematics of the *Residual Reduction Algorithm* (RRA) Tool. This tool has the purpose of minimizing the effects of modelling and marker data processing errors that lead to large non-physical compensatory forces called residuals. Specifically, it alters the torso mass center of a subject-specific model and permits the kinematics of the model to vary from Inverse Kinematics output in order to be more dynamically consistent with the ground reaction force data.

The working principle of the algorithm that lays behind the tool has been described in [50]. At user-specified time intervals during a simulation, the CMC

Tool computes muscle excitation levels that will drive the generalized coordinates of the dynamic musculoskeletal model towards a desired kinematic trajectory. CMC does this by using a combination of proportional-derivative (PD) control and static optimization (see figure 4.2).

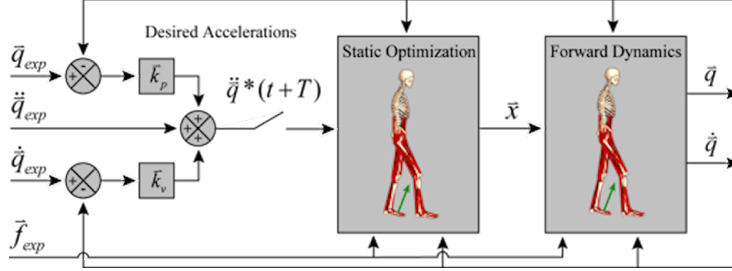


Figure 4.2: Schematic of the Computed Muscle Control Algorithm

Before starting the CMC algorithm, initial states for the model are computed. The states comprise the generalized coordinates, generalized speeds, plus any muscle states (i.e. muscle activation levels and fiber lengths). While the initial values of the generalized coordinates and speeds can be taken from the desired kinematics that you specify, the initial values of the muscle states are generally unknown. To compute viable starting muscle states, CMC is applied to the first 0.030 seconds of the desired movement. Because the muscle states are generally out of equilibrium and muscle forces can change dramatically during this initial time interval, the simulation results during this interval are generally not valid.

The first step in the CMC algorithm is to compute a set of desired accelerations ($\ddot{\mathbf{q}}^*$) which, when achieved, will drive the model coordinates (\mathbf{q}) toward the experimentally-derived coordinates (\mathbf{q}_{exp}). The desired accelerations are computed using the following PD control law:

$$\ddot{\mathbf{q}}^*(t+T) = \ddot{\mathbf{q}}_{exp}(t+T) + \mathbf{k}_v [\dot{\mathbf{q}}_{exp}(t) - \dot{\mathbf{q}}(t)] + \mathbf{k}_p [\mathbf{q}_{exp}(t) - \mathbf{q}(t)] \quad (4.3)$$

where \mathbf{k}_v and \mathbf{k}_p are the feedback gains on the velocity and position errors. Because the forces that muscles apply to the body cannot change instantaneously, the desired accelerations are computed for some small time T in the future. For musculoskeletal models, T is typically chosen to be about 0.010 seconds. This time interval is short enough to allow adequate control, but long enough to allow muscle forces to change. If these desired accelerations are achieved, errors between the model coordinates and experimentally-derived coordinates will be driven to zero. To drive these errors to zero in a critically damped fashion (i.e. without over-shooting or over-damping), the velocity gains can be chosen using the following relation:

$$\mathbf{k}_v = 2\sqrt{\mathbf{k}_p} \quad (4.4)$$

For musculoskeletal models, it works well if the error gains are chosen to drive any errors to zero slowly. The next step in CMC is to compute the actuator controls ($\mathbf{x}(t)$) that will achieve the desired accelerations ($\ddot{\mathbf{q}}^*(t+T)$). Most of the time, the controls are predominantly comprised of muscle excitations, but this is not required. Any kind of actuator can be used with CMC. Static optimization is used to distribute the load across synergistic actuators. It is

called “static” optimization because the performance criterion must be confined to quantities that can be computed at any instant in time during a simulation. Two formulations of the static optimization problem are currently available in CMC. The first formulation, called *the slow target*, consists of a performance criterion (J) that is a weighted sum of squared actuator controls plus the sum of desired acceleration errors:

$$J = \sum_{i=1}^{n_x} x_i^2 + \sum_{j=1}^{n_q} w_j (\ddot{q}_j^* - \ddot{q}_j)^2 \quad (4.5)$$

The first summation minimizes and distributes loads across actuators and the second drives the model accelerations (\ddot{q}_j) toward the desired accelerations (\ddot{q}_j^*). The second formulation, called *the fast target*, is the sum of squared controls augmented by a set of equality constraints ($C_j = 0$) that requires the desired accelerations to be achieved within the tolerance set for the optimizer:

$$J = \sum_{i=1}^{n_x} x_i^2; \quad \forall j \in \{1, \dots, n_q\} C_j = \ddot{q}_j^* - \ddot{q}_j \quad (4.6)$$

The fast target is both faster and generally produces better tracking. However, if the constraints cannot be met, the fast target will fail and CMC will exit with an error message. Often the reason for the failure is that the musculoskeletal model is not strong enough. The final step in the CMC algorithm is to use the computed controls to conduct a standard forward dynamic simulation, advancing forward in time by T . These steps, computing the desired accelerations, static optimization, and forward dynamic simulation, are repeated until time is advanced to the end of the desired movement interval.

If desired, constraints can be placed on the upper and lower bounds of the controls $\mathbf{x}(t)$ as a function of simulation time: this could be useful, for example, to make the computed muscle excitation patterns similar to prototypical ones or the electromyographical measurements. The bounds on the controls $\mathbf{x}(t)$ are specified in an XML input file. For muscle excitations, the default upper bound is typically 1.0 (full excitation), and the default lower bound is typically a small number just above 0.0 (no excitation), such as 0.01 or 0.02. The lower bound is not set at precisely 0.0 because mathematical models of muscle are often not as well-behaved when excitation goes all the way to 0.0.

For more informations about this tool, visit the *User’s Guide* documentation at this link <http://simtk-confluence.stanford.edu:8080/display/OpenSim/Computed+Muscle+Control>.

4.3 Implementation and integration of the actuator model

This section explains the steps that has been accomplished in order to implement and integrate the actuator model explained in chapter 3 into an OPENSIM model of the lower limb, simulating a normal gait movement. The integration had to overcome the limitations of the simulator: we cannot have at the same time a forward simulation of the gait with the exoskeleton controller enabled, to see the resulting movement and an inverse simulation to see the values of the generated

4.3. IMPLEMENTATION AND INTEGRATION OF THE ACTUATOR MODEL³⁵

internal forces. Indeed, the controller of the exoskeleton needs to know at the same time the model configuration, result of the forward simulation, *and* the reference torques, results of the inverse dynamics. So the solution that has been found is to firstly perform the inverse dynamics on the normal model, without the exoskeleton, in order to obtain the reference torques and then call another time the inverse dynamics tool with the exoskeleton controller enabled. The simulated exoskeleton, applying to the model external forces that the tool will take into account, will change the internal forces profile.

4.3.1 OPENSIM model

The OPENSIM model used for the simulation is the *Gait2354*², a three dimensional model of the human musculoskeletal system, with 23 degrees of freedom and 54 muscolotendon actuators representing 76 muscles in the human lower extremities and torso. This model derives from the *Gait2392* by reducing the number of muscolotendon actuators to improve the simulation speed. The models, with the addition of experimental data, were developed by Darryl Thelen (University of Wisconsin-Madison) and Ajay Seth, Frank C. Anderson, and Scott L. Delp (Stanford University) and are available in the standard OPENSIM model distribution.

For this thesis, the *Gait2354* has been modified by adding two torque actuators to the hip joints, that apply their torque on the transverse axis. These are model components of type `OpenSim::TorqueActuator`, that apply a torque to the given axis of an intensity equal to the command value. Then adding a new custom controller for these two actuators, written in C++ and named `ExoController`, they can be used to simulate the behaviour of the proposed single actuator. This controller reads from a given file the desired angle positions of the single actuator over the time, i.e. the $\theta_a(t)$ function of the angular (section 3.3.2) or the *extended* angular model (section 3.4). Then, knowing the hip joints' coordinates, it computes the command to give to the torque actuators accordingly to the model, as if there were the elastic bands.

4.3.2 Command computation

The computation of the angle command $\theta_a(t)$ that controls the `ExoController`, is done externally to the simulator. It has been used a set of MatLab® scripts that:

- gather the torques needed for the flexion of the hips from the results of the Inverse Dynamics Tool, executed on the normal model;
- gather the angles of the hip joints from the results of the Inverse Kinematics Tool;
- compute for each time frame the desired position command of the actuator;
- write out on a file the computed position commands, in such a way that can be used by the modified model controller.

²A detailed documentation of this model can be found at: <http://simtk-confluence.stanford.edu:8080/display/OpenSim/Gait+2392+and+2354+Models>.

The torques computed by the Inverse Dynamics cannot be directly used as reference for the actuator because they are both negative and positive. Moreover, they must be reduced to make the actuator giving only a portion of the torques required for the movement, because it may be useful to leave some work to be done by the user. Indeed, the active role of patients is essential for improving rehabilitation [55]. Choosing a reduction ratio p^{red} and having $\tau_l^m(t)$ and $\tau_r^m(t)$ the “experimental” torque profiles obtained from the ID (the ones generated by the muscles without the exoskeleton), the references for the actuator are computed as follows:

$$\tau_l(t) := \begin{cases} p^{red}\tau_l^m(t), & \text{if } \tau_l^m(t) > \tau_r^m(t) \text{ and } \tau_l^m(t) > T_{min} \\ 0, & \text{otherwise} \end{cases} \quad (4.7a)$$

$$\tau_r(t) := \begin{cases} p^{red}\tau_r^m(t), & \text{if } \tau_r^m(t) > \tau_l^m(t) \text{ and } \tau_r^m(t) > T_{min} \\ 0, & \text{otherwise} \end{cases} \quad (4.7b)$$

In the equations there is also the T_{min} parameter that is a minimum threshold for the application of the command. The resulting torques $\tau_l(t)$ and $\tau_r(t)$ are used as input for the model control law and they respect all the assumptions (B1), (B2), (B3) and (B4) of the problem 2.

Then there is a script that computes the actuator angles $\theta_a(t)$, using the control law described in the section 3.3.2, and also the corresponding applied torques. These values are stored to a text file with a line for each time frame containing four values: simulation time t , $\theta_a(t)$, the left and the right applied torques.

The applied torques, given the actuator angles, are computed as follows:

$$\tau_l^+(t) = \begin{cases} K_l(-\theta_l(t)R_l - \theta_a(t)R_a)R_l, & \text{if } -\theta_l(t)R_l - \theta_a(t)R_a > 0 \\ 0, & \text{otherwise} \end{cases} \quad (4.8a)$$

$$\tau_r^+(t) = \begin{cases} K_r(-\theta_r(t)R_r + \theta_a(t)R_a)R_r, & \text{if } -\theta_r(t)R_r + \theta_a(t)R_a > 0 \\ 0, & \text{otherwise} \end{cases} \quad (4.8b)$$

4.3.3 Extensions

The MatLab® scripts and the `ExoController` implement also the *extended* angular model (section 3.4). It can be enabled by changing from 0 to a positive number both the linear spring constant of the lower elastic bands. The actual version of the code for the computation of the command angle is the same for both the implemented models. The code that changes is the one that computes the applied torques, taking into account that some of the context assumptions could not be satisfied in every time frame. Recalling the equations for the torques applied by the lower elastic bands, 3.12 for the left side and 3.13 for the right side, the total torques applied to the two joints are:

$$\tau_l^{act}(t) = \tau_l^+(t) + \tau_l^-(t) \quad (4.9a)$$

$$\tau_r^{act}(t) = \tau_r^+(t) + \tau_r^-(t) \quad (4.9b)$$

where τ_l^+ and τ_r^+ are the torques applied by the upper elastic bands as defined in 4.8. The superscript *act* stands for *actuator*.

4.4 Simulation workflow

This subsection resumes the simulation workflow that has been developed to integrate the proposed actuator into an OPENSIM simulation. These are the main steps:

1. perform the *Inverse Kinematics* Tool on the model *Gait2354* of the lower limbs with the desired experimental marker data;
2. perform the *Inverse Dynamics* Tool on the normal model with the motion generated by the IK;
3. calculate the actuator angle commands $\theta_a(t)$ using the developed MatLab® scripts;
4. perform the *Inverse Dynamics* Tool on the model with the addition of the *ExoController* activated by the commands computed in the previous step;
5. compare the results of the two executions of the *Inverse Dynamics* Tool to evaluate the effectiveness of the exoskeleton.

The first step can be omitted if we already have the motion data.

4.5 Conclusion

This chapter presented the validation method that has been adopted for the proposed actuator. It consists of an integration of the actuator within a musculoskeletal OPENSIM model of the human lower limbs. The integration modifies the model *Gait2354*, adding two torque actuators components and a specific controller for them to emulate the behaviour of the single actuator model. Then it uses a set of MatLab® scripts to compute the actuator angles knowing the torques required for the desired movement. Section 4.2 described the OPENSIM framework; section 4.3 described the integration and section 4.4 summarized the workflow developed. The next chapter will collect the results of the validation in a specific test case.

Results

5.1 Introduction

This chapter will present the validation results of the proposed actuation method. The following will use the methods described in the previous chapter and will consider specific test cases and relative interesting measurements.

The chapter is organised as follows: section 5.2 will describe the test cases and how they have been evaluated; section 5.3 will contain the simulation results. In section 5.4 the results will be discussed and in section 5.5 there will be the conclusion of the chapter.

5.2 Test cases evaluation

The validation of the model presented in chapter 3 will be done by means of a simulation of the exoskeleton coupled with a model of the human lower limbs, *Gait2354* model within the OPENSIM framework. The implementation and the integration between the actuator model and the simulator has been described in section 4.3 of the previous chapter. Briefly, the movement data are firstly used to compute the inverse dynamics without the exoskeleton, to gain the reference “normal” toques; then, the simulation is run with the active exoskeleton and the new inverse dynamics results are compared to the ones of the previous simulation. The movement data come from the study described in the article of Chand et al. [29], and they are available within the model distribution.

The outcome of the simulation experiments has been evaluated in term of:

- the root mean square error between the torques applied by the single actuator and the reference torques, respectively for the left and the right side;

- the ratio between the energy generated by the muscles with the exoskeleton and without, considering only the instants where the exoskeleton was giving torque to that side;
- the power generated by the muscles with the exoskeleton and without.

In the validation process some parameters have been varied, in particular we considered:

- the reduction ratio of the reference torques;
- the smoothing of the actuator angle;
- extended version of the model enabled, with different radii of the pulley.

For simplicity the radii of the pulleys for the upper elastic and the linear spring constants have not been modified.

5.2.1 Evaluation method

This subsection will describe in detail the evaluation measurements. In the following, $\tau_l(k)$ and $\tau_r(k)$ are the reference torques (obtained by the reduction defined in equations 4.7), $\tau_l^{act}(k)$ and $\tau_r^{act}(k)$ are the torques applied by the actuator (the superscript *act* stands for *actuator*), $\tau_l^m(k)$ and $\tau_r^m(k)$ are the torques generated by the muscles without the exoskeleton and $\tau_l^{me}(k)$ and $\tau_r^{me}(k)$ are the torques generated with the exoskeleton (the superscript *m* stands for *muscles* and *me* for *muscles with exoskeleton*). Moreover, it has been defined a function that states if the actuator is giving force to the left joint, to the right or neither, called $s(k)$:

$$s(k) := \begin{cases} 1, & \text{if } \tau_r(k) > 0 \\ -1, & \text{if } \tau_l(k) > 0 \\ 0, & \text{otherwise} \end{cases} \quad (5.1)$$

These are all discrete functions at a sampling rate of $60Hz$. The number of samples is N .

The root mean square errors are computed as follows:

$$RMS_l = \sqrt{\frac{\sum_{k=1}^N [\tau_l(k) - \tau_l^{act}(k)]^2}{N}} \quad (5.2a)$$

$$RMS_r = \sqrt{\frac{\sum_{k=1}^N [\tau_r(k) - \tau_r^{act}(k)]^2}{N}} \quad (5.2b)$$

The energy generated by the muscles with the exoskeleton is computed as fol-

lows:

$$E_l^+ = \sum_{\substack{i \in \{k \mid s(k)=-1\} \\ 1 \leq i \leq N-1}} |\tau_l^{me}(i)(\theta_l(i+1) - \theta_l(i))| \quad (5.3a)$$

$$E_l^- = \sum_{\substack{i \in \{k \mid s(k)=1\} \\ 1 \leq i \leq N-1}} |\tau_l^{me}(i)(\theta_l(i+1) - \theta_l(i))| \quad (5.3b)$$

$$E_r^+ = \sum_{\substack{i \in \{k \mid s(k)=1\} \\ 1 \leq i \leq N-1}} |\tau_r^{me}(i)(\theta_r(i+1) - \theta_r(i))| \quad (5.3c)$$

$$E_r^- = \sum_{\substack{i \in \{k \mid s(k)=-1\} \\ 1 \leq i \leq N-1}} |\tau_r^{me}(i)(\theta_r(i+1) - \theta_r(i))| \quad (5.3d)$$

The energy generated by the muscles without the exoskeleton is computed in the same way, except that $\tau_l^{me}(k)$ and $\tau_r^{me}(k)$ are substituted respectively by $\tau_l^m(k)$ and $\tau_r^m(k)$. The values obtained are called $E_l^{+,m}$, $E_l^{-,m}$, $E_r^{+,m}$ and $E_r^{-,m}$. The effectiveness of the solution is then evaluated for the positive torques with $\eta_l^+ = \frac{E_l^+}{E_l^{+,m}}$ and $\eta_r^+ = \frac{E_r^+}{E_r^{+,m}}$, and for the negative torques with $\eta_l^- = \frac{E_l^-}{E_l^{-,m}}$ and $\eta_r^- = \frac{E_r^-}{E_r^{-,m}}$. This definition of effectiveness is such that an higher value means a less effective result, because we have more energy consumed.

The powers generated by the muscles is then computed as follows:

$$P_l(k) = \tau_l^{me}(k)\omega_l(k), \quad P_r(k) = \tau_r^{me}(k)\omega_r(k) \quad (5.4a)$$

$$P_l^m(k) = \tau_l^m(k)\omega_l(k), \quad P_r^m(k) = \tau_r^m(k)\omega_r(k) \quad (5.4b)$$

where $\omega_l(k) = \frac{\theta_l(k+1) - \theta_l(k-1)}{t_{k+1} - t_{k-1}}$ and $\omega_r(k) = \frac{\theta_r(k+1) - \theta_r(k-1)}{t_{k+1} - t_{k-1}}$ are approximations of the angular velocities of the joints.

We also evaluated the possibility of smoothing the desired actuator position before applying them to the single actuator: this has the purpose of having a smoother transition from a operation mode to the other, so the its parameter is choose in such a way that it only smooth the major discontinuities, while minimally affecting the command elsewhere.

5.3 Simulation results

This section is devoted to report the results of the simulations that have been performed. We only validated two of the models proposed in chapter 3: in subsection 5.3.1 there are the validation results of the base *angular* model (described in section 3.3.2); in subsection 5.3.2 there are the validation results of the *extended* angular model (described in section 3.4).

5.3.1 The *angular* model

This subsection will present the results of the simulations with the base *angular* model. The table 5.1 describes the configuration of the considered test cases. The parameters taken into account are the reduction factor of the input torques, i.e. how much the exoskeleton must help the walking, and if the actuator angles

have been smoothed before giving them to the **ExoController**. The smoothing is performed by using a MatLab® smoothing spline with the parameter $p = 0.9999$.

In every test case the actuator parameters are set as follows:

- K_l and K_r were set to 40 N/m;
- R_a , R_l and R_r were all set al to 1 m.

| | Reduction factor | Smoothed |
|--------|------------------|----------|
| Case 1 | 0.3 | ✗ |
| Case 2 | 0.3 | ✓ |
| Case 3 | 0.5 | ✗ |
| Case 4 | 0.5 | ✓ |
| Case 5 | 0.8 | ✗ |
| Case 6 | 0.8 | ✓ |

Table 5.1: Test cases configurations of the *angular* model validation

For each test case we present four graphs:

- *Actuator angle command*: this graph contains the angles of the left joint (blue), the right joint (red) and the angle command to the single actuator (green). There is also the plot of the status function ($s(k)$).
- *Applied torques*: this graph contains the torques applied to the left (blue dash-dotted) and the right joint (red dash-dotted) and the target torques $p^{red}\tau_l^m$ and $p^{red}\tau_r^m$, for the left (blue dashed) and the right side (red dashed). Note that when $s(k) \neq 1$ the reference torque for the right joint is 0, while when $s(k) \neq -1$ the reference torque for the left joint is 0.
- *Inverse dynamics results*: this graph contains the results of the ID applied to the model without the exoskeleton (dashed line) and applied to the model *with* the exoskeleton (solid line).
- *Generated power (positive torque)*: this graph is meaningful for the evaluation of the effectiveness of the solution. It contains the bar plot of the functions $P_l(k)$ and $P_l^m(k)$ (blue) when the status is $s(k) = -1$, active exoskeleton on the left side, and $P_r(k)$ and P_r^m (red) when the status is $s(k) = 1$, active exoskeleton on the right side.

Case 1: the graphs are in the figures 5.1 and 5.2.

Case 2: the graphs are in the figures 5.3 and 5.4.

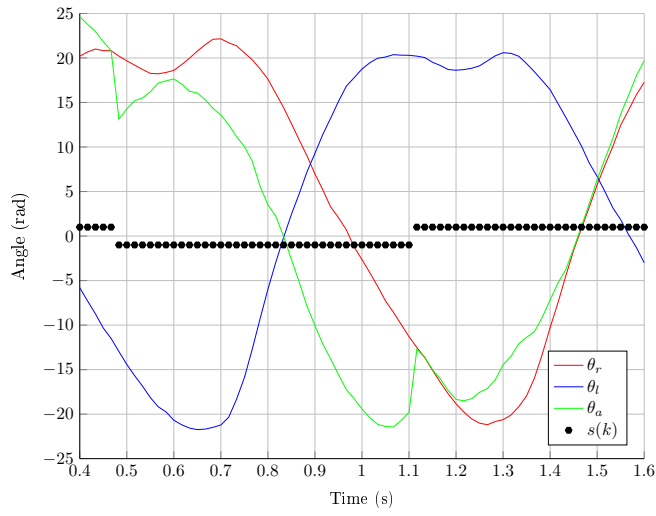
Case 3: the graphs are in the figures 5.5 and 5.6.

Case 4: the graphs are in the figures 5.7 and 5.8.

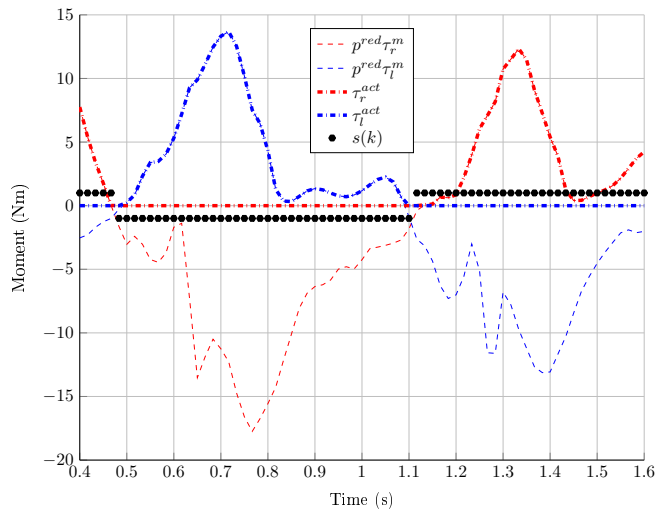
Case 5: the graphs are in the figures 5.9 and 5.10.

Case 6: the graphs are in the figures 5.11 and 5.12.

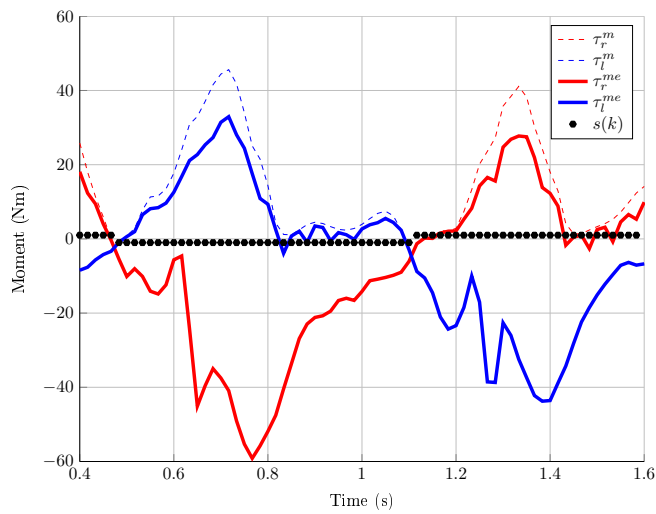
The table 5.2 shows for each the test case the values of the quantitative evaluations defined in subsection 5.2.1. The table 5.3 contains the execution time of the Inverse Dynamics Tool invocations.



(a) Case 1 – Actuator angle command



(b) Case 1 – Applied torques



(c) Case 1 – Inverse dynamics results

Figure 5.1: Case 1 – Results

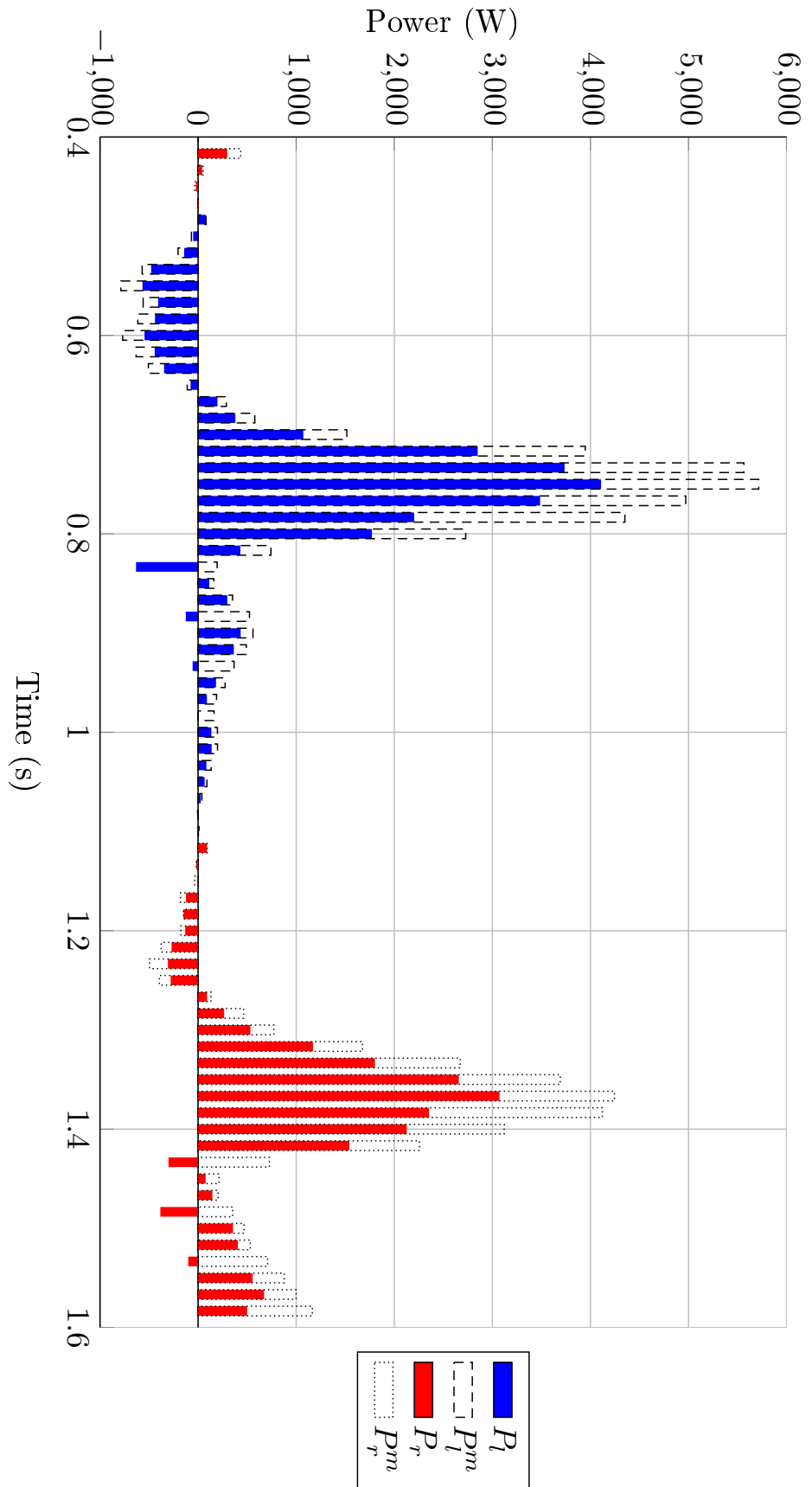
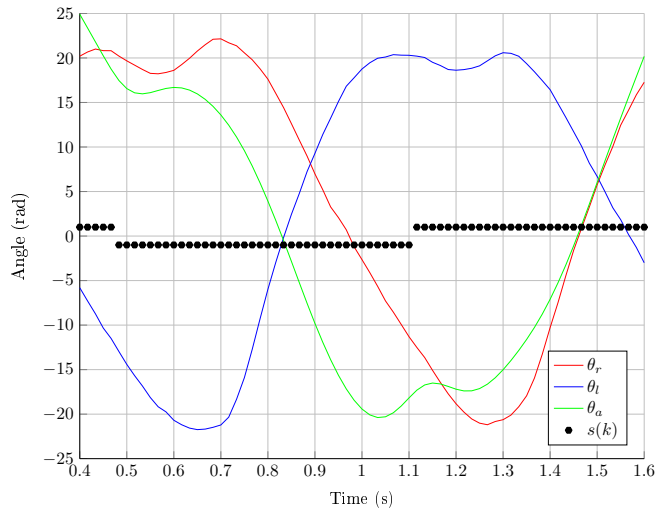
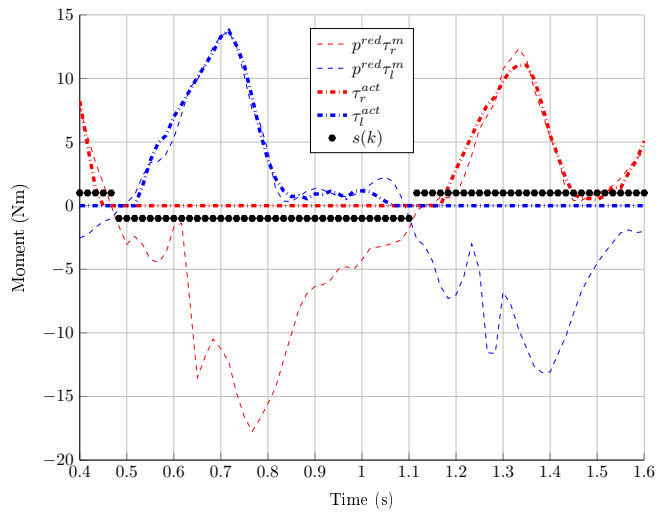


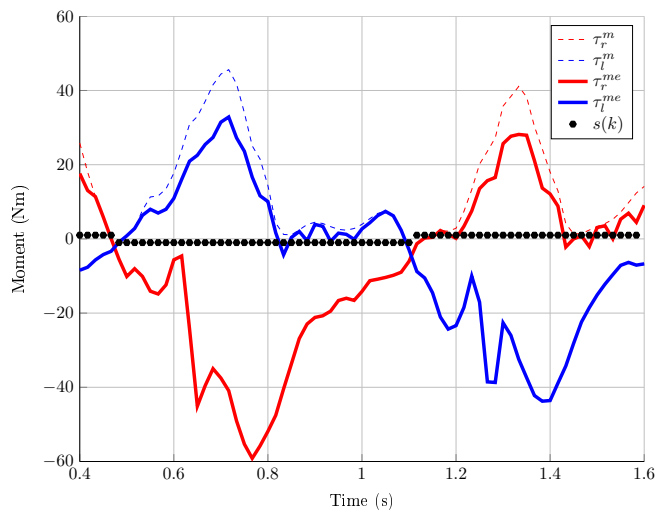
Figure 5.2: Case 1 – Generated power (positive torque)



(a) Case 2 – Actuator angle command



(b) Case 2 – Applied torques



(c) Case 2 – Inverse dynamics results

Figure 5.3: Case 2 – Results

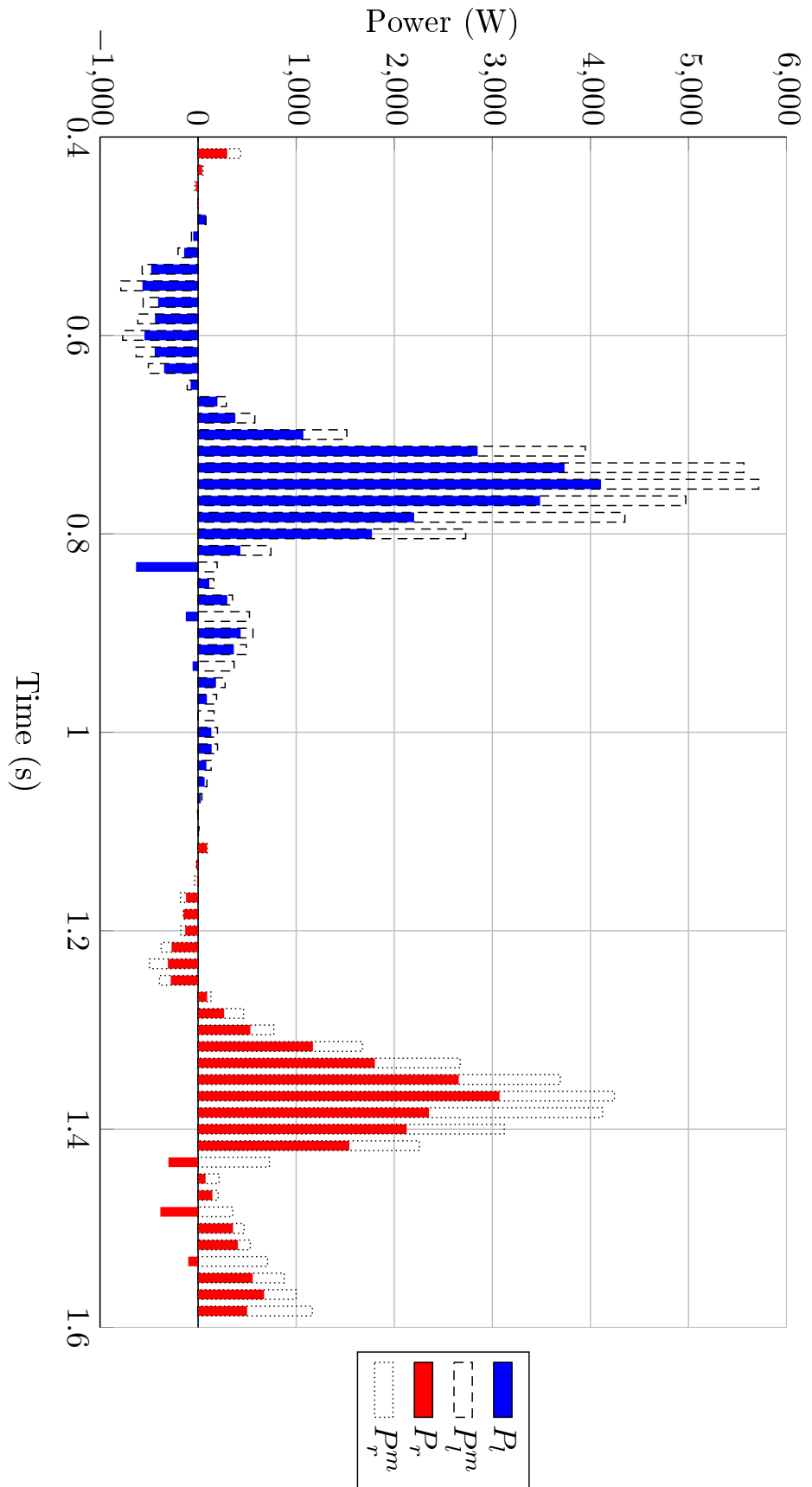
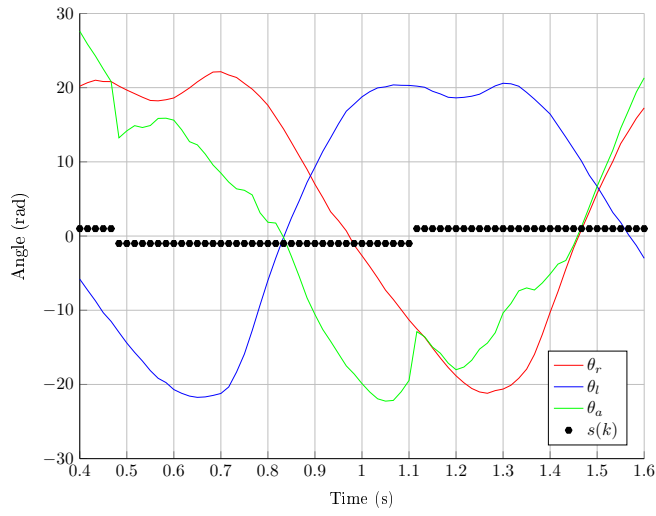
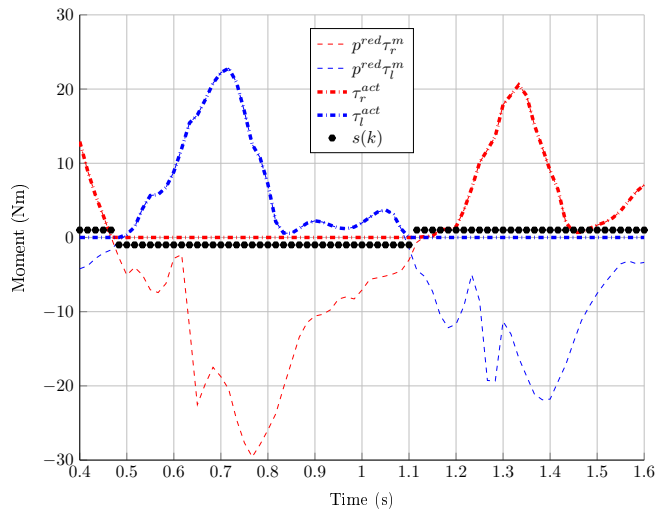


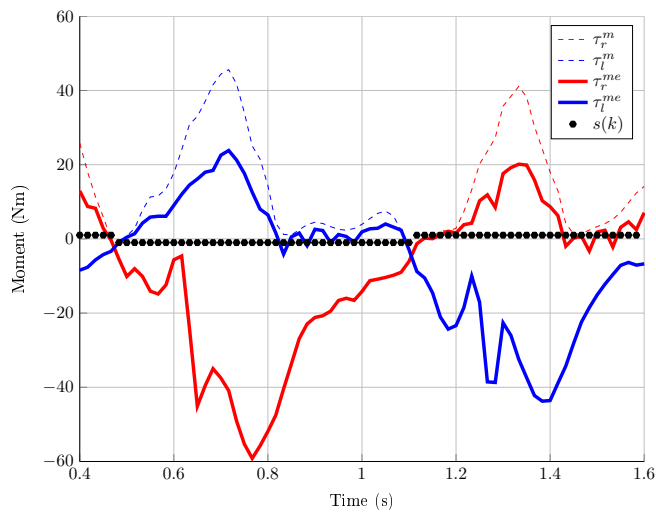
Figure 5.4: Case 2 – Generated power (positive torque)



(a) Case 3 – Actuator angle command



(b) Case 3 – Applied torques



(c) Case 3 – Inverse dynamics results

Figure 5.5: Case 3 – Results

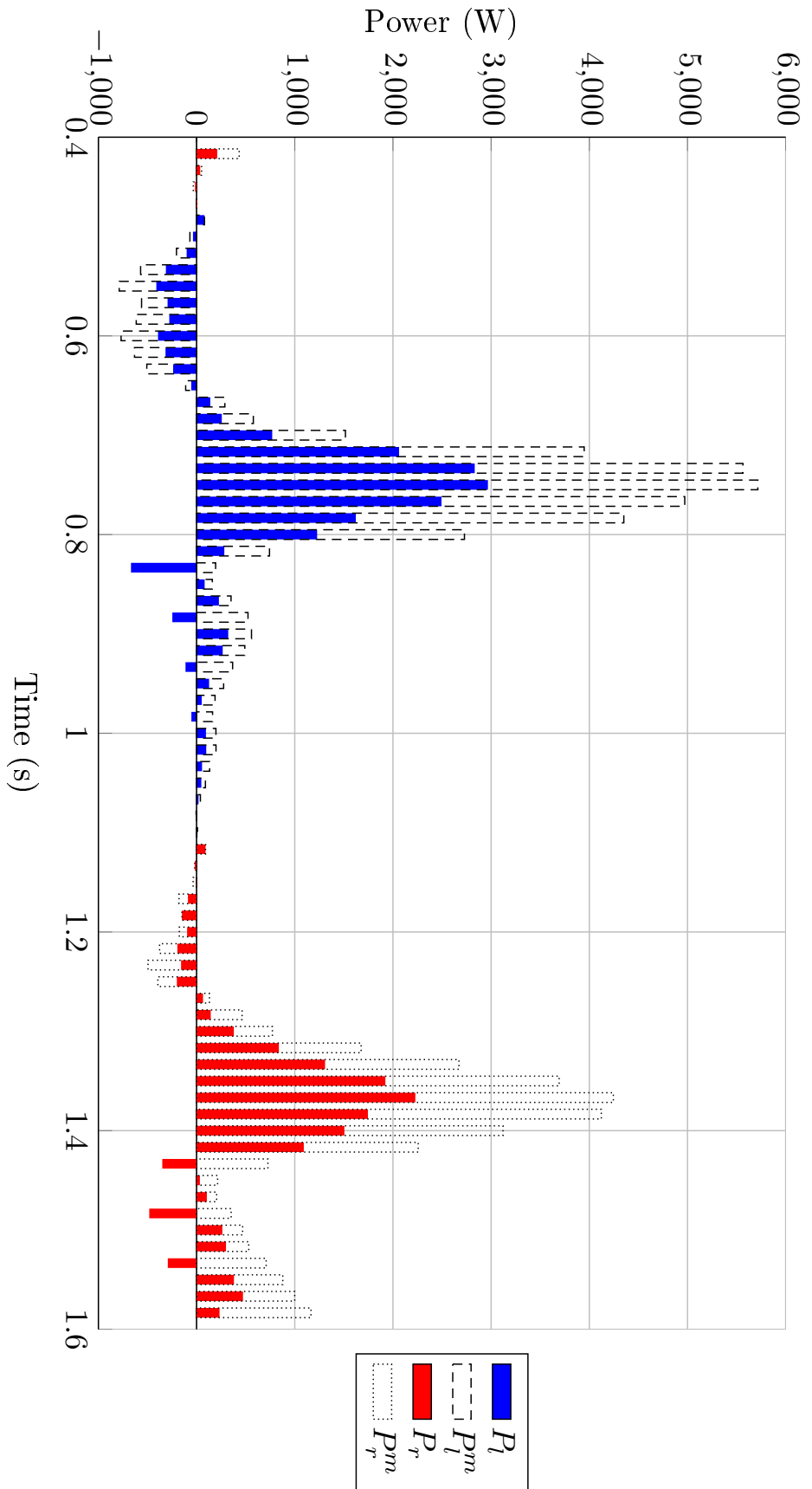
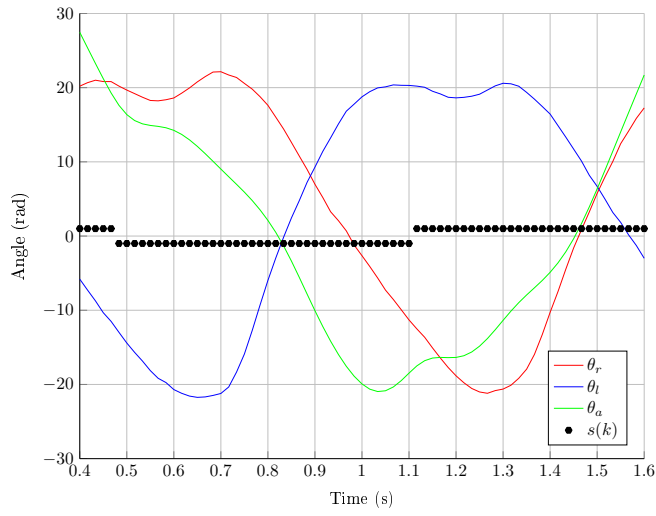
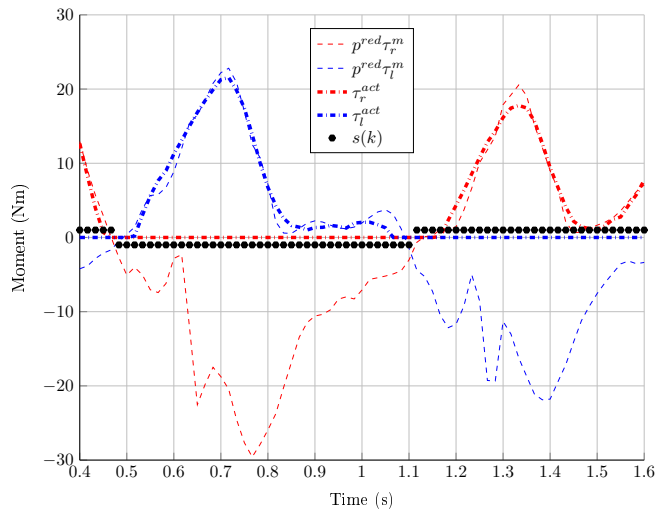


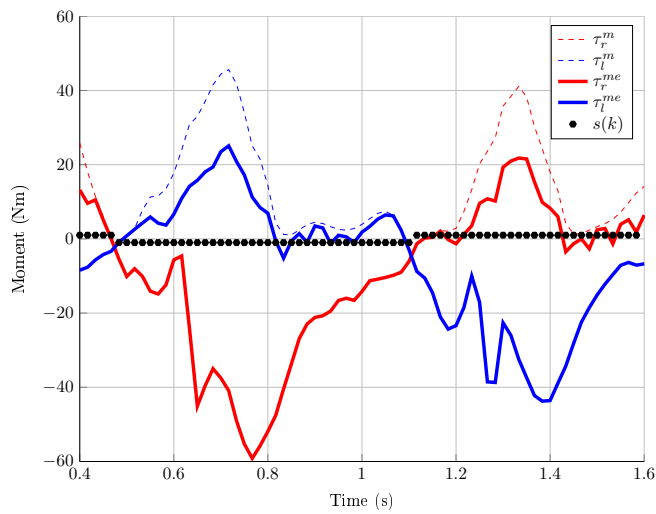
Figure 5.6: Case 3 – Generated power (positive torque)



(a) Case 4 – Actuator angle command



(b) Case 4 – Applied torques



(c) Case 4 – Inverse dynamics results

Figure 5.7: Case 4 – Results

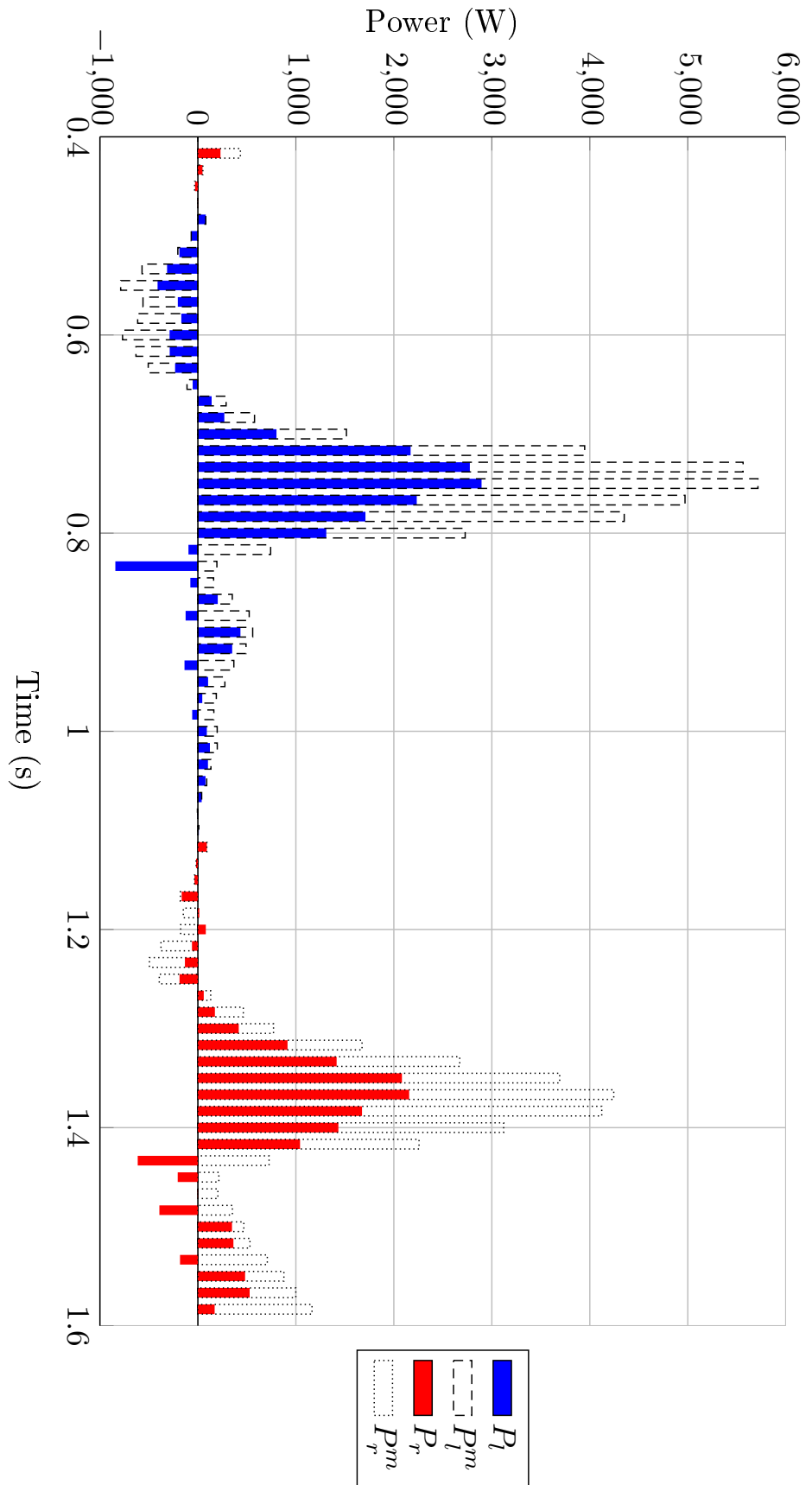
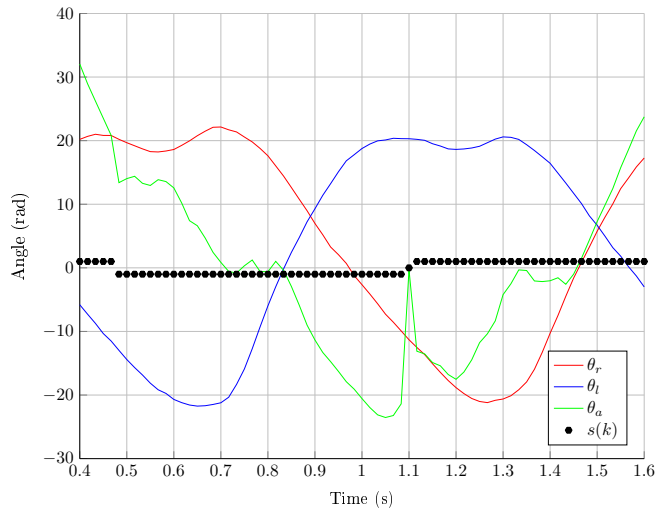
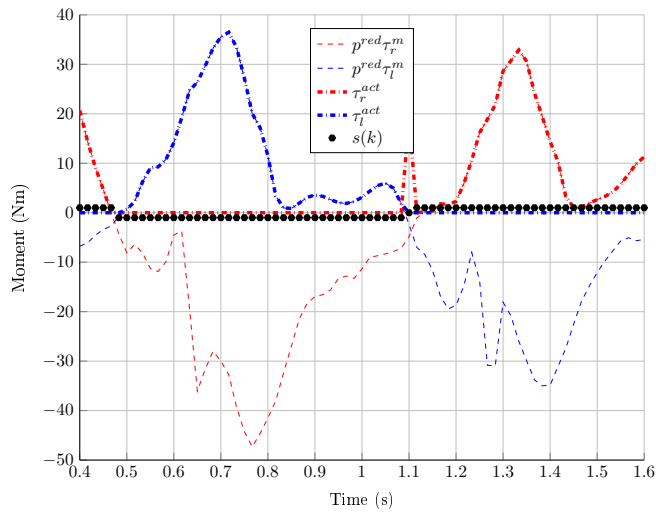


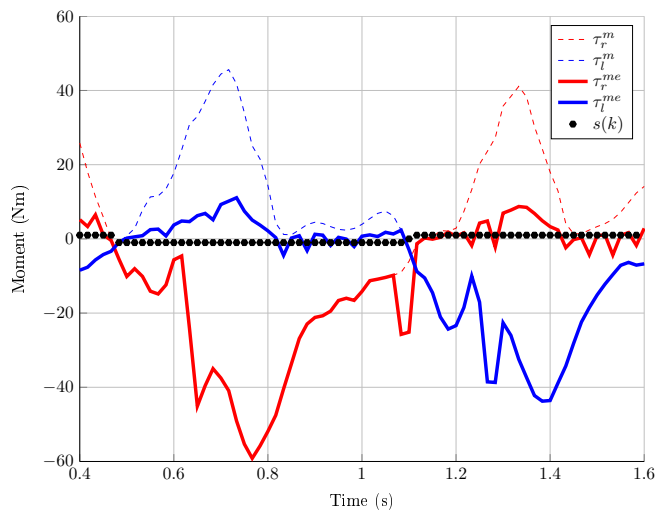
Figure 5.8: Case 4 – Generated power (positive torque)



(a) Case 5 – Actuator angle command



(b) Case 5 – Applied torques



(c) Case 5 – Inverse dynamics results

Figure 5.9: Case 5 – Results

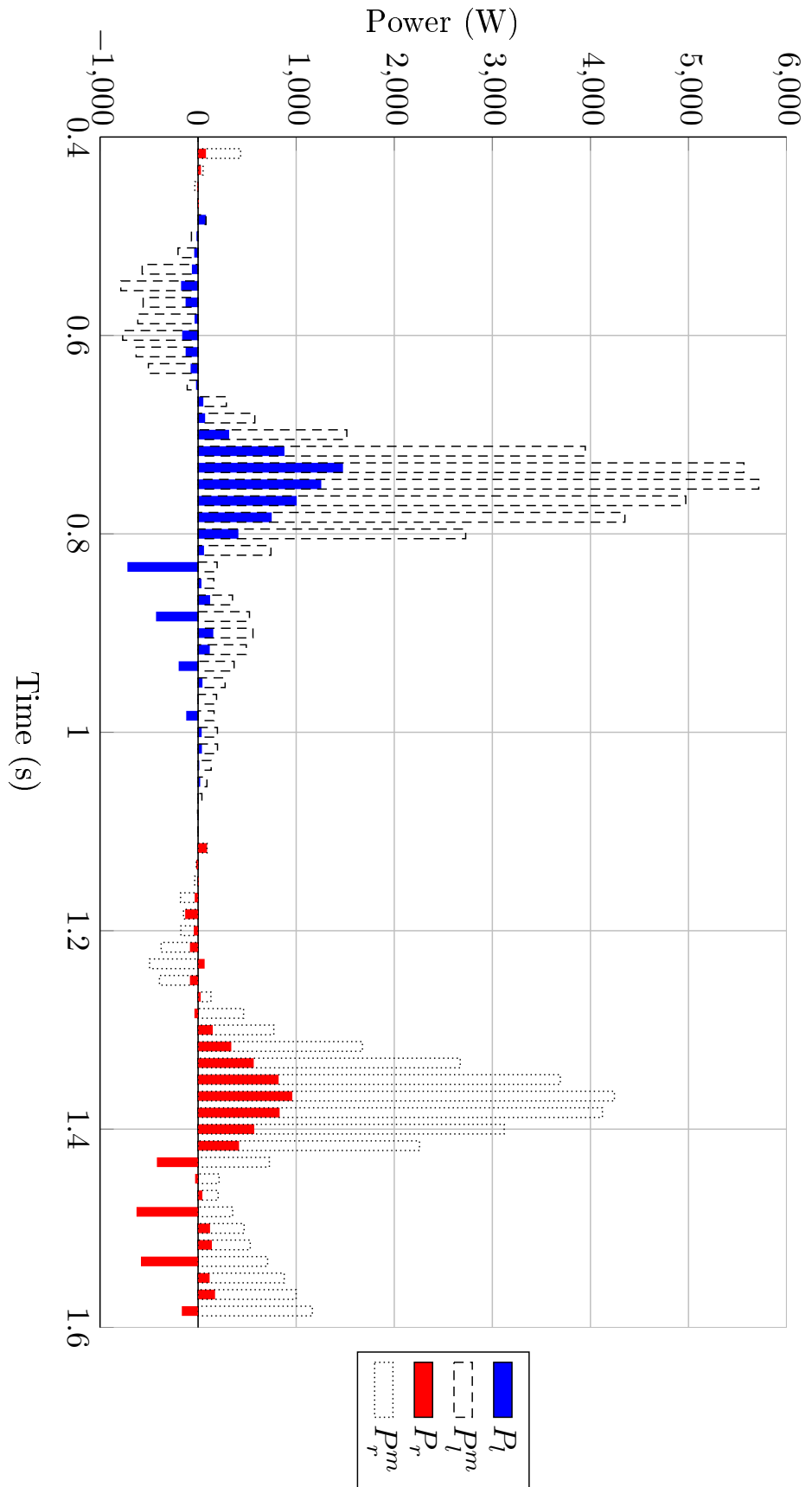
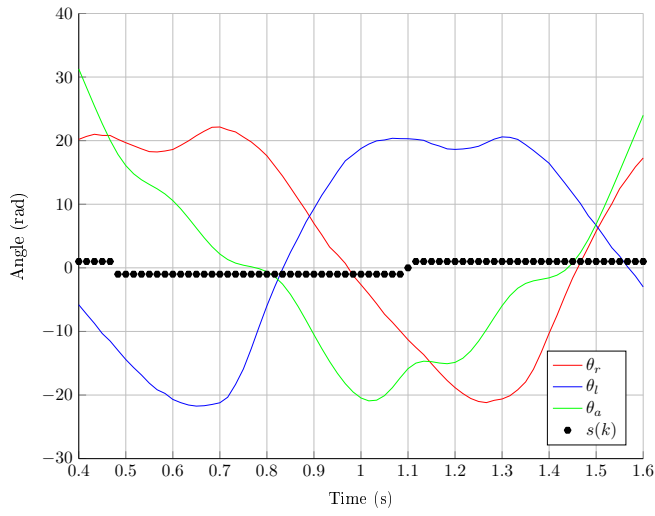
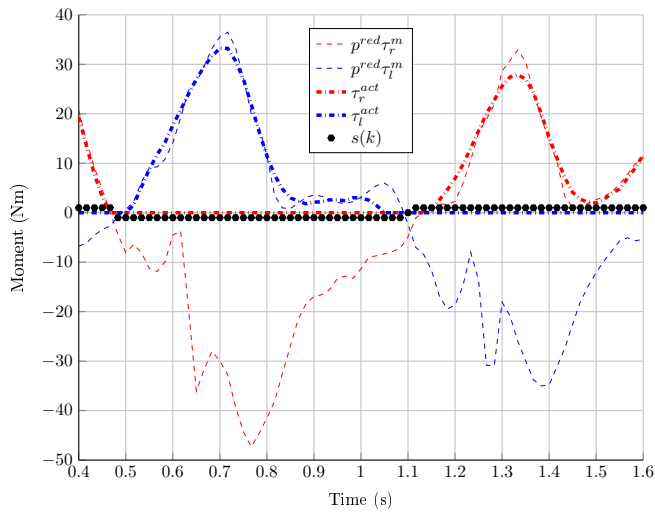


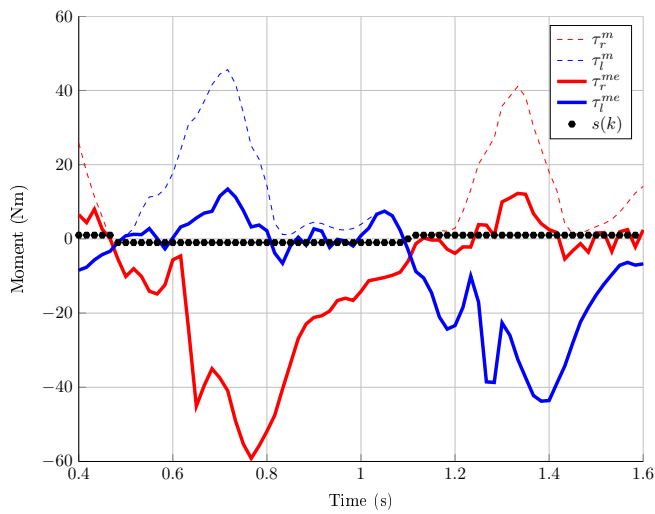
Figure 5.10: Case 5 – Generated power (positive torque)



(a) Case 6 – Actuator angle command



(b) Case 6 – Applied torques



(c) Case 6 – Inverse dynamics results

Figure 5.11: Case 6 – Results

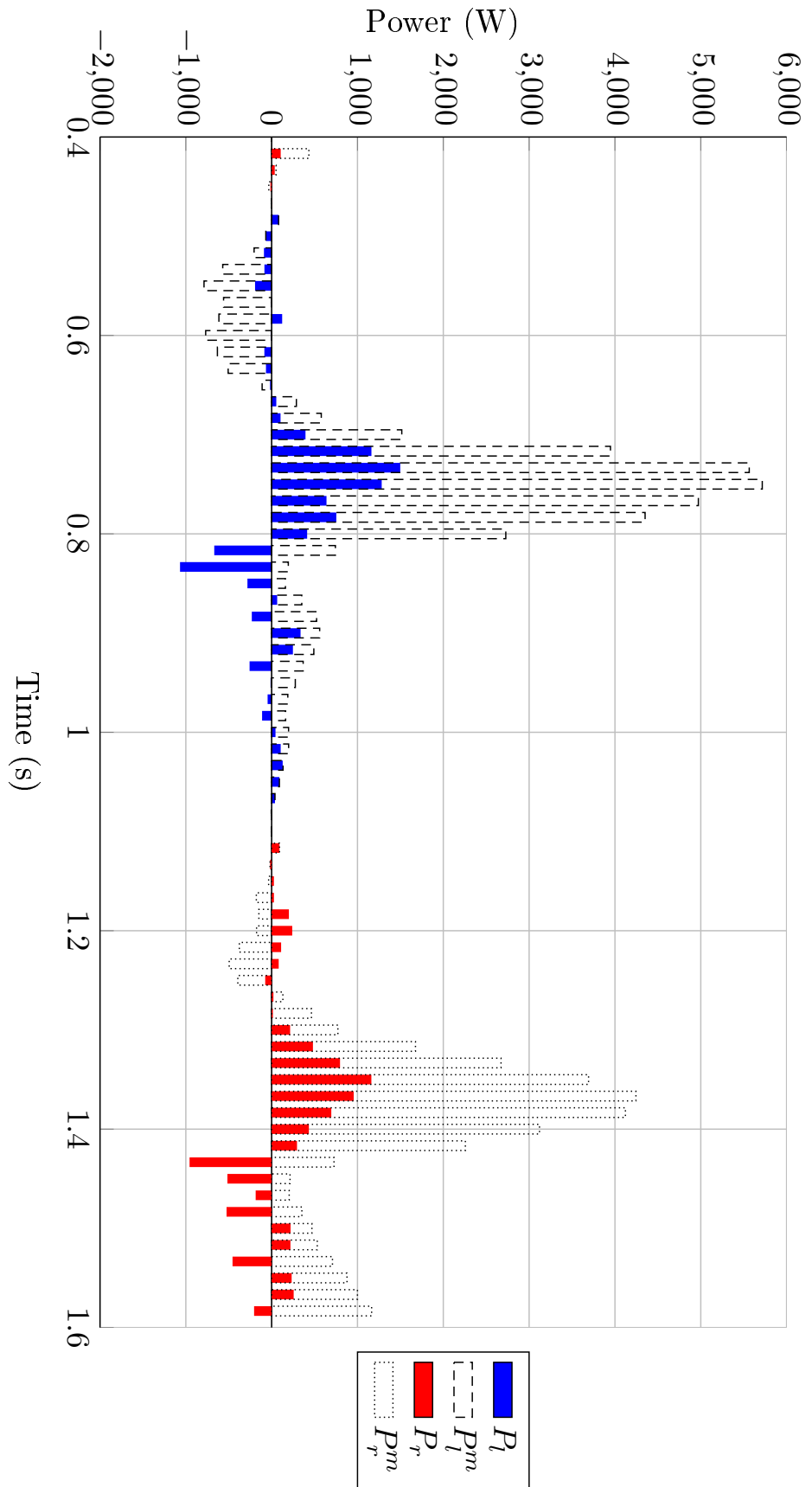


Figure 5.12: Case 6 – Generated power (positive torque)

| | RMS_l (Nm) | RMS_r (Nm) | E_l^+ (J) | $E_l^{+,m}$ (J) | η_l^+ | E_r^+ (J) | $E_r^{+,m}$ (J) | η_r^+ |
|--------|-----------------|-----------------|----------------|--------------------|------------|----------------|--------------------|------------|
| Case 1 | 0.1076 | 0.0457 | 479.3765 | 704.1514 | 0.6808 | 385.8981 | 583.6577 | 0.6612 |
| Case 2 | 0.5817 | 0.6225 | 472.8912 | 704.1514 | 0.6716 | 381.4024 | 583.6577 | 0.6535 |
| Case 3 | 0.1793 | 0.0762 | 353.7495 | 704.1514 | 0.5024 | 285.5184 | 583.6577 | 0.4892 |
| Case 4 | 0.9078 | 0.9076 | 352.2267 | 704.1514 | 0.5002 | 291.8513 | 583.6577 | 0.5000 |
| Case 5 | 0.0866 | 2.2563 | 165.1192 | 703.8709 | 0.2346 | 143.3586 | 583.6577 | 0.2456 |
| Case 6 | 1.6225 | 1.4369 | 193.8951 | 703.8709 | 0.2755 | 178.5881 | 583.6577 | 0.3060 |

Table 5.2: Test cases evaluation of the *angular* model validation

| | ID time (s) |
|--------|-------------|
| Case 1 | 0.119 |
| Case 2 | 0.153 |
| Case 3 | 0.126 |
| Case 4 | 0.112 |
| Case 5 | 0.110 |
| Case 6 | 0.109 |

Table 5.3: ID execution time of the *angular* model validation

5.3.2 The *extended* angular model

This subsection will present the results of the simulations with the *extended* angular model. The table 5.4 describes the configuration of the considered test cases. The parameters taken into account are the reduction factor of the input torques, i.e. how much the exoskeleton must help the walking, if the actuator angles have been smoothed before giving them to the `ExoController` and the radii length of the pulleys for the lower elastic bands, the ones that apply the negative torques. The smoothing is performed, as for the *angular* model, by using a MatLab® smoothing spline with the parameter $p = 0.9999$.

In every test case the actuator parameters are set as follows:

- K_l and K_r were set to 100 N/m;
- R_a , R_l and R_r were all set to 1 m;
- K_l^I and K_r^I were set to 40 N/m

| | Reduction factor | Smoothed | R_l^I (m) | R_r^I (m) |
|---------|------------------|----------|-------------|-------------|
| Case 1a | 0.3 | ✗ | 1.0 | 1.0 |
| Case 1b | 0.3 | ✗ | 1.5 | 1.5 |
| Case 2a | 0.3 | ✓ | 1.0 | 1.0 |
| Case 2b | 0.3 | ✓ | 1.5 | 1.5 |
| Case 3a | 0.5 | ✗ | 1.0 | 1.0 |
| Case 3b | 0.5 | ✗ | 1.5 | 1.5 |
| Case 4a | 0.5 | ✓ | 1.0 | 1.0 |
| Case 4b | 0.5 | ✓ | 1.5 | 1.5 |
| Case 5a | 0.8 | ✗ | 1.0 | 1.0 |
| Case 5b | 0.8 | ✗ | 1.5 | 1.5 |
| Case 6a | 0.8 | ✓ | 1.0 | 1.0 |
| Case 6b | 0.8 | ✓ | 1.5 | 1.5 |

Table 5.4: Test cases configurations of the *extended* angular model validation

For each test case we present six graphs:

- *Actuator angle command*: this graph contains the angles of the left joint (blue), the right joint (red) and the angle command to the single actuator (green). There is also the plot of the status function ($s(k)$).
- *Applied torques*: this graph contains the torques applied to the left (blue dash-dotted) and the right joint (red dash-dotted) and the target torques $p^{red}\tau_l^m$ and $p^{red}\tau_r^m$, for the left (blue dashed) and the right side (red dashed). As stated in 3.4, the actuator is set to actively follow only the positive torques.
- *Inverse dynamics results*: this graph contains the results of the ID applied to the model without the exoskeleton (dashed line) and applied to the model *with* the exoskeleton (solid line).
- *Generated power (positive torque)*: this graph is meaningful for the evaluation of the effectiveness of the solution for the actuation of the positive

reference torques. It contains the bar plot of the functions $P_l(k)$ and $P_l^{old}(k)$ (blue) when the status is $s(k) = -1$, active exoskeleton on the left side, and $P_r(k)$ and P_r^{old} (red) when the status is $s(k) = 1$, active exoskeleton on the right side.

- *Generated power (negative torque)*: this graph is meaningful for the evaluation of the effectiveness of the solution for the actuation of the negative reference torques. It contains the bar plot of the functions $P_l(k)$ and $P_l^{old}(k)$ (blue) when the status is $s(k) = 1$, exoskeleton giving positive torque to the right side, and $P_r(k)$ and P_r^{old} (red) when the status is $s(k) = -1$, exoskeleton giving positive torque to the right side.

Case 1a: the graphs are in the figures 5.13, 5.14a and 5.14b.

Case 1b: the graphs are in the figures 5.15, 5.16a and 5.14b.

Case 2a: the graphs are in the figures 5.17, 5.18a and 5.18b.

Case 2b: the graphs are in the figures 5.19, 5.20a and 5.20b.

Case 3a: the graphs are in the figures 5.21, 5.22a and 5.22b.

Case 3b: the graphs are in the figures 5.23, 5.24a and 5.24b.

Case 4a: the graphs are in the figures 5.25, 5.26a and 5.26b.

Case 4b: the graphs are in the figures 5.27, 5.28a and 5.28b.

Case 5a: the graphs are in the figures 5.29, 5.30a and 5.30b.

Case 5b: the graphs are in the figures 5.31, 5.32a and 5.32b.

Case 6a: the graphs are in the figures 5.33, 5.34a and 5.34b.

Case 6b: the graphs are in the figures 5.35, 5.36a and 5.36b.

The tables 5.5 and 5.6 show for each the test case the values of the quantitative evaluations defined in subsection 5.2.1. The only difference is that there are two versions of the *RMS*, in the table 5.6 there is the one computed on all the reference torques (both positive and negative), while the one in the table 5.5 is only relative to the positive reference torques. The table 5.7 contains the execution time of the Inverse Dynamics Tool invocations.

| | RMS_l (Nm) | RMS_r (Nm) | E_l^+ (J) | $E_l^{+,m}$ (J) | η_l^+ | E_r^+ (J) | $E_r^{+,m}$ (J) | η_r^+ |
|---------|-----------------|-----------------|----------------|--------------------|------------|----------------|--------------------|------------|
| Case 1a | 5.0381 | 6.0292 | 478.1077 | 704.1514 | 0.6790 | 387.4181 | 583.6577 | 0.6638 |
| Case 1b | 11.2805 | 13.1053 | 555.2333 | 704.1514 | 0.7885 | 436.2853 | 583.6577 | 0.7475 |
| Case 2a | 4.9561 | 5.9697 | 475.9070 | 704.1514 | 0.6759 | 387.0937 | 583.6577 | 0.6632 |
| Case 2b | 11.2898 | 13.1050 | 551.3844 | 704.1514 | 0.7830 | 439.9148 | 583.6577 | 0.7537 |
| Case 3a | 5.7121 | 6.6540 | 352.5579 | 704.1514 | 0.5007 | 286.6183 | 583.6577 | 0.4911 |
| Case 3b | 12.3559 | 14.2719 | 421.2368 | 704.1514 | 0.5982 | 322.7510 | 583.6577 | 0.5530 |
| Case 4a | 5.6581 | 6.6268 | 354.5565 | 704.1514 | 0.5035 | 297.1360 | 583.6577 | 0.5091 |
| Case 4b | 12.3821 | 14.2776 | 416.8457 | 704.1514 | 0.5920 | 332.0270 | 583.6577 | 0.5689 |
| Case 5a | 7.0688 | 8.1126 | 164.3128 | 703.8709 | 0.2334 | 143.9357 | 583.6577 | 0.2466 |
| Case 5b | 14.5594 | 16.4017 | 218.9384 | 703.8709 | 0.3110 | 168.6830 | 583.6577 | 0.2890 |
| Case 6a | 6.9668 | 7.7412 | 195.9180 | 703.8709 | 0.2783 | 178.6631 | 583.6577 | 0.3061 |
| Case 6b | 14.5086 | 16.1767 | 245.0473 | 703.8709 | 0.3481 | 208.3884 | 583.6577 | 0.3570 |

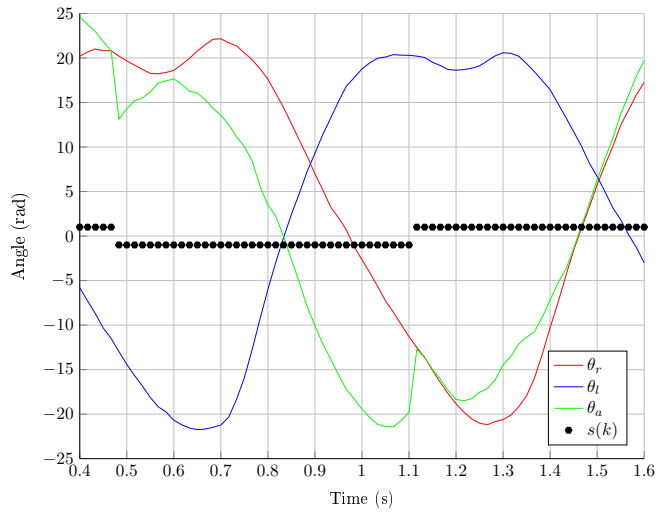
Table 5.5: Test cases evaluation of the *extended* angular model validation

| | $RMS_l -$ all (Nm) | $RMS_r -$ all (Nm) | E_l^- (J) | $E_l^{-,m}$ (J) | η_l^- | E_r^- (J) | $E_r^{-,m}$ (J) | η_r^- |
|---------|-----------------------|-----------------------|----------------|--------------------|------------|----------------|--------------------|------------|
| Case 1a | 4.3645 | 4.1651 | 492.5994 | 669.1069 | 0.7362 | 627.8097 | 1011.9191 | 0.6204 |
| Case 1b | 7.7043 | 7.9495 | 348.1907 | 669.1069 | 0.5204 | 382.1591 | 1011.9191 | 0.3777 |
| Case 2a | 4.2883 | 4.1083 | 487.9656 | 669.1069 | 0.7293 | 634.7857 | 1011.9191 | 0.6273 |
| Case 2b | 7.7334 | 7.9719 | 340.9803 | 669.1069 | 0.5096 | 380.2865 | 1011.9191 | 0.3758 |
| Case 3a | 6.0301 | 6.2030 | 484.0660 | 669.1069 | 0.7235 | 602.4670 | 1011.9191 | 0.5954 |
| Case 3b | 6.8686 | 6.2266 | 341.0576 | 669.1069 | 0.5097 | 365.7145 | 1011.9191 | 0.3614 |
| Case 4a | 5.9947 | 6.2100 | 478.7707 | 669.1069 | 0.7155 | 604.4024 | 1011.9191 | 0.5973 |
| Case 4b | 6.9361 | 6.2933 | 330.7734 | 669.1069 | 0.4944 | 357.8712 | 1011.9191 | 0.3537 |
| Case 5a | 9.4994 | 10.9097 | 471.2733 | 669.1069 | 0.7043 | 601.0443 | 1004.6158 | 0.5983 |
| Case 5b | 7.8482 | 6.5972 | 334.0522 | 669.1069 | 0.4993 | 370.7643 | 1004.6158 | 0.3691 |
| Case 6a | 9.3524 | 10.7267 | 463.4970 | 669.1069 | 0.6927 | 569.6953 | 1004.6158 | 0.5671 |
| Case 6b | 7.6230 | 6.2520 | 318.6708 | 669.1069 | 0.4763 | 326.3962 | 1004.6158 | 0.3249 |

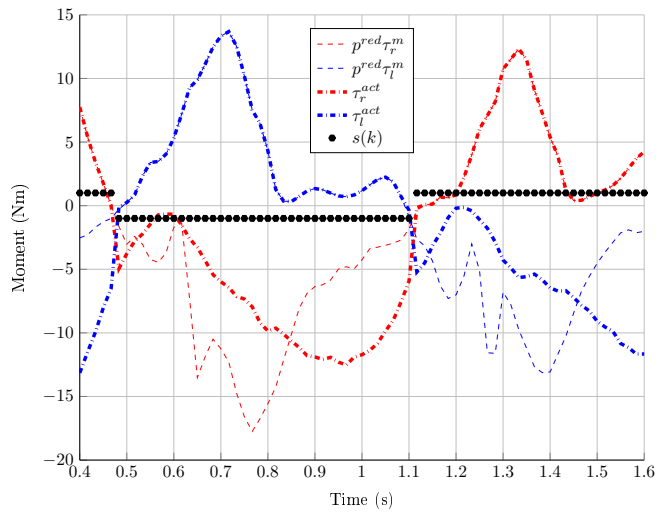
Table 5.6: Test cases evaluation of the *extended* angular model validation (negative torques)

| | ID time (s) |
|---------|-------------|
| Case 1a | 0.110 |
| Case 1b | 0.109 |
| Case 2a | 0.109 |
| Case 2b | 0.109 |
| Case 3a | 0.110 |
| Case 3b | 0.109 |
| Case 4a | 0.109 |
| Case 4b | 0.109 |
| Case 5a | 0.109 |
| Case 5b | 0.109 |
| Case 6a | 0.110 |
| Case 6b | 0.094 |

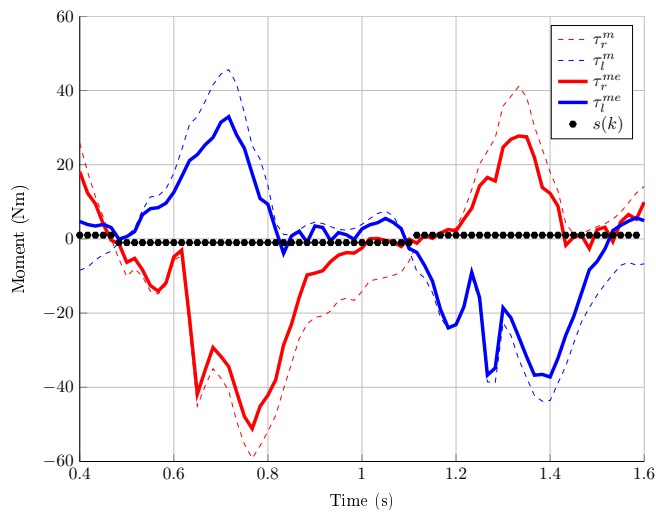
Table 5.7: ID execution time of the *extended* angular model validation



(a) Case 1a - Actuator angle command

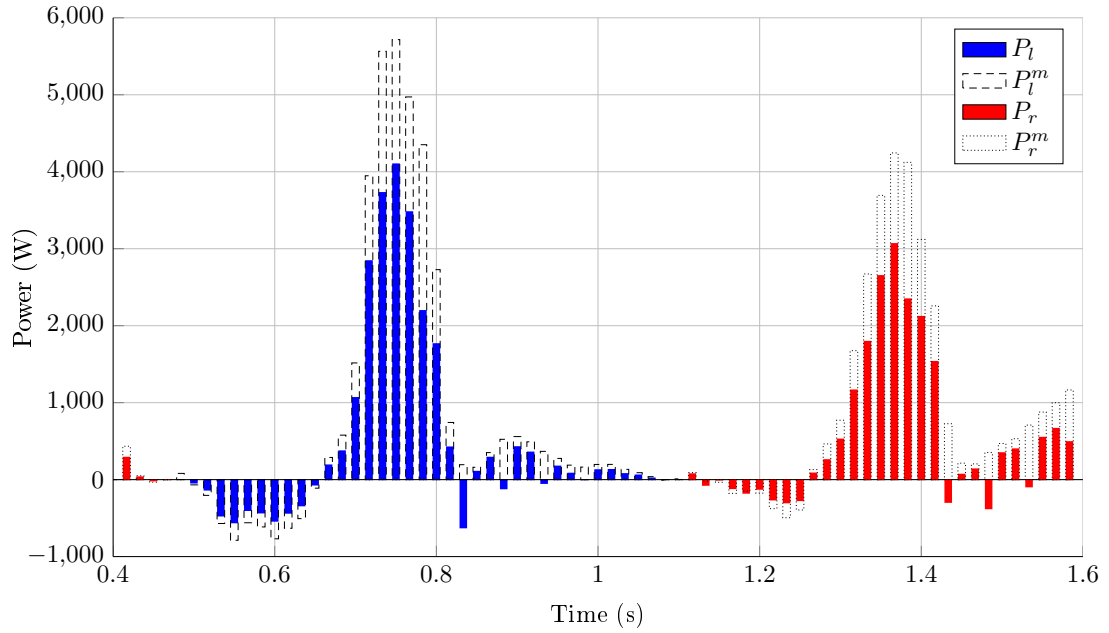


(b) Case 1a - Applied torques

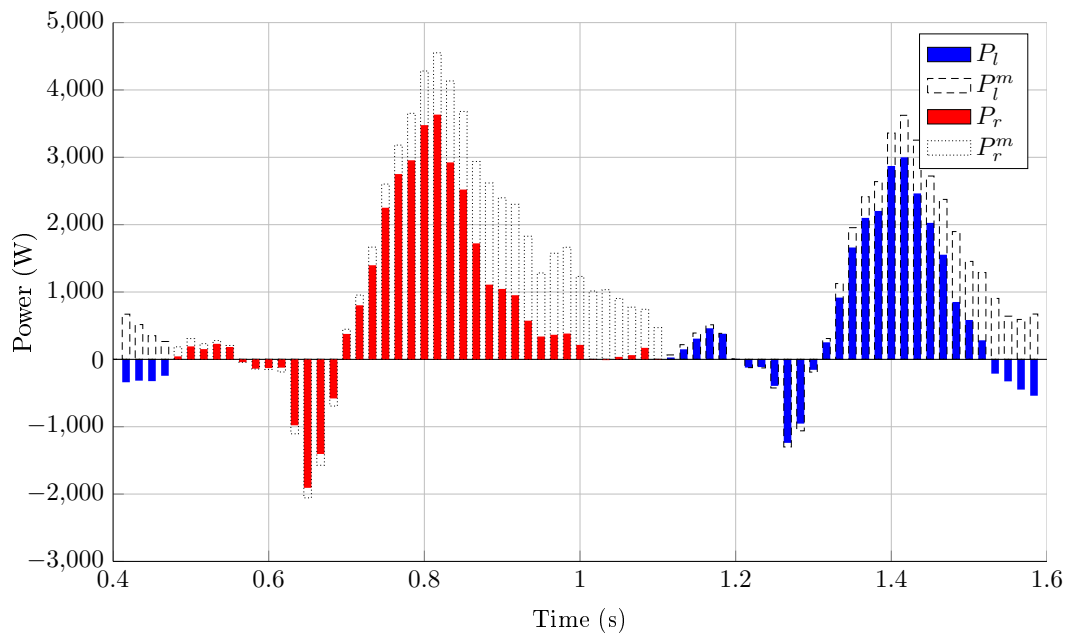


(c) Case 1a - Inverse dynamics results

Figure 5.13: Case 1a - Results

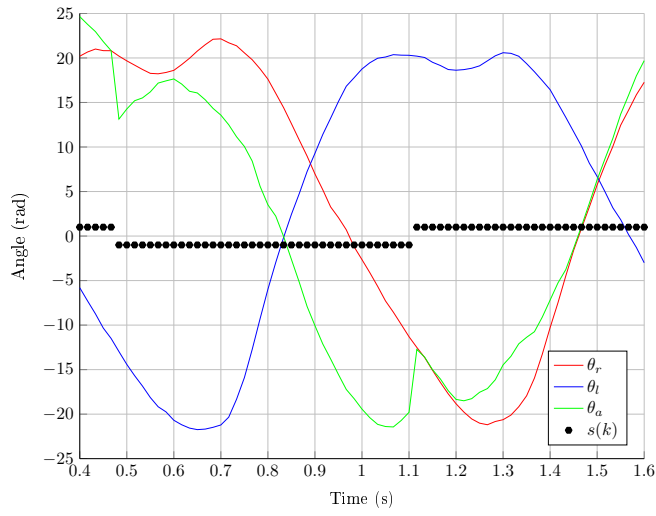


(a) Case 1a – Generated power (positive torque)
Effectiveness (only inferior)

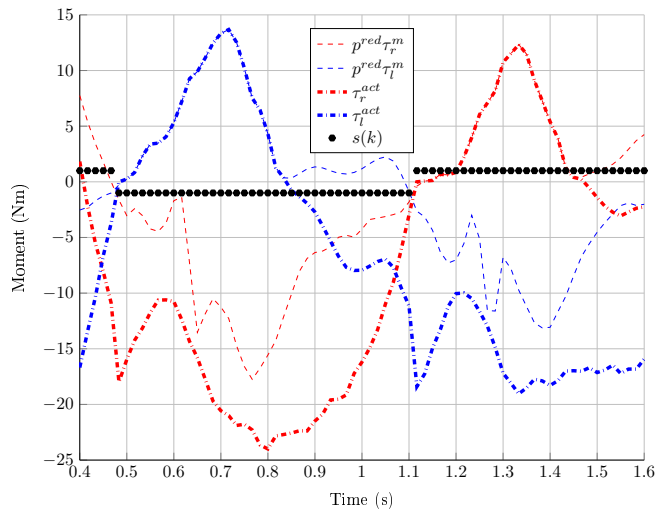


(b) Case 1a – Generated power (negative torque)

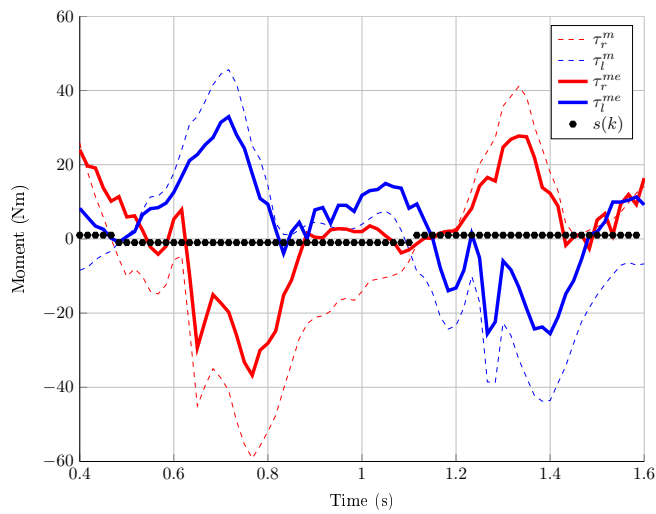
Figure 5.14: Case 1a – Generated power



(a) Case 1b – Actuator angle command

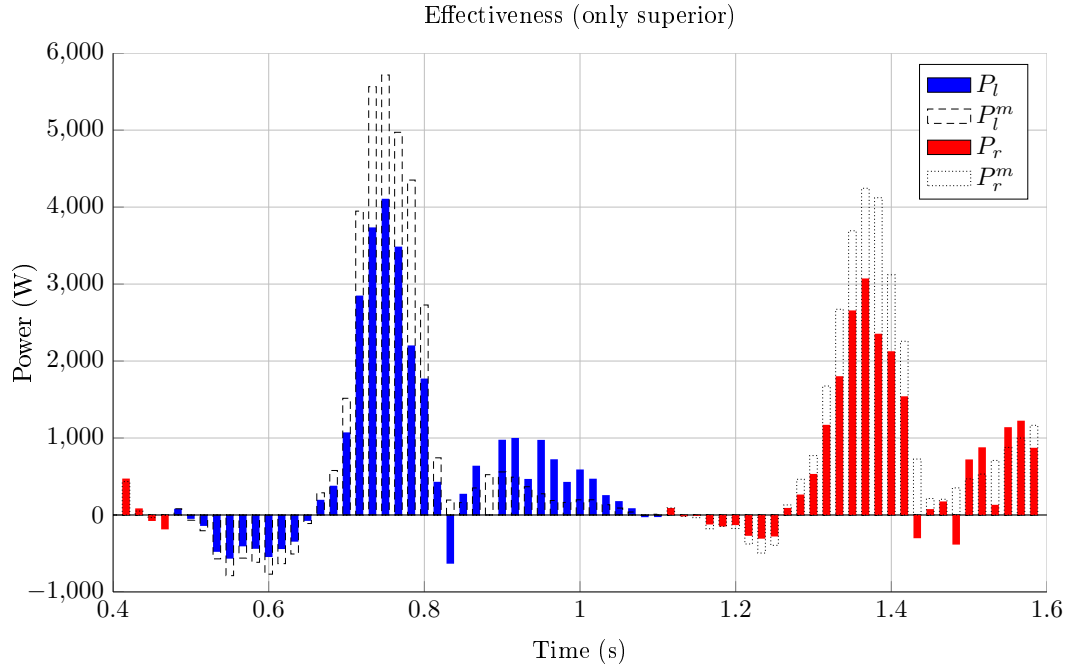


(b) Case 1b – Applied torques

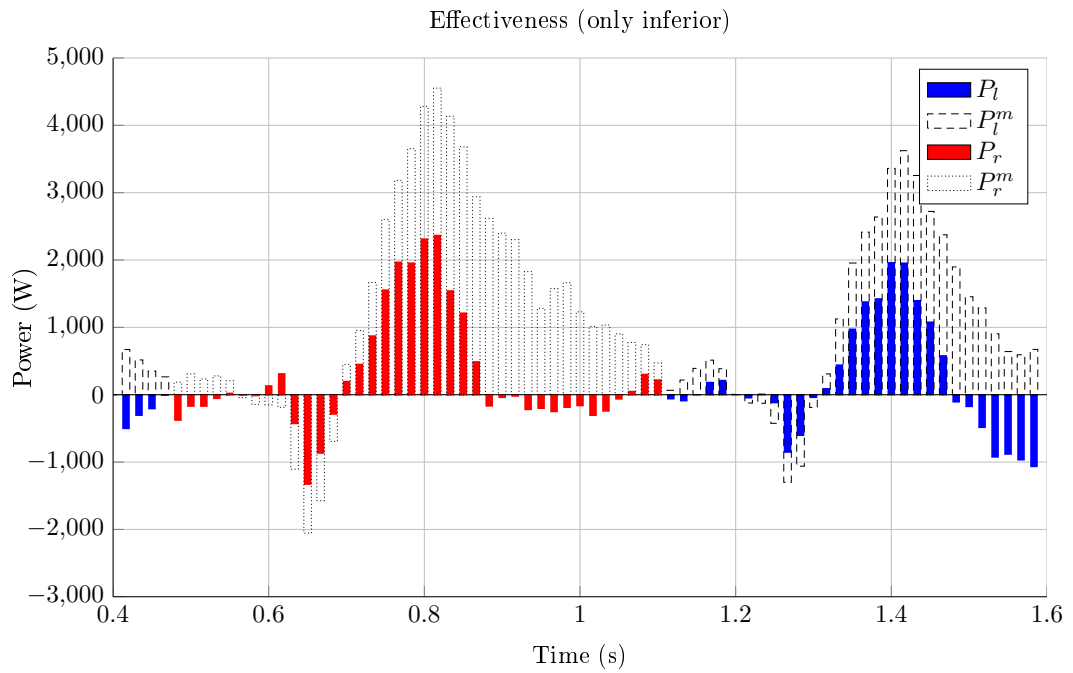


(c) Case 1b – Inverse dynamics results

Figure 5.15: Case 1b – Results

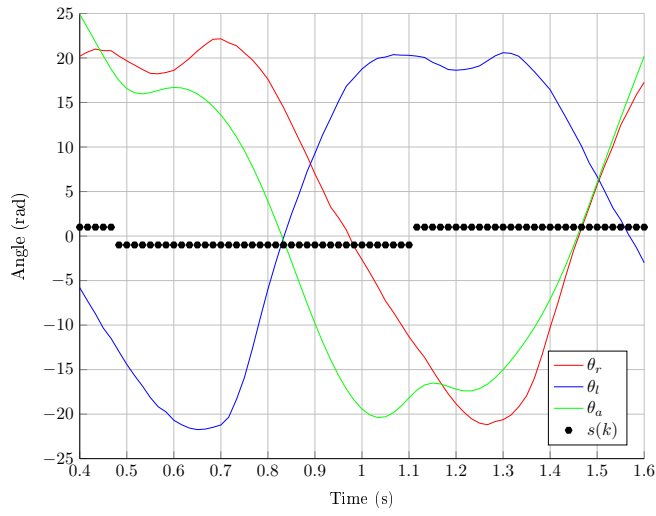


(a) Case 1b – Generated power (positive torque)

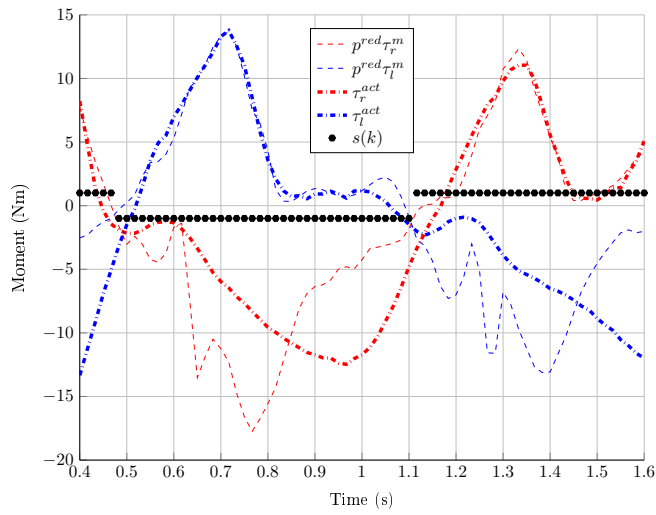


(b) Case 1b – Generated power (negative torque)

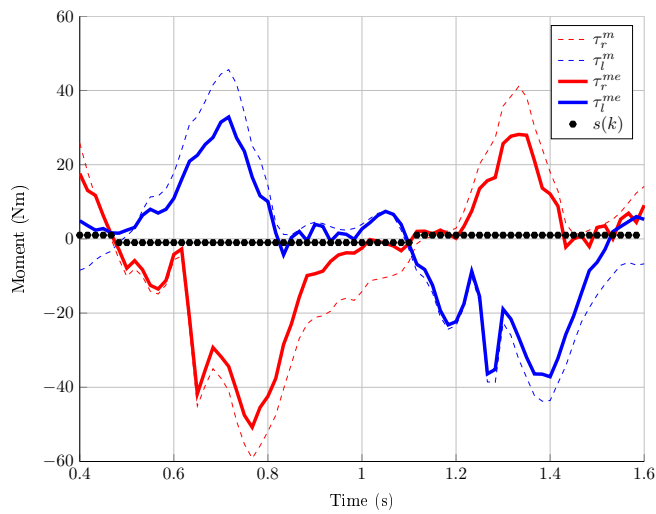
Figure 5.16: Case 1b – Generated power



(a) Case 2a - Actuator angle command

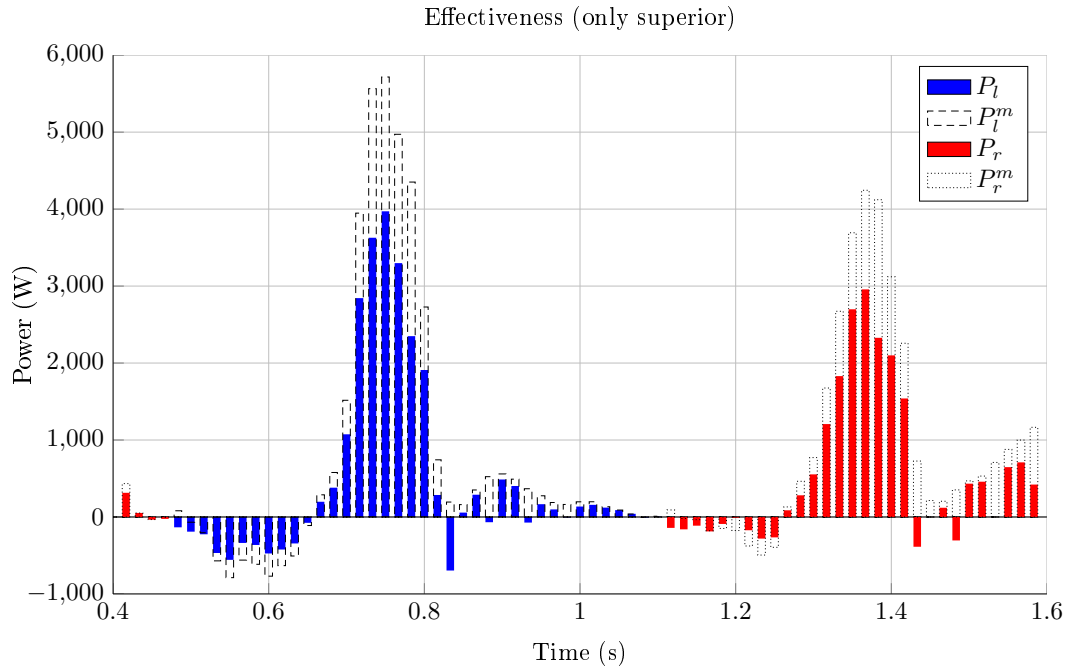


(b) Case 2a - Applied torques

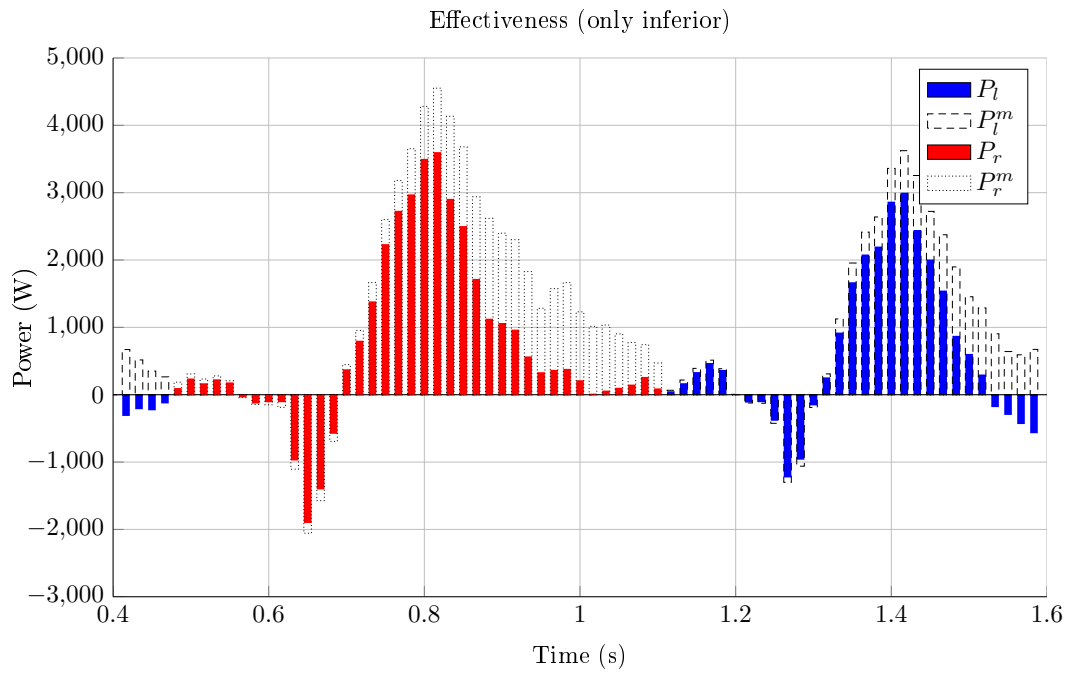


(c) Case 2a - Inverse dynamics results

Figure 5.17: Case 2a - Results

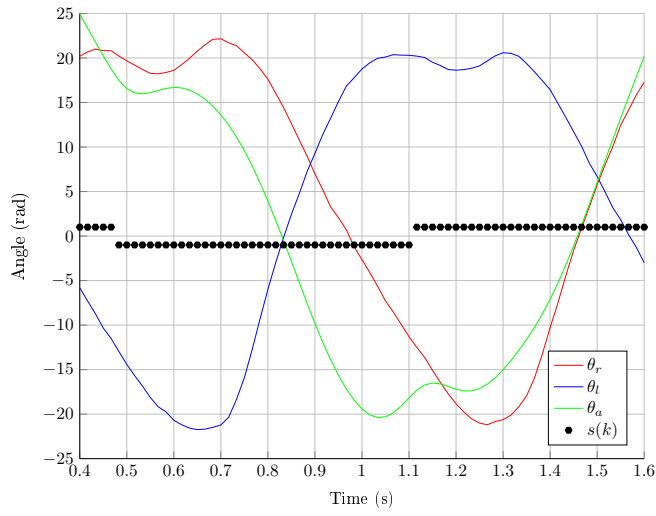


(a) Case 2a – Generated power (positive torque)

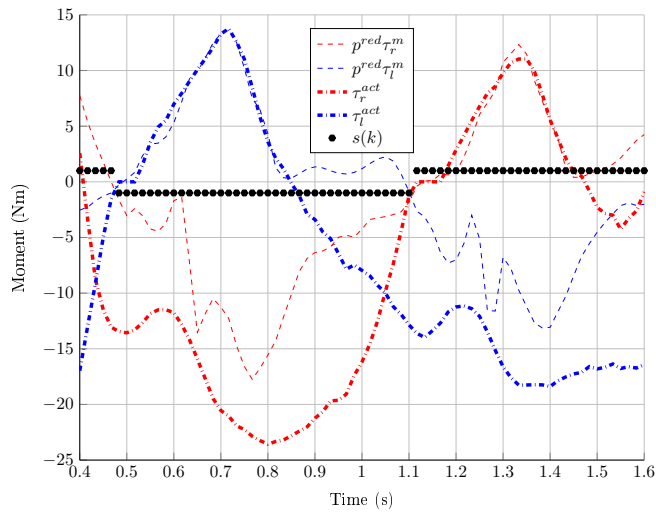


(b) Case 2a – Generated power (negative torque)

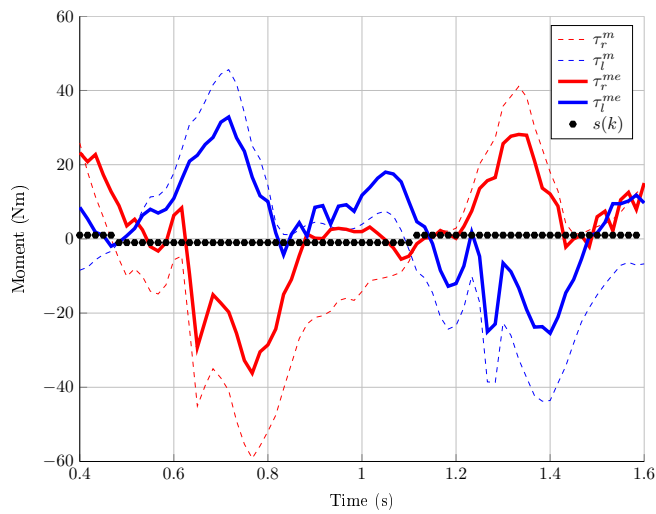
Figure 5.18: Case 2a – Generated power



(a) Case 2b – Actuator angle command

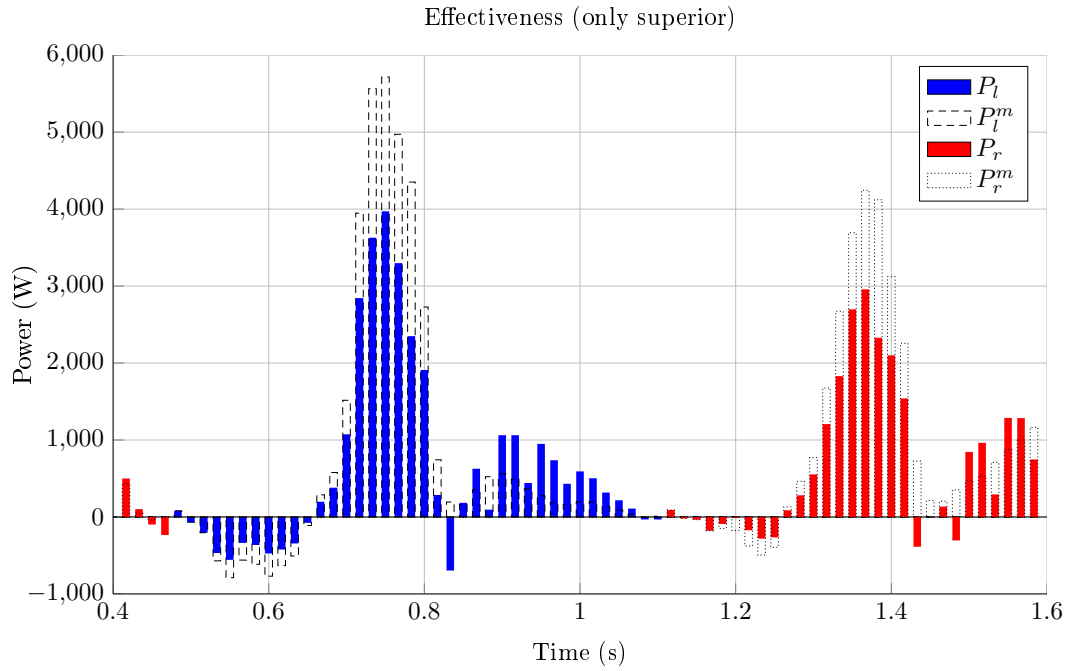


(b) Case 2b – Applied torques

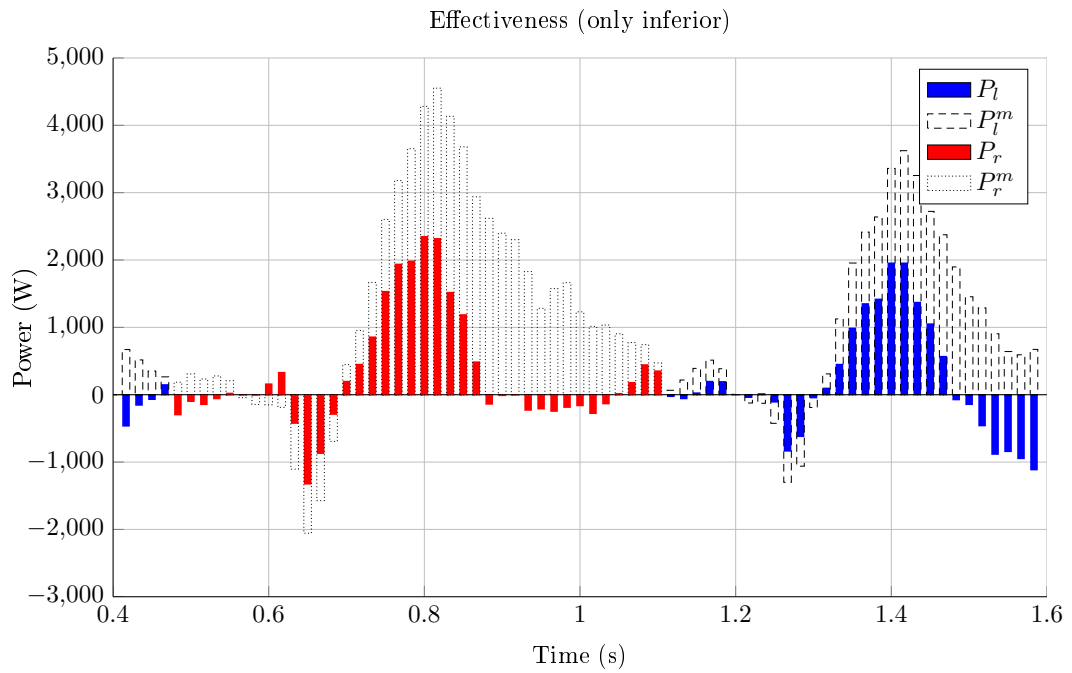


(c) Case 2b – Inverse dynamics results

Figure 5.19: Case 2b – Results

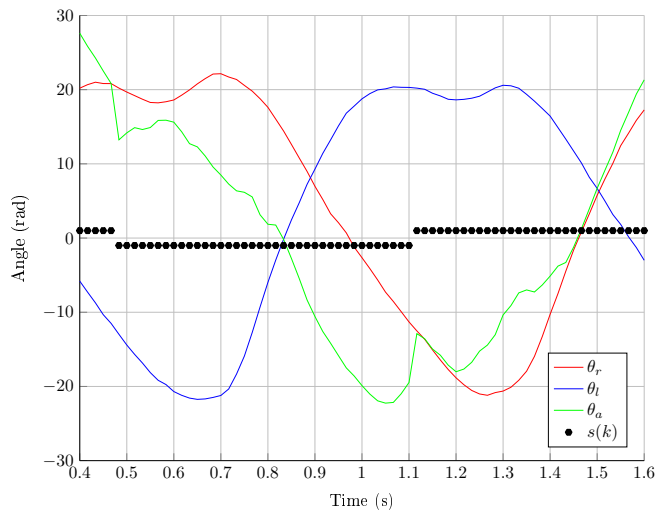


(a) Case 2b – Generated power (positive torque)

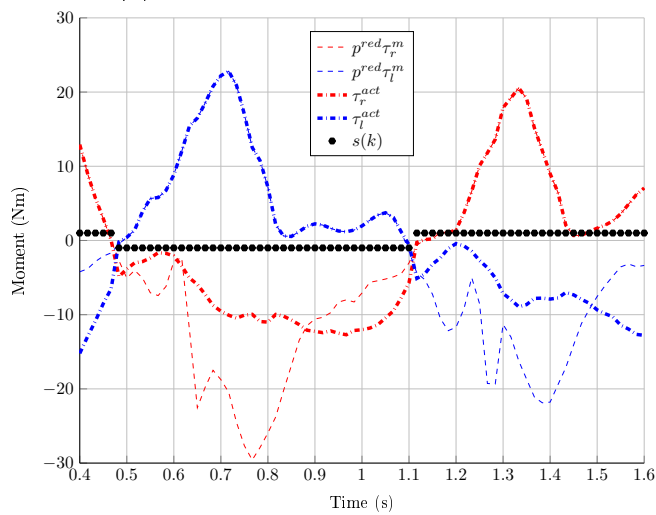


(b) Case 2b – Generated power (negative torque)

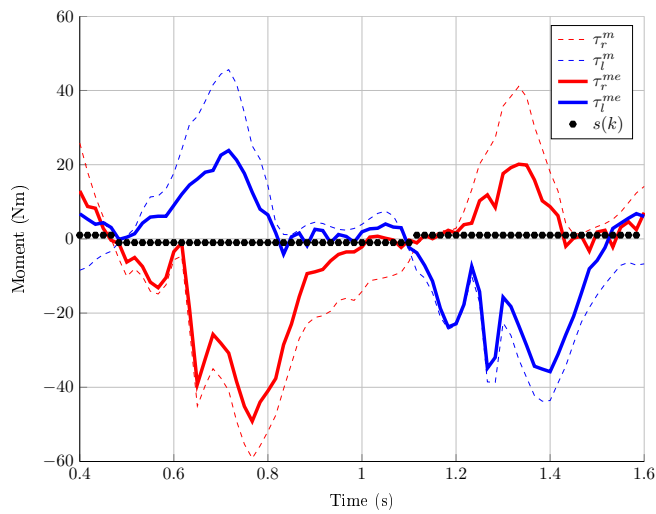
Figure 5.20: Case 2b – Generated power



(a) Case 3a - Actuator angle command

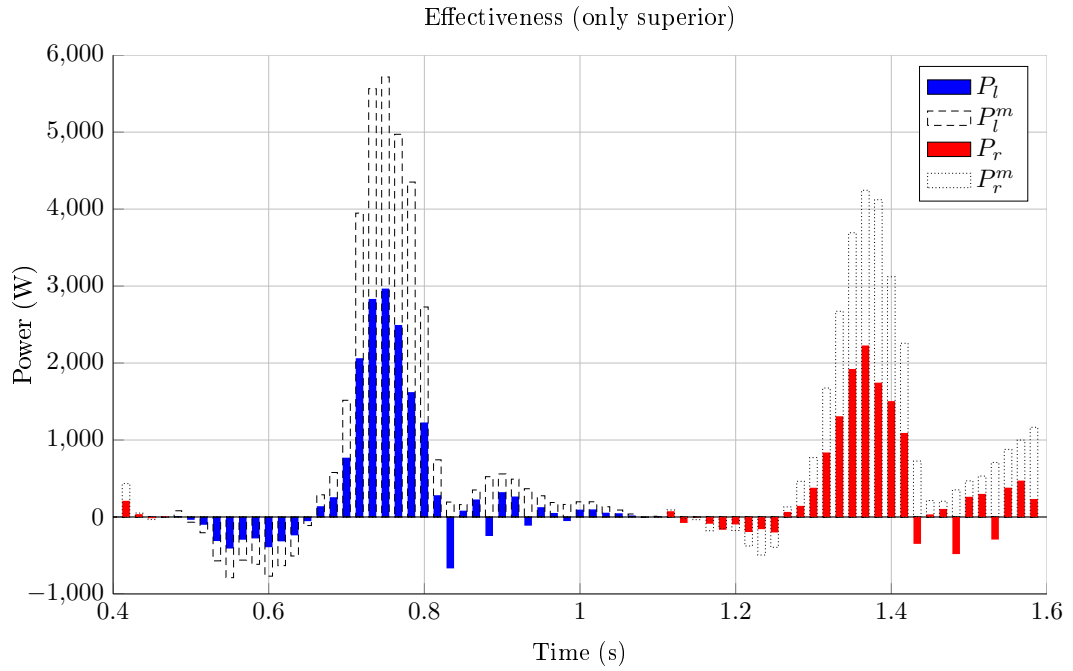


(b) Case 3a - Applied torques

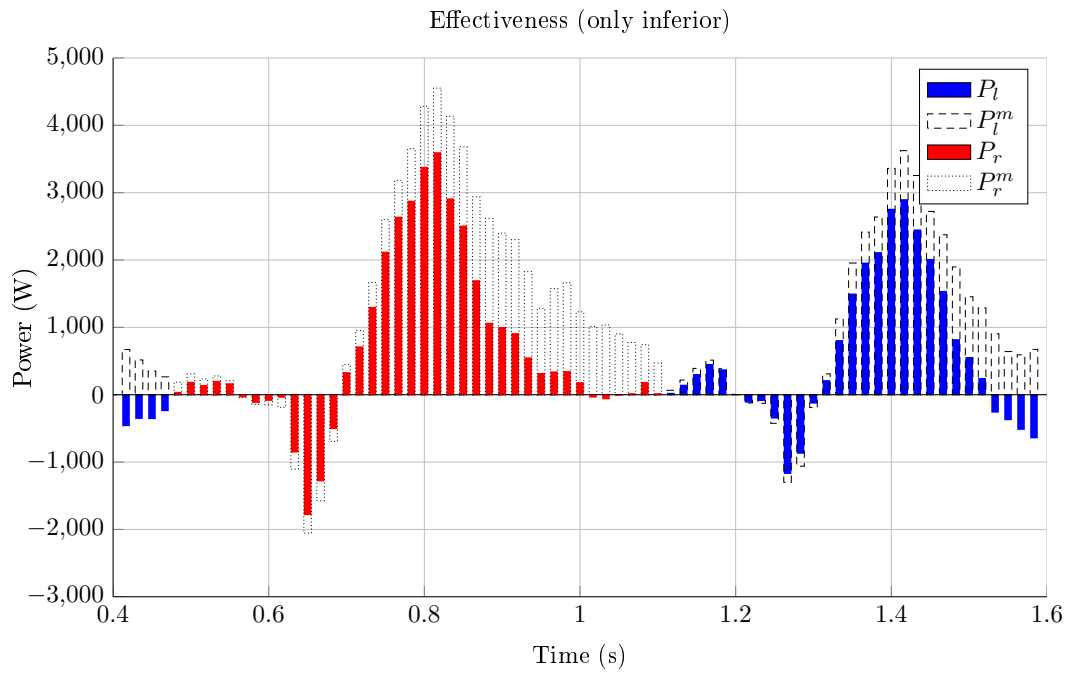


(c) Case 3a - Inverse dynamics results

Figure 5.21: Case 3a - Results

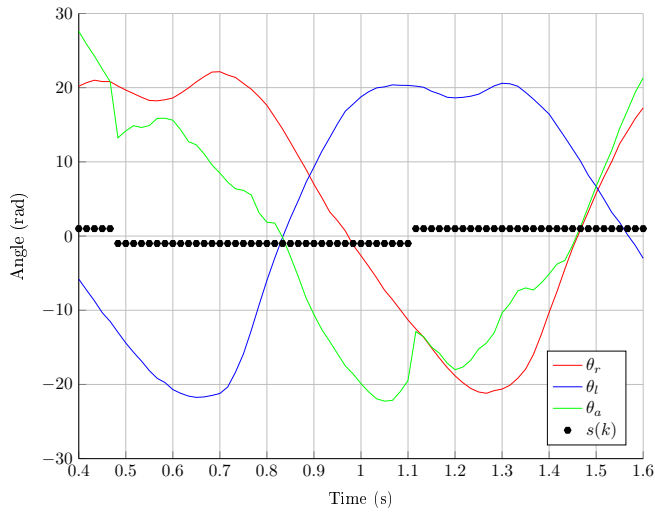


(a) Case 3a – Generated power (positive torque)

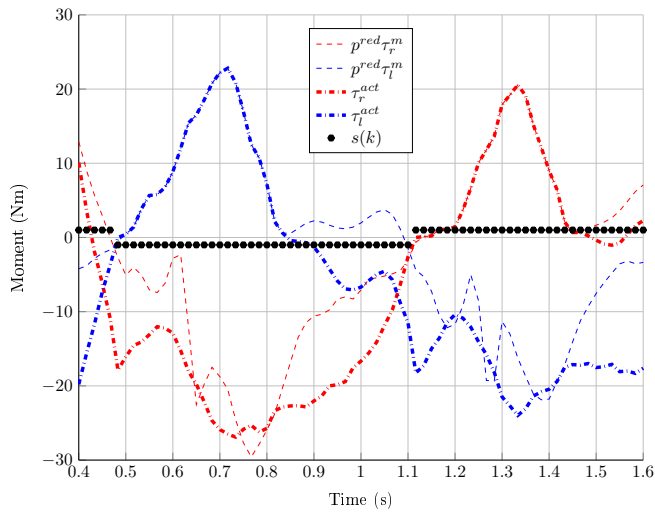


(b) Case 3a – Generated power (negative torque)

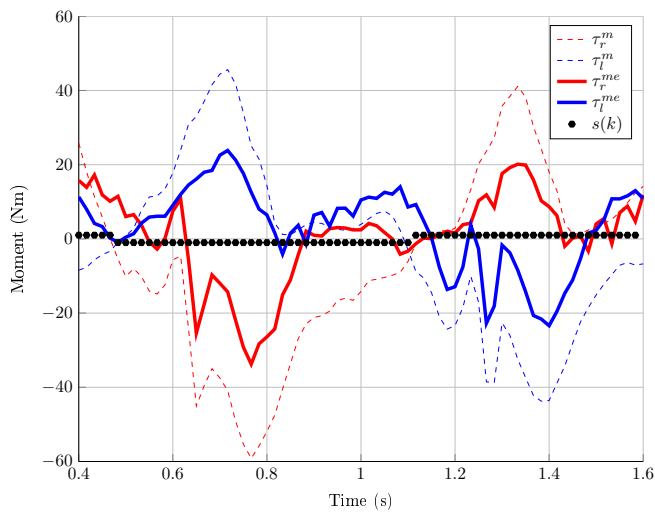
Figure 5.22: Case 3a – Generated power



(a) Case 3b – Actuator angle command

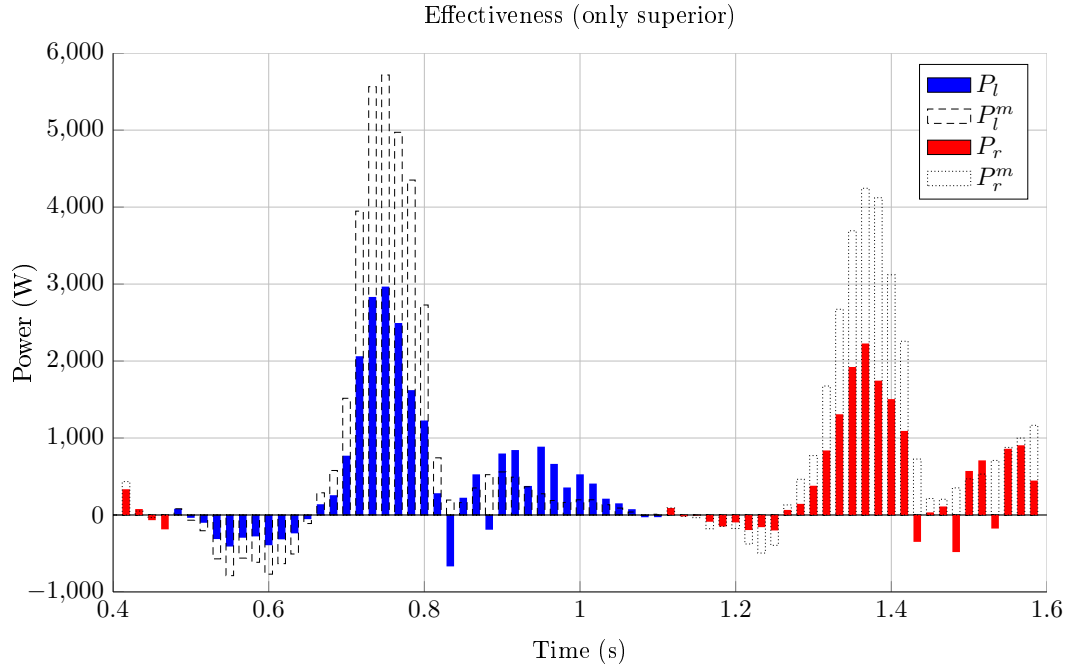


(b) Case 3b – Applied torques

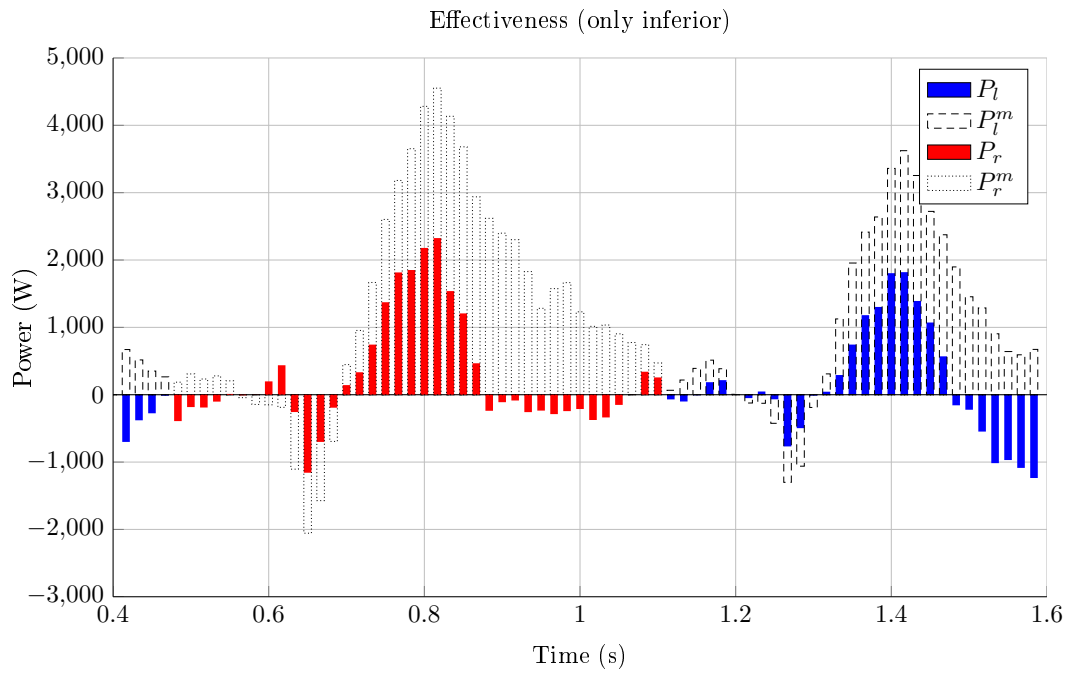


(c) Case 3b – Inverse dynamics results

Figure 5.23: Case 3b – Results

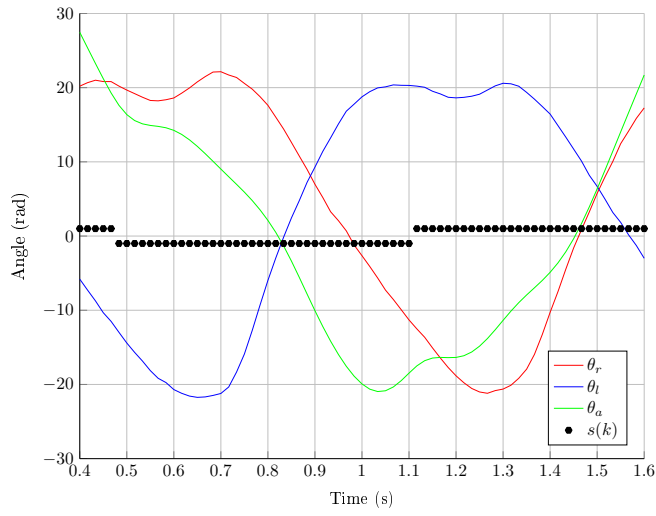


(a) Case 3b – Generated power (positive torque)

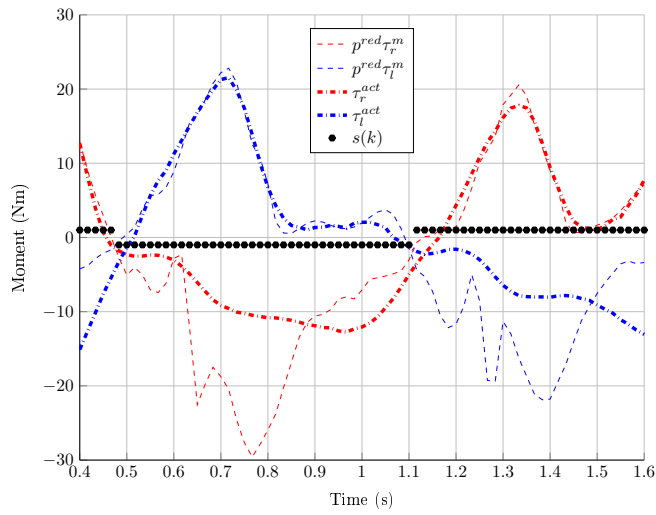


(b) Case 3b – Generated power (negative torque)

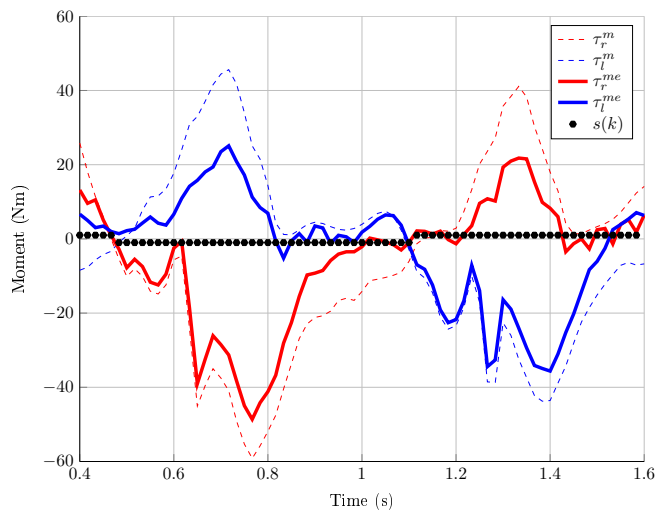
Figure 5.24: Case 3b – Generated power



(a) Case 4a - Actuator angle command

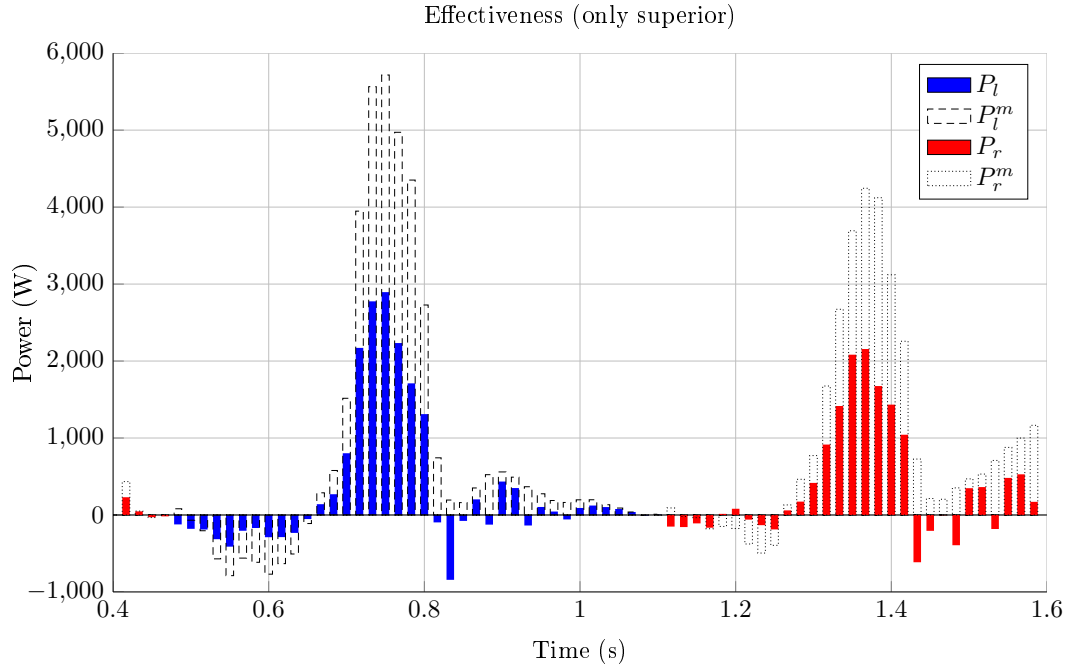


(b) Case 4a - Applied torques

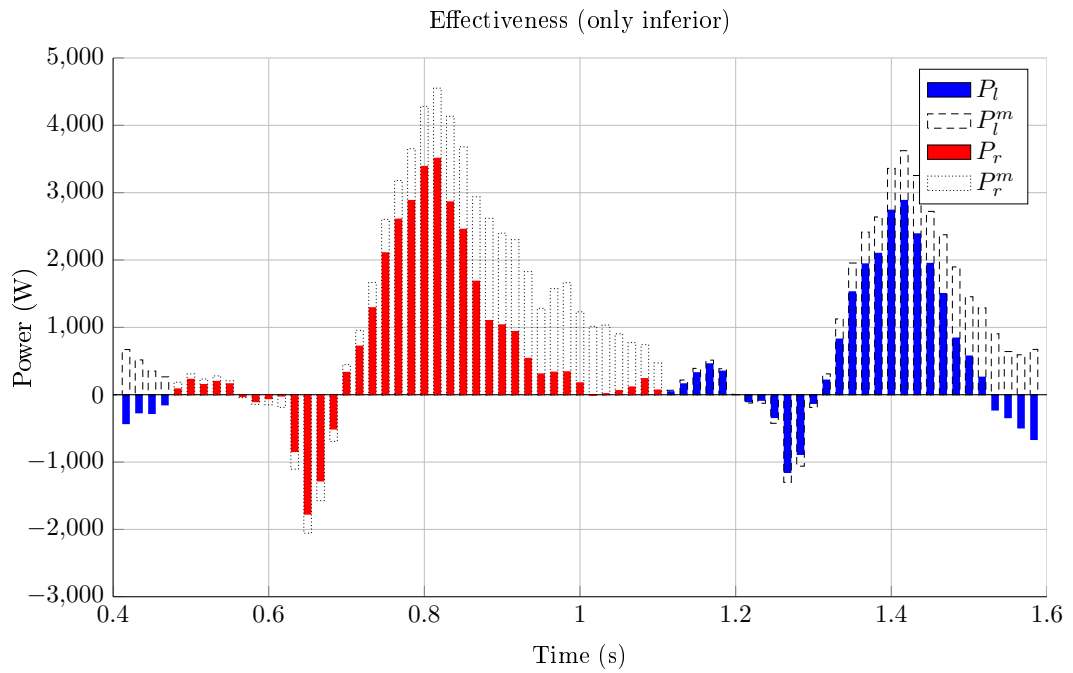


(c) Case 4a - Inverse dynamics results

Figure 5.25: Case 4a - Results

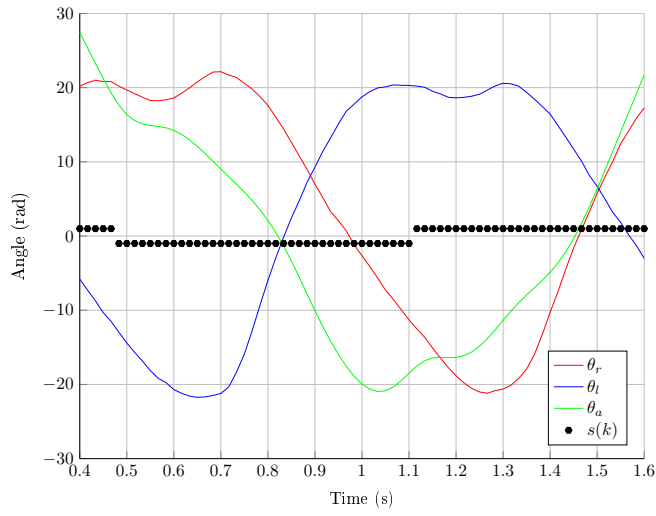


(a) Case 4a – Generated power (positive torque)

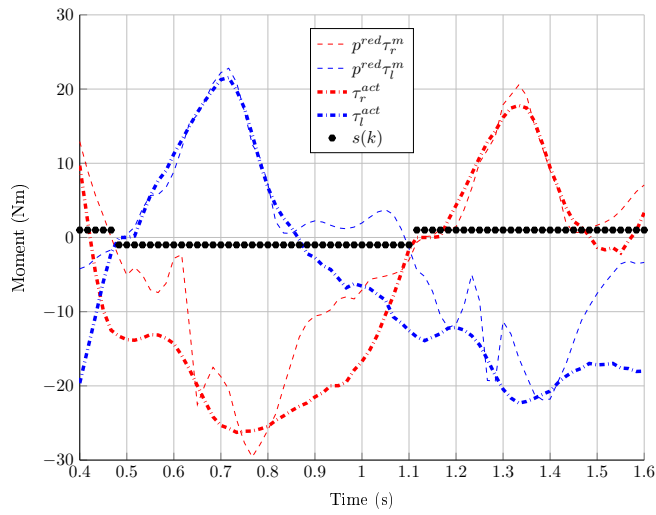


(b) Case 4a – Generated power (negative torque)

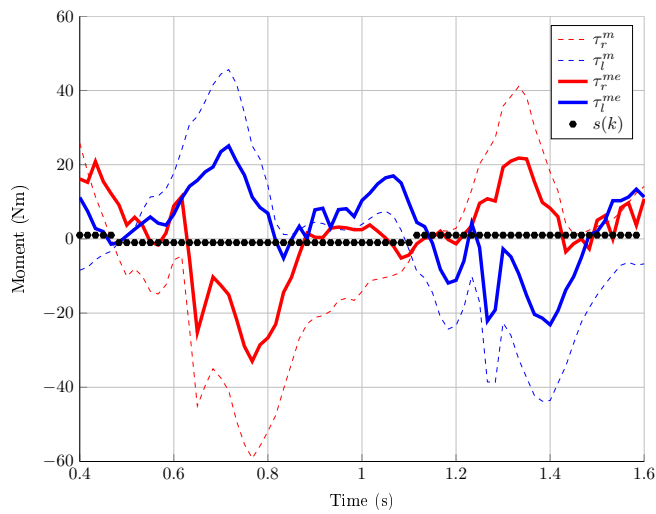
Figure 5.26: Case 4a – Generated power



(a) Case 4b – Actuator angle command

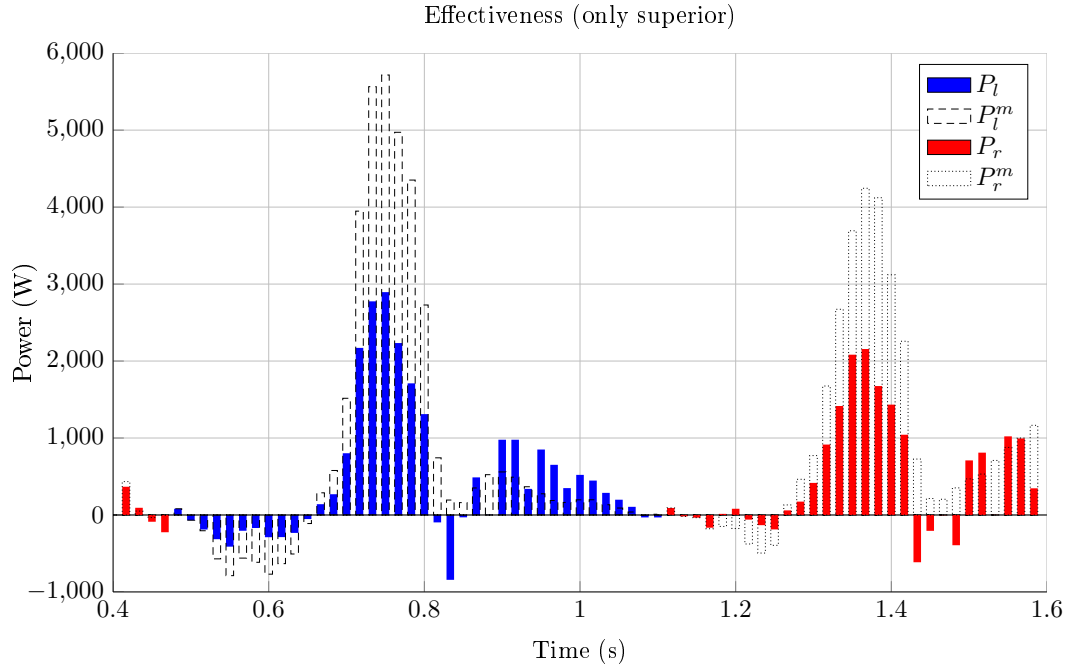


(b) Case 4b – Applied torques

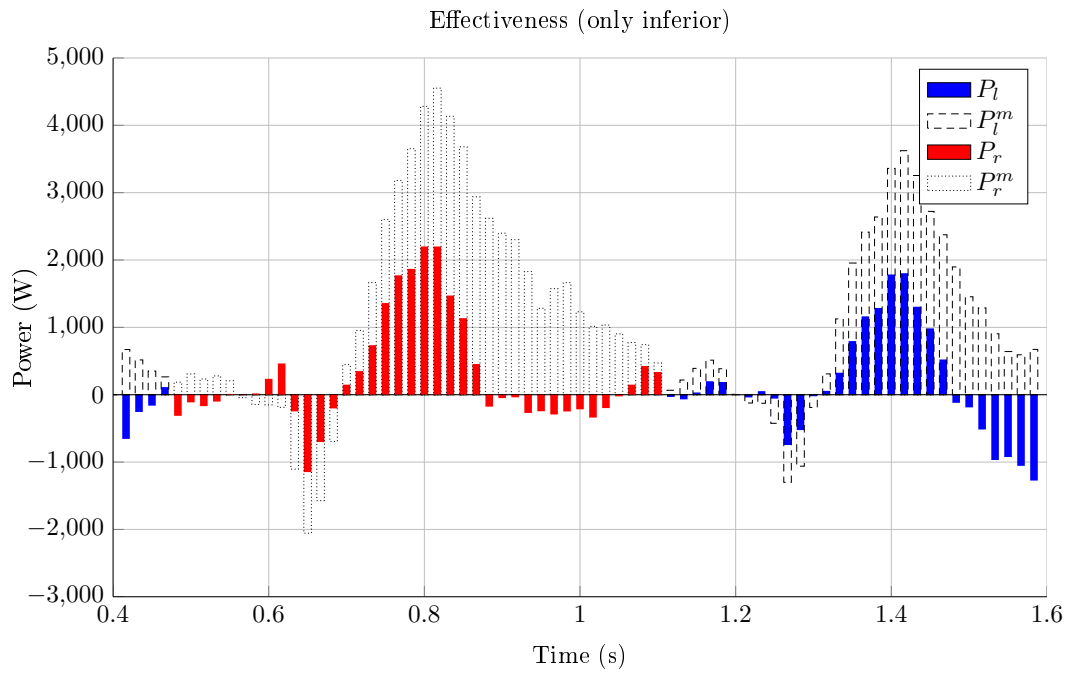


(c) Case 4b – Inverse dynamics results

Figure 5.27: Case 4b – Results

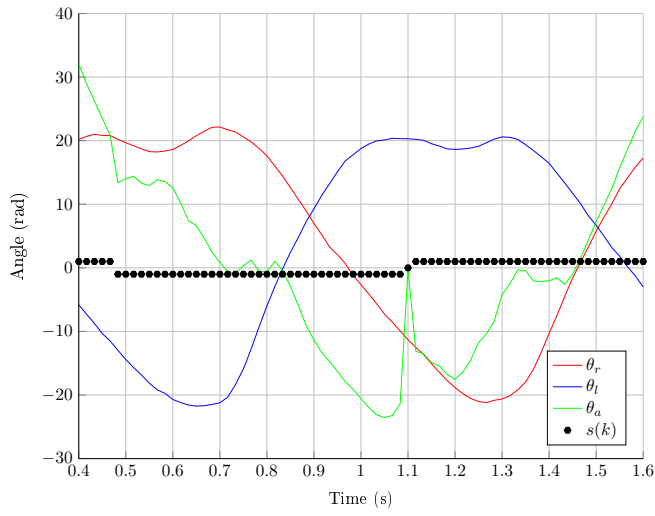


(a) Case 4b – Generated power (positive torque)

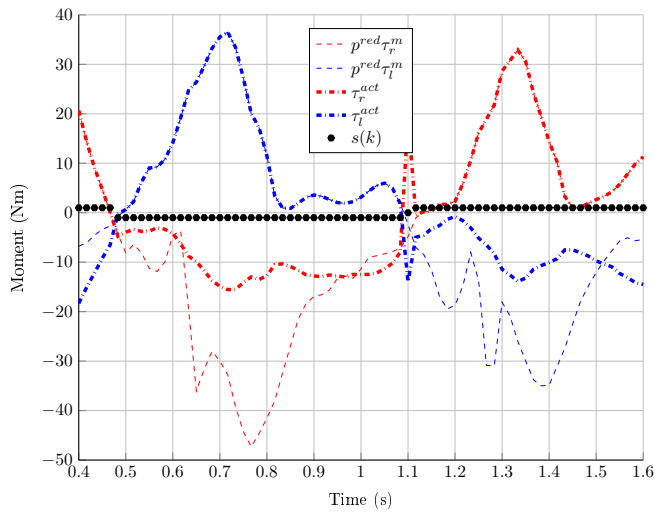


(b) Case 4b – Generated power (negative torque)

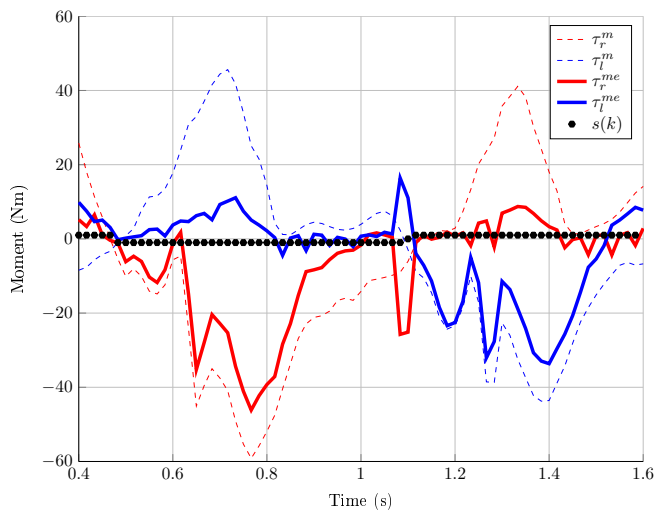
Figure 5.28: Case 4b – Generated power



(a) Case 5a - Actuator angle command

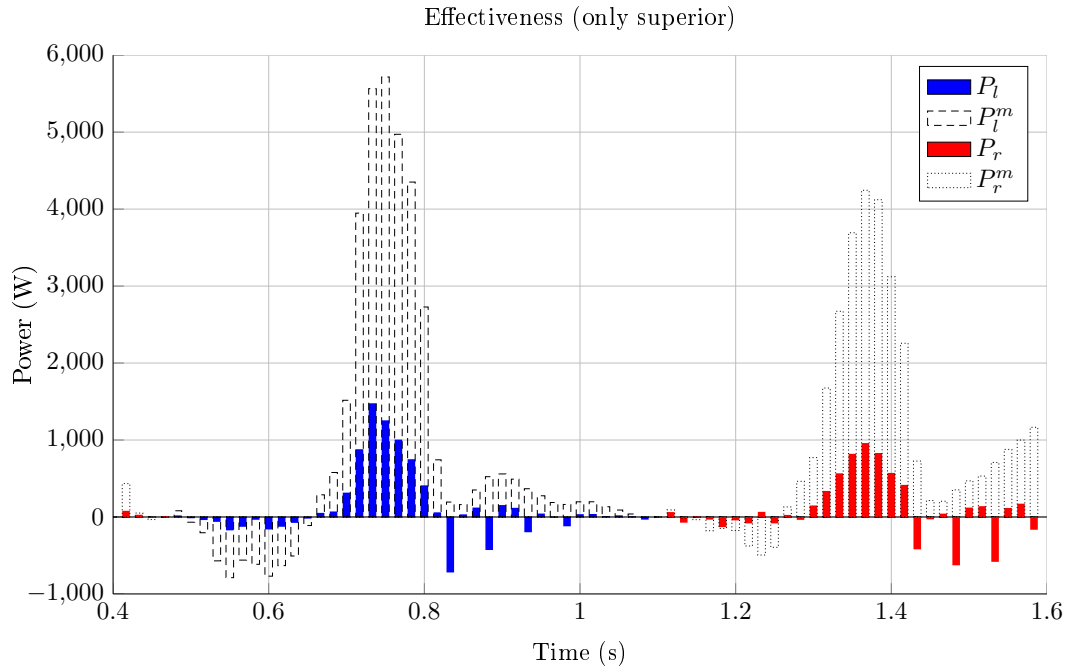


(b) Case 5a - Applied torques

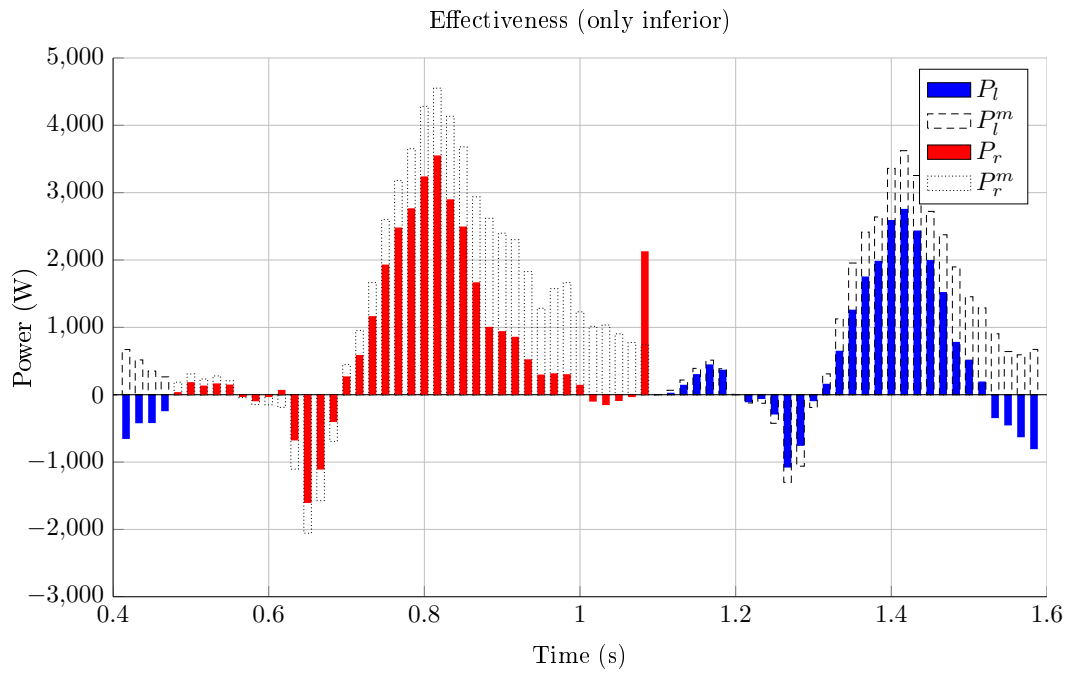


(c) Case 5a - Inverse dynamics results

Figure 5.29: Case 5a - Results

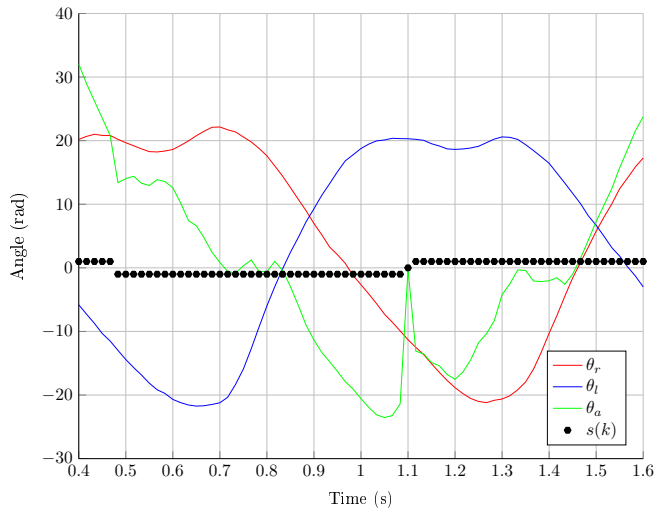


(a) Case 5a – Generated power (positive torque)

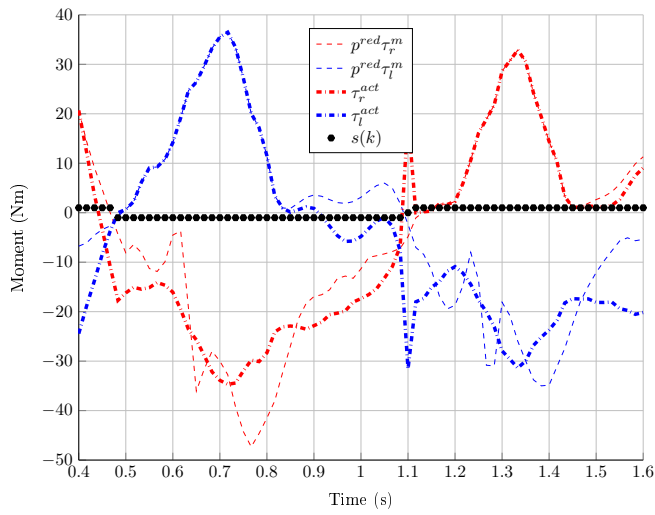


(b) Case 5a – Generated power (negative torque)

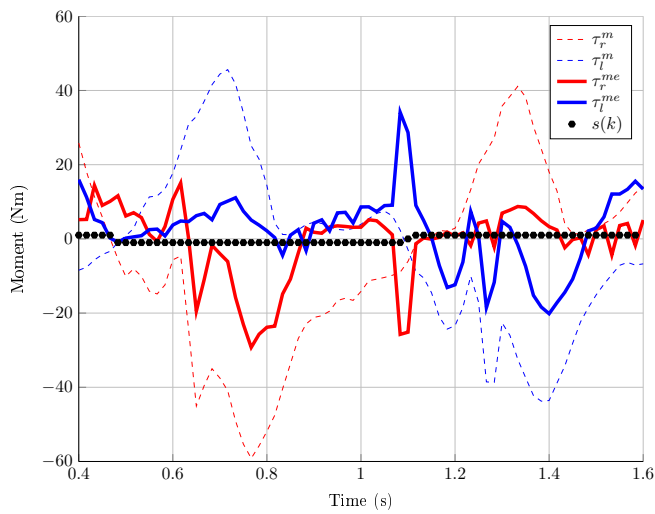
Figure 5.30: Case 5a – Generated power



(a) Case 5b – Actuator angle command

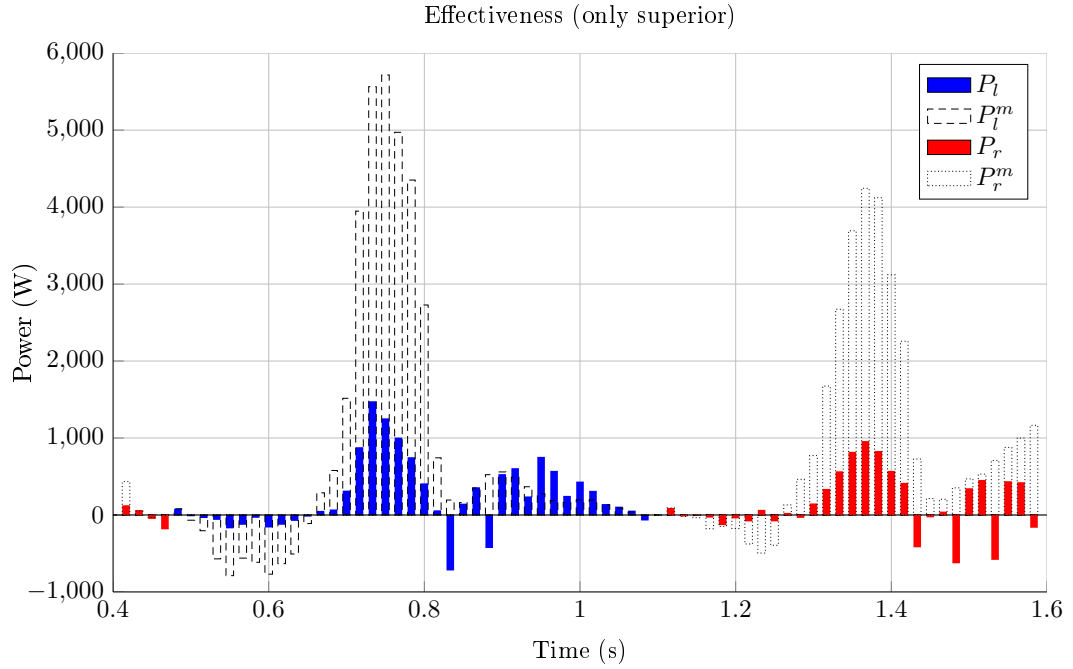


(b) Case 5b – Applied torques

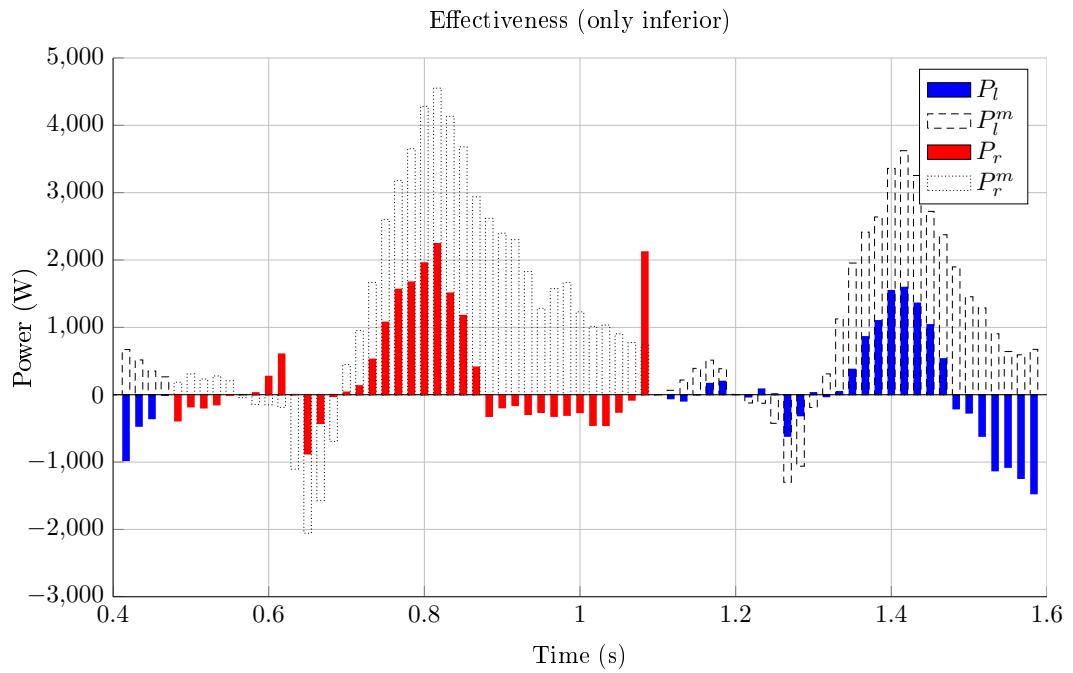


(c) Case 5b – Inverse dynamics results

Figure 5.31: Case 5b – Results

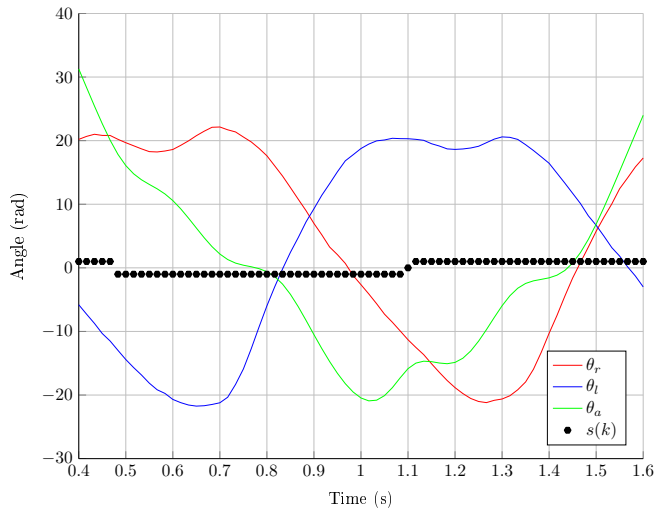


(a) Case 5b – Generated power (positive torque)

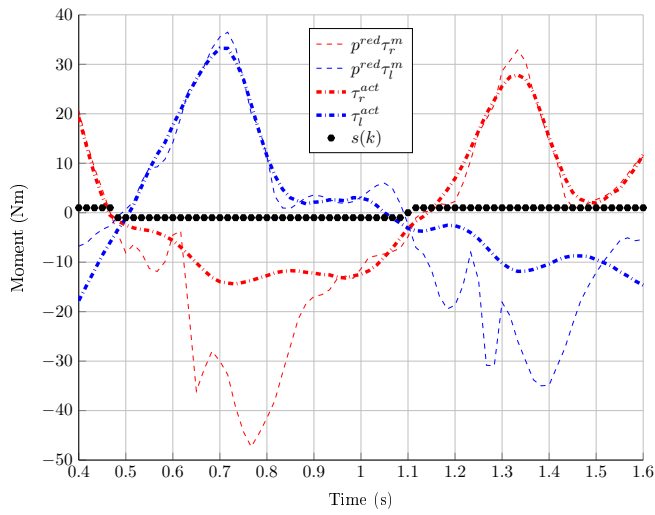


(b) Case 5b – Generated power (negative torque)

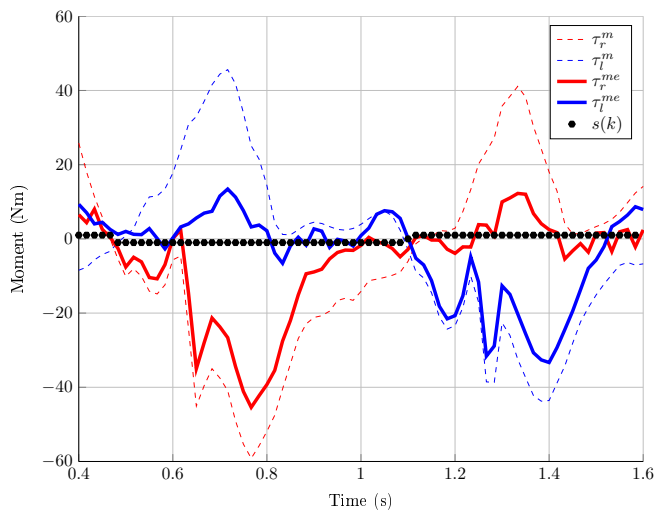
Figure 5.32: Case 5b – Generated power



(a) Case 6a – Actuator angle command

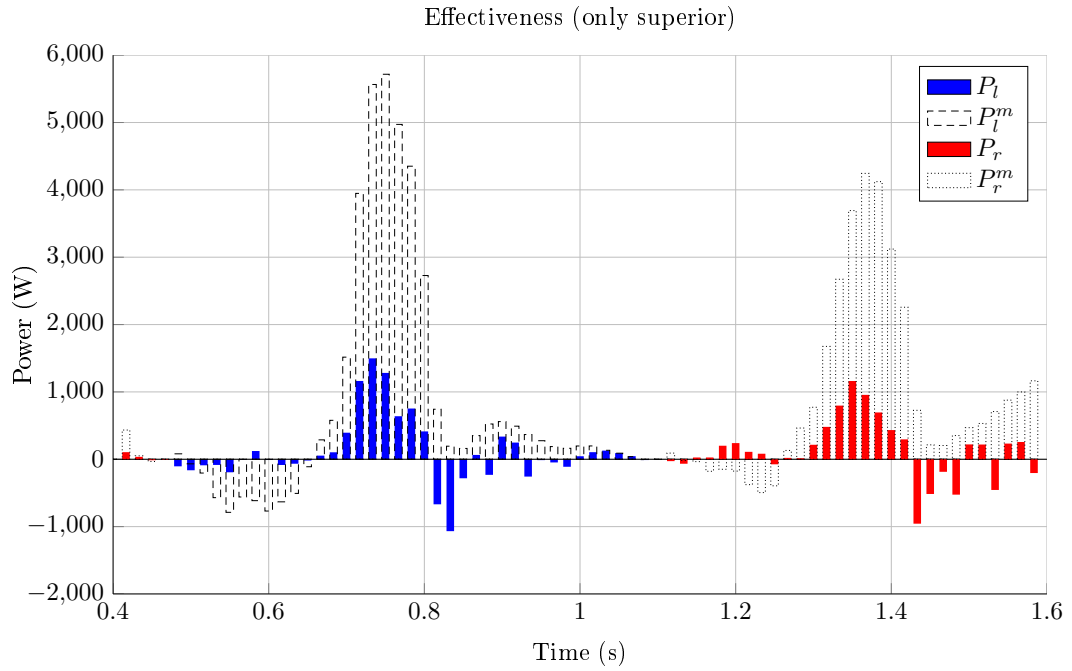


(b) Case 6a – Applied torques

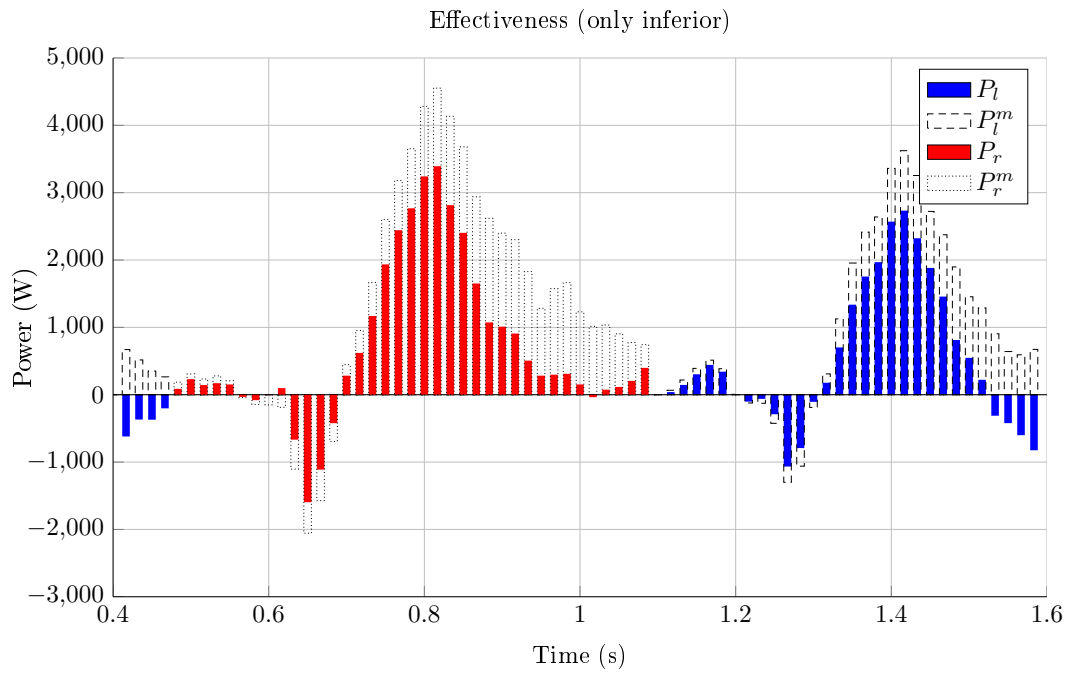


(c) Case 6a – Inverse dynamics results

Figure 5.33: Case 6a – Results

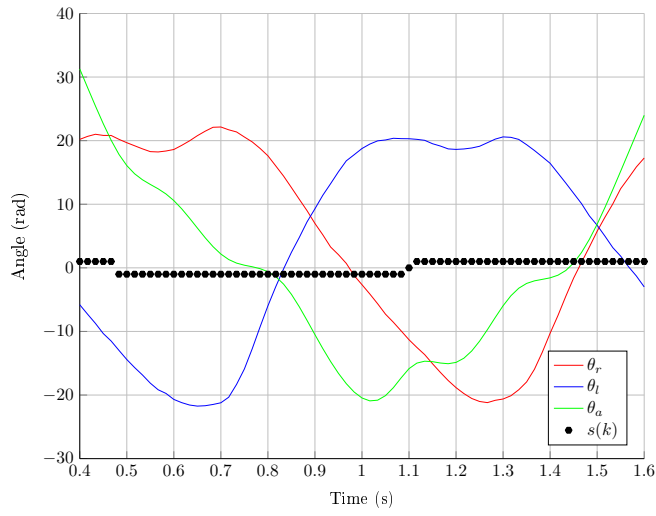


(a) Case 6a – Generated power (positive torque)

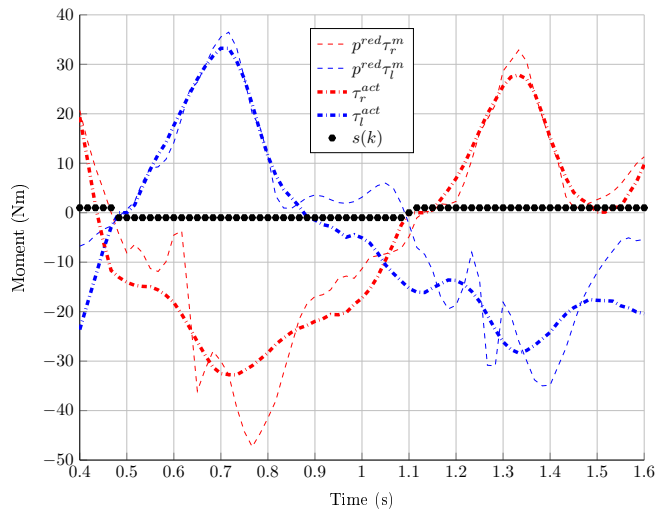


(b) Case 6a – Generated power (negative torque)

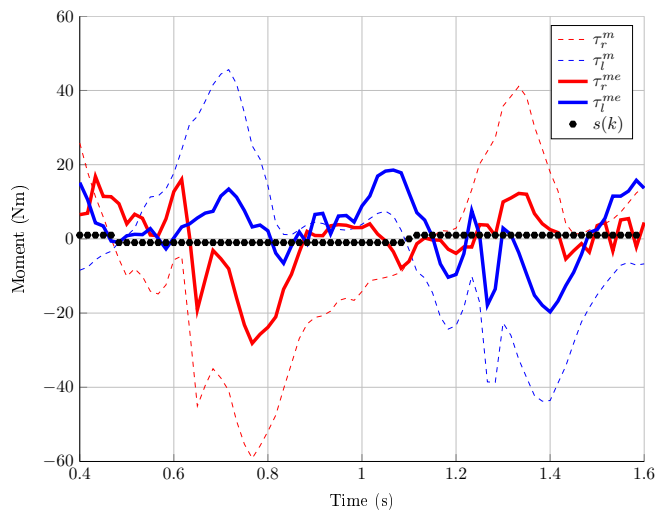
Figure 5.34: Case 6a – Generated power



(a) Case 6b – Actuator angle command



(b) Case 6b – Applied torques



(c) Case 6b – Inverse dynamics results

Figure 5.35: Case 6b – Results

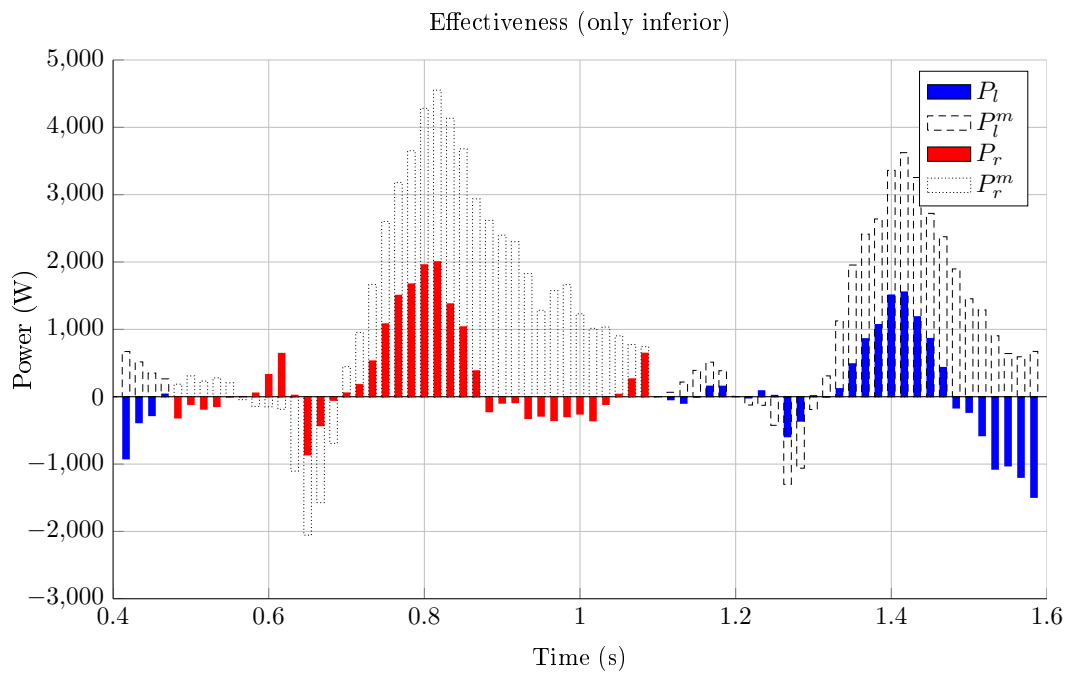
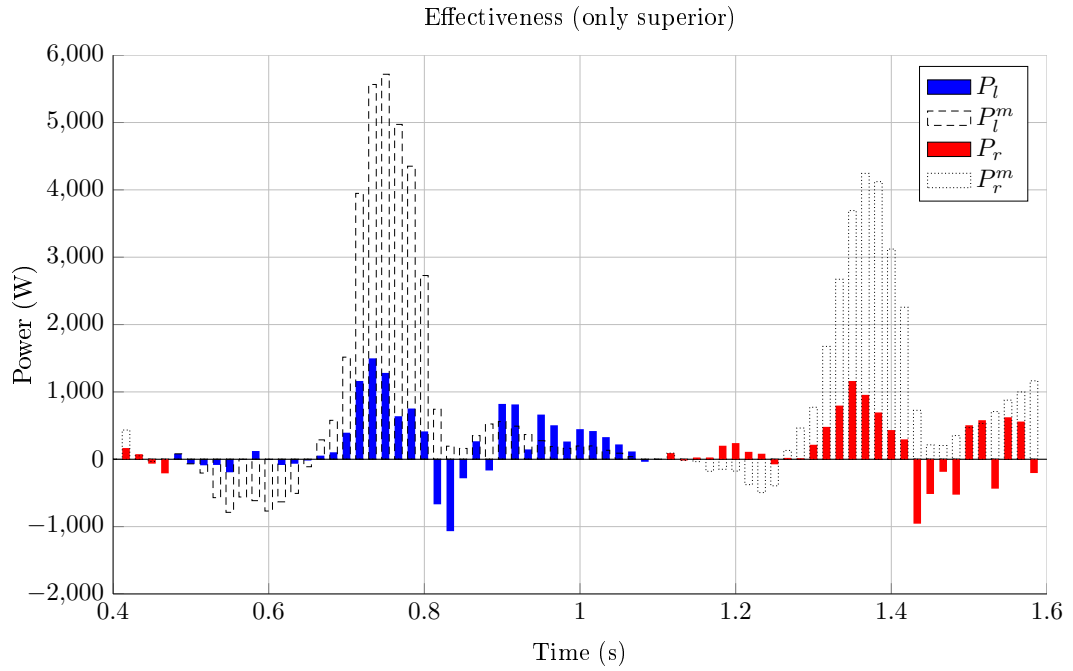


Figure 5.36: Case 6b – Generated power

5.4 Discussion

In this section the previously presented results will be discussed. The test cases for the *angular* model will be distinguished from the ones for the *extended* angular model.

5.4.1 Discussion of the *angular* model validation

The graph of figure 5.37 shows the summary results of the *angular* model validation with respect to the user energy expense. For the considered task, the work done by the muscles is always decreased of a factor that is proportional to the reduction factor used: in theory, if we have a reduction factor on the input torques of p^{red} , the effectiveness factor η_l or η_r should be less or equal to $1 - p^{red}$. The theoretical results are reflected in simulation for reduction factors of 0.3 and 0.5, where sometimes the effectiveness factor is even lower than expectations (so more effective), while for a reduction factor of 0.8, although we still have a decrease, the results show that the effectiveness factor is up to half times higher than theory (so less effective than expected). As regards the tracking error between the reference and the applied torques, looking at the table 5.2 we can see that it is always less than 1.6 Nm for the left side and 2.3 Nm for the right side. Given that the maximum value for the references is about 35 Nm, we can consider this a good result. Another important observation is that if we smooth the angle commands, the tracking error values most often are higher than the corresponding *not* smoothed test, while for the energy values the smoothed test is similar or worse than the *not* smoothed test.

If we look at the power graphs we see that, even if we have an overall decrease of the energy consumption, in some cases the muscles must counteract the exoskeleton, producing a sort of braking power opposite in sign to the one generated without the exoskeleton. This occurs occasionally in the test cases with a reduction factor of 0.3 and 0.5, but it is more frequent when the reduction factor is 0.8. From the point of view of motor learning this is an issue, because we do not limit our action to reduce the force the user must generate, but we also force the user to a muscle activation pattern different from the normal one we want to teach him.

5.4.2 Discussion of the *extended* angular model validation

The graphs of figures 5.38 and 5.39 show the summary results of the *extended* angular model validation with respect to the user energy expense. For the considered task, the work done by the muscles is always decreased of a factor that is proportional to the reduction factor used, as for the *angular* model. Also for this model, while giving positive torques the theoretical results are reflected in simulation for reduction factors of 0.3 and 0.5, but for a reduction factor of 0.8, although we still have a decrease, the results show that the effectiveness factor is up to half times higher than theory (so less effective than expected). Instead, the decrease of the energy for the negative torques, seems not to be influenced by the reduction factor, but only by the pulleys radii: when the radii are increased, the effectiveness factor is almost reduced of an half. The energy quantities show two different trends: the “*a*” test cases, the ones with both lower radii set to 1.0 m, have energy expense for the positive torques lower than

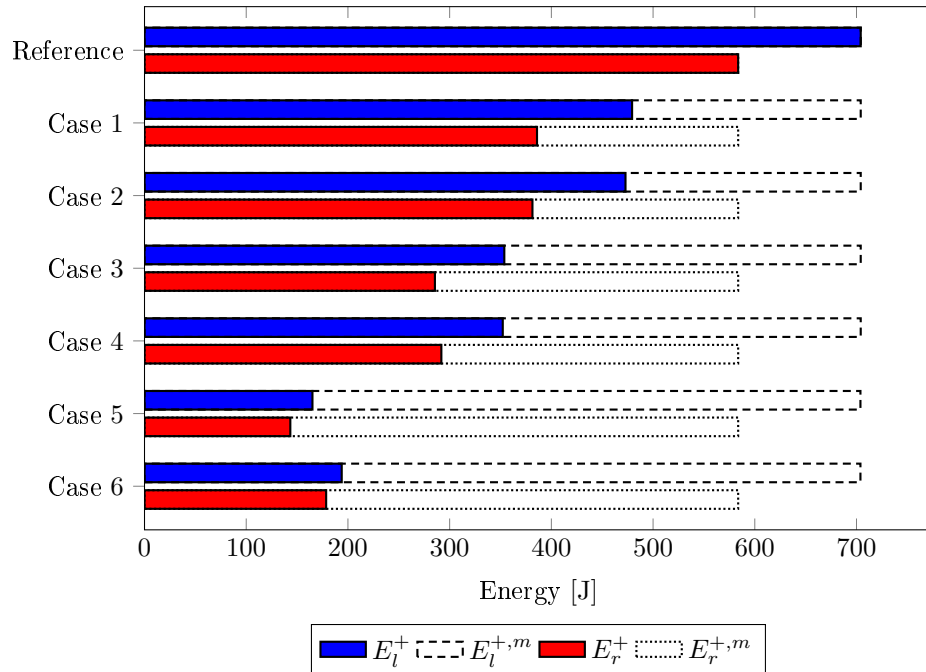


Figure 5.37: Summary results – *angular* model

the “*b*” test cases, the ones with both lower radii set to 1.5 m. On the other hand, the “*b*” test cases have energy expense lower than the “*a*” tests for the negative torques. As regards the tracking error between the reference and the applied torques, looking at the tables 5.5 and 5.6, we can see that it is always higher with respect to the base model, for both the sides. Also for this quantity, the values show two different trends: the “*a*” test cases have a tracking error comprised between 5.0 Nm and 7.0 Nm for the left side and 6.0 Nm and 8.1 Nm for the right side; the “*b*” test cases have a tracking errors that is higher, almost double, than the other group, comprised between 11.3 Nm and 14.6 Nm for the left side and 13.1 Nm and 16.4 Nm for the right side. Given that the maximum value for the references is about 35 Nm, we can not consider this a good result. Another important observation is that if we smooth the angle commands, the tracking error values are slightly lower than the corresponding *not* smoothed test, while for the energy values the smoothed test is similar or worst than the *not* smoothed test, as in the *angular* model.

In this model too, if we look at the power graphs we see that in some cases the muscles must counteract the exoskeleton, producing a braking power, but there are also some cases such that the power generated with the enabled exoskeleton is greater in module than the one generated without the exoskeleton, although having the same sign. The occurrence of the braking power is the same as the *angular* model. The second issue always happens when we have the lower elastic bands radii set to 1.5 m and only while giving positive torques to the joints. It never occurs in the other test cases, except to the test case 5a because of the failure in choosing which joint follow: this problem is solved by the smoothed

version of this test case, i.e. 6a. From the point of view of motor learning this second situation is not an issue, but for the reduction of required force it is.

5.5 Conclusion

This chapter presented the results of the validation of the proposed actuator. The methodology adopted has been described in the chapter 4; this chapter specified the test cases and the measurement accomplished. The results, as stated in section 5.4, show that the adopted solution for the *angular* model is effective for the task considered. This is encouraging for the feasibility of the model. However, the results for the *extended* angular model are not as good as the ones for the base model, but there is room for improvement. It is a good starting point, but it still needs investigations.

There is also a need for extending the results, by considering different walking tasks, other from the one considered for the test cases. Indeed, the exoskeleton should show its effectiveness in many and different types of walking, so as to exhibit adaptability. This will be a requirement to build a real implementation.

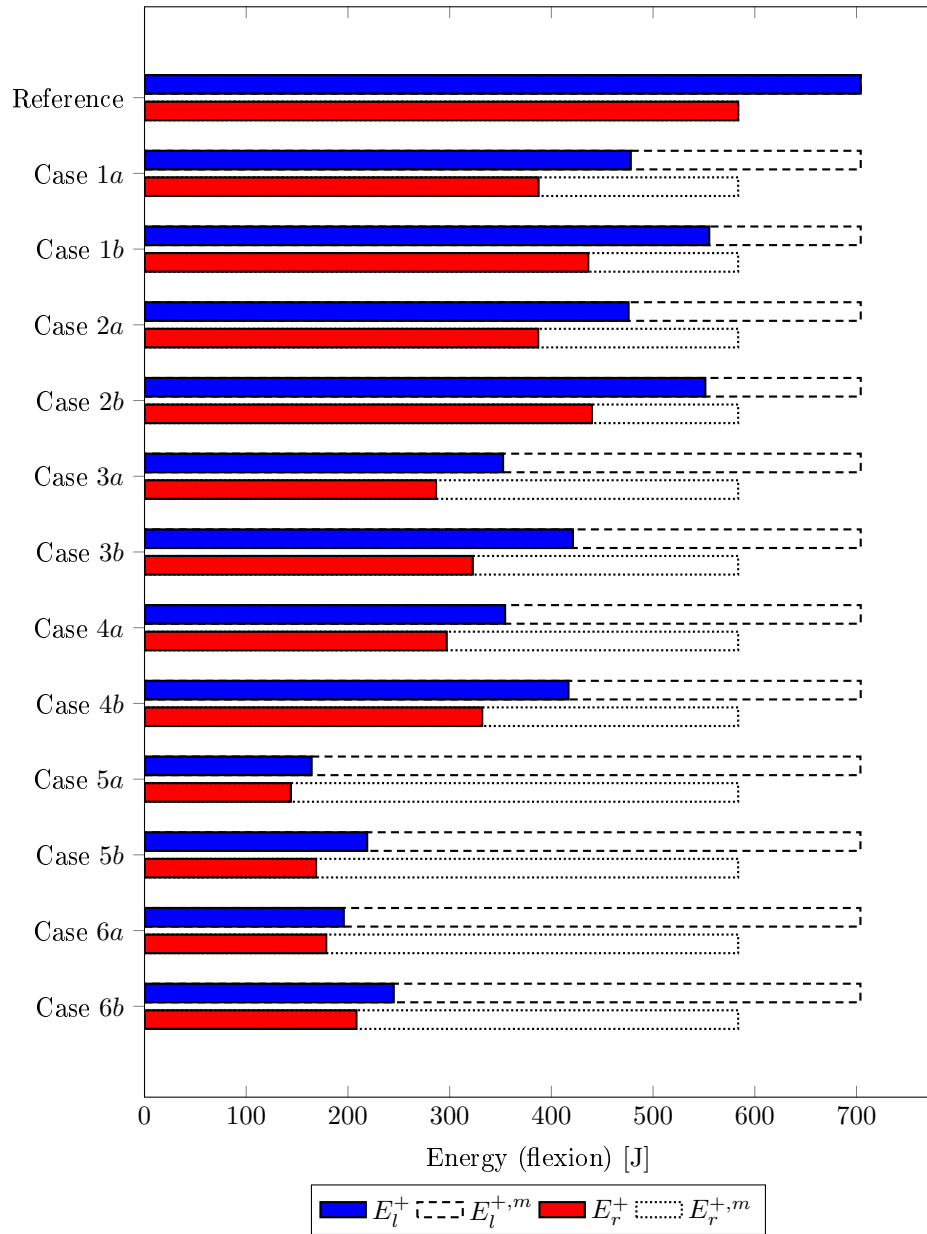


Figure 5.38: Summary results (flexion) – *extended* angular model

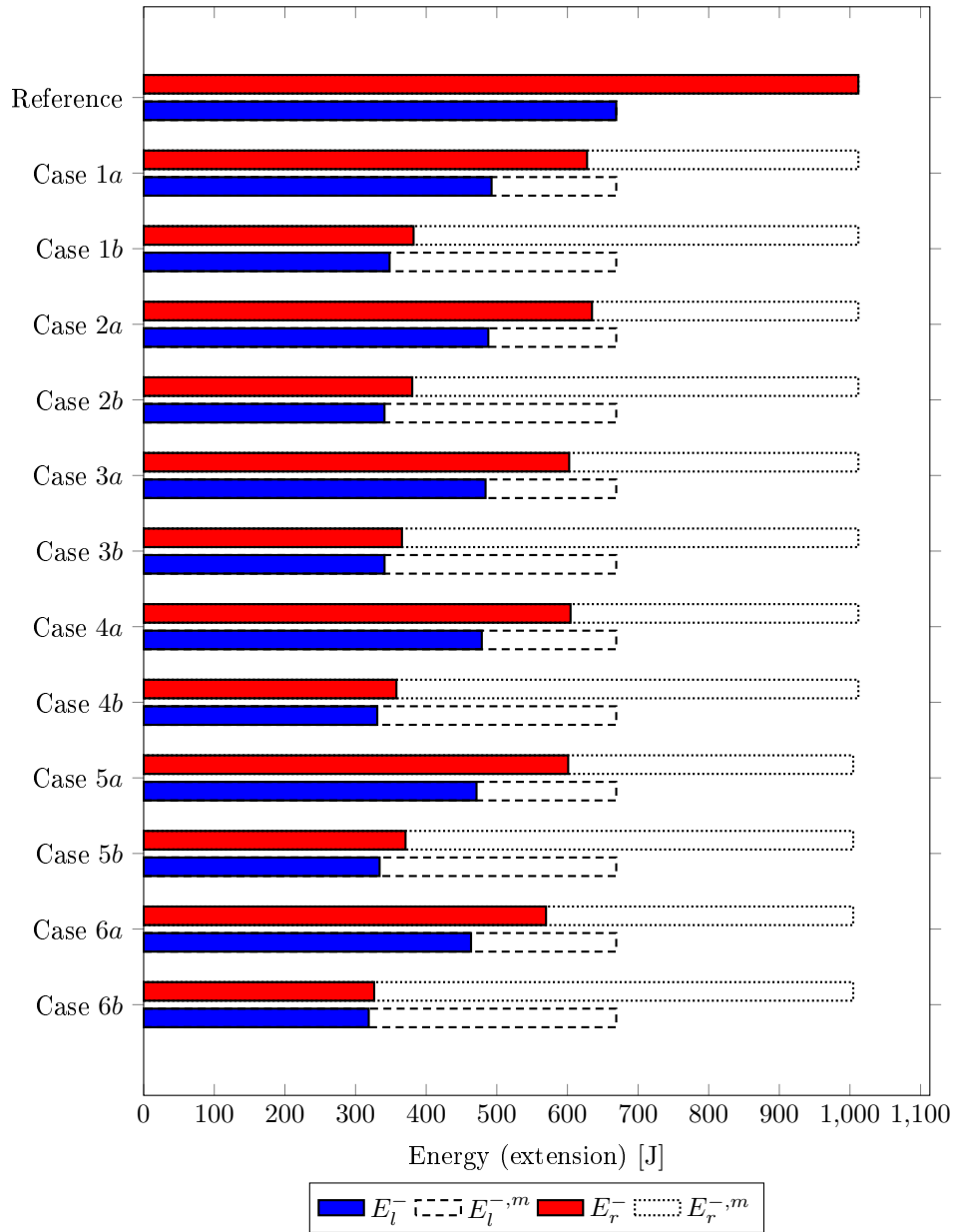


Figure 5.39: Summary results (extension) – *extended* angular model

Conclusions and future work

The purpose of this thesis was to show that it is possible to design a mechanical structure that using a *single* rotational electric motor is able to actuate the hip of an exoskeleton. Moreover, it is by using an elastic actuator, so that we can have a compliant interaction with the user of the exoskeleton.

In this project we were only interested in the design and validation of a mechanical model that could be controlled by means of a single actuator, leaving the definition of a proper control strategy to further developments. The proposed actuation system receives the torque command from the control layer and then, knowing the positions of the two joints left free to follow their trajectories, it controls the single actuator to give the desired torques to the controlled joints. The two models that have been developed and validated are the *angular* that only gives positive torques to the two joints, and the *extended* angular that tries to give both positive and negative torques, being controlled only for the positive one.

The proposed single actuator exoskeleton has been validated by simulating it with the OPENSIM simulator [66]. This is a biomechanical simulator developed at the Stanford University that allows to simulate a complex body model. This simulator provides two main analysis: the first one is a forward dynamics analysis, that given the muscle excitation commands, returns the resulting generalized force at the joints in each time frame, from which it is possible to compute the resulting movement. The second is an inverse dynamics analysis, that given the joints' positions in each frame, returns the generalized forces generated at each joint by the muscles that are needed to produce the movement, also taking into account the presence of external forces, if any. This simulator has been used to validate the proposed actuator. The exoskeleton has been simulated coupled with the model of the lower limbs of the human body for a walking task, using a movement based on real data of a normal gait. Then,

using an inverse dynamics analysis, the forces generated by the muscles with and without the contribution of the exoskeleton will be compared.

The results of these simulations has shown that the energy generated by the muscles with the enabled exoskeleton, was less than the one without external help: this make us confident of the effectiveness of the solution.

The future prospective of this work is to apply it to some real exoskeletons, such as the one developed by Andrea Calanca and others [11]. Nevertheless, the principle of this work could be applied to a large variety of exoskeletons and it could probably be extended in order to control with a single actuator not only the two hip joints, but also others, like the knee or ankle ones. Further work must be done in order to achieve the result of a real implementation of this actuator: the models must be validated with respect to other data of walking tasks to be sure that it would work in many conditions. The abstract mathematical models would have to be extended in such a way that some of the assumptions could be relaxed. Moreover, the *extended* angular model would have to be more analysed to work better, maybe changing the control law in a way that it could mediate between the correct application of the positive torques and of the negative torques.

Bibliography

- [1] Abhishek Agrawal, Sai K Banala, Sunil K Agrawal, and Stuart A Binner-macleod. “Design of a Two Degree-of-freedom Ankle-Foot Orthosis for Robotic Rehabilitation”. In: *Rehabilitation Robotics, 2005. ICORR 2005. 9th International Conference on* (2005), pp. 41–44.
- [2] Argomedtec. URL: <http://www.argomedtec.com/>.
- [3] Alan T. Asbeck, Robert J. Dyer, Arnar F. Larusson, and Conor J. Walsh. “Biologically-inspired soft exosuit”. In: *IEEE International Conference on Rehabilitation Robotics* June (2013), pp. 1–8. ISSN: 19457898. DOI: [10.1109/ICORR.2013.6650455](https://doi.org/10.1109/ICORR.2013.6650455).
- [4] Alan T. Asbeck, Kai Schmidt, and Conor J. Walsh. “Soft exosuit for hip assistance”. In: *Robotics and Autonomous Systems* (2014). ISSN: 09218890. DOI: [10.1016/j.robot.2014.09.025](https://doi.org/10.1016/j.robot.2014.09.025).
- [5] Ruth Nancy Barker, Sandra Brauer, and Richard Carson. “Training-induced changes in the pattern of triceps to biceps activation during reaching tasks after chronic and severe stroke.” In: *Experimental Brain Research* 196.4 (2009), pp. 483–496.
- [6] Berkeleybionics. URL: <http://berkeleybionics.com/>.
- [7] Ekso Bionics. URL: <http://intl.eksobionics.com/>.
- [8] Rex Bionics. URL: <http://www.rexbionics.com/>.
- [9] Joaquin Blaya and Hugh Herr. “Adaptive control of a variable-impedance ankle-foot orthosis to assist drop-foot gait.” In: *IEEE transactions on neural systems and rehabilitation engineering : a publication of the IEEE Engineering in Medicine and Biology Society* 12.1 (Mar. 2004), pp. 24–31. ISSN: 1534-4320. DOI: [10.1109/TNSRE.2003.823266](https://doi.org/10.1109/TNSRE.2003.823266).
- [10] A. Calanca, S Piazza, and P Fiorini. “Force Control System for Pneumatic Actuators of an Active Gait Orthosis”. In: *Biomedical Robotics and Biomechanics (BioRob), 2010 3rd IEEE RAS and EMBS International Conference on. 26-29 Sep, 849-854, 2010*. Tokyo, 2010, pp. 64–69.
- [11] Andrea Calanca, Stefano Piazza, and Paolo Fiorini. “A Motor Learning Oriented, Compliant and Mobile Gait Orthosis”. In: *Appl. Bionics Biomechanics* (Jan. 2012).

- [12] C.P. Chou and B. Hannaford. “Measurement and Modeling of McKibben Pneumatic Artificial Muscles”. In: *IEEE Transactions on Robotics and Automation* 12.1 (1996), pp. 90–102.
- [13] Ed Colgate and Neville Hogan. “An Analysis of Contact Instability in Terms of Passive Analysis of Lumped Models Coupled Performance”. In: *Proceedings of the IEEE* (1989).
- [14] Steve Collins, Andy Ruina, Russ Tedrake, and Martijn Wisse. “Efficient bipedal robots based on passive-dynamic walkers”. In: *Science (New York, N.Y.)* 307.5712 (Feb. 2005), pp. 1082–5. ISSN: 1095-9203. DOI: [10.1126/science.1107799](https://doi.org/10.1126/science.1107799).
- [15] Frank Daerden and Dirk Lefeber. “Pneumatic Artificial Muscles: actuators for robotics and automation”. In: *European journal of mechanical and environmental engineering* 47.1 (2002), pp. 11–21.
- [16] Brian Dellon and Yokyo Matsuoka. “Prosthetics, exoskeletons, and rehabilitation [Grand challenges of robotics]”. In: *IEEE Robotics and Automation Magazine* 14.1 (2007), pp. 30–34. ISSN: 10709932. DOI: [10.1109/MRA.2007.339622](https://doi.org/10.1109/MRA.2007.339622).
- [17] S.L. Delp, F.C. Anderson, A.S. Arnold, P. Loan, A. Habib, C.T. John, E. Guendelman, and D.G. Thelen. “OpenSim: Open-Source Software to Create and Analyze Dynamic Simulations of Movement”. In: *Biomedical Engineering, IEEE Transactions on* 54.11 (Nov. 2007), pp. 1940–1950. ISSN: 0018-9294. DOI: [10.1109/TBME.2007.901024](https://doi.org/10.1109/TBME.2007.901024).
- [18] Ye Ding, Ignacio Galiana, Alan Asbeck, Brendan Quinlivan, Stefano Marco Maria De Rossi, Conor Walsh, Stefano Marco, and Maria De Rossi. “Multi-joint actuation platform for lower extremity soft exosuits”. In: *2014 IEEE International Conference on Robotics and Automation (ICRA)* (2014), pp. 1327–1334. DOI: [10.1109/ICRA.2014.6907024](https://doi.org/10.1109/ICRA.2014.6907024).
- [19] Aaron M. Dollar and Hugh Herr. “Lower Extremity Exoskeletons and Active Orthoses: Challenges and State-of-the-Art”. In: *IEEE Transactions on Robotics* 24.1 (2008), pp. 144–158. ISSN: 1552-3098. DOI: [10.1109/TR0.2008.915453](https://doi.org/10.1109/TR0.2008.915453).
- [20] R. Ekkelenkamp, J. Veneman, and Herman van der Kooij. “LOPES : Selective Control of Gait Functions During the Gait Rehabilitation of CVA Patients”. In: *9th International Conference on Rehabilitation Robotics, 2005. ICORR 2005.* (2005), pp. 361–364. DOI: [10.1109/ICORR.2005.1501120](https://doi.org/10.1109/ICORR.2005.1501120).
- [21] Jeremy L Emken and David J Reinkensmeyer. “Robot-enhanced motor learning: accelerating internal model formation during locomotion by transient dynamic amplification.” In: *IEEE transactions on neural systems and rehabilitation engineering : a publication of the IEEE Engineering in Medicine and Biology Society* 13.1 (Mar. 2005), pp. 33–9. ISSN: 1534-4320. DOI: [10.1109/TNSRE.2004.843173](https://doi.org/10.1109/TNSRE.2004.843173).
- [22] Ryan J. Farris, Hugo A. Quintero, and Michael Goldfarb. “Preliminary evaluation of a powered lower limb orthosis to aid walking in paraplegic individuals”. In: *IEEE Transactions on Neural Systems and Rehabilitation Engineering* 19.6 (2011), pp. 652–659. ISSN: 15344320. DOI: [10.1109/TNSRE.2011.2163083](https://doi.org/10.1109/TNSRE.2011.2163083).

- [23] Daniel P Ferris, Keith E Gordon, Gregory S Sawicki, and Ammanath Peethambaran. “An improved powered ankle-foot orthosis using proportional myoelectric control.” In: *Gait & posture* 23.4 (June 2006), pp. 425–8. ISSN: 0966-6362. DOI: [10.1016/j.gaitpost.2005.05.004](https://doi.org/10.1016/j.gaitpost.2005.05.004).
- [24] Christian Fleischer and Günter Hommel. “Torque control of an exoskeletal knee with EMG signals”. In: *VDI BERICHTE* 1956 (2006), p. 79.
- [25] Christian Fleischer, Christian Reinicke, and Günter Hommel. “Predicting the intended motion with EMG signals for an exoskeleton orthosis controller”. In: *Intelligent robots and systems, 2005.(IROS 2005). 2005 IEEE/RSJ international conference on*. IEEE. 2005, pp. 2029–2034.
- [26] Francesco Giovacchini, Federica Vannetti, Matteo Fantozzi, Marco Cempini, Mario Cortese, Andrea Parri, Tingfang Yan, Dirk Lefeber, and Nicola Vitello. “A light-weight active orthosis for hip movement assistance”. In: *Robotics and Autonomous Systems* (2014). ISSN: 0921-8890. DOI: [10.1016/j.robot.2014.08.015](https://doi.org/10.1016/j.robot.2014.08.015).
- [27] Hugh Herr. “Exoskeletons and orthoses: classification, design challenges and future directions.” In: *Journal of neuroengineering and rehabilitation* 6 (2009), p. 21. ISSN: 1743-0003. DOI: [10.1186/1743-0003-6-21](https://doi.org/10.1186/1743-0003-6-21).
- [28] Kevin W Hollander, Thomas G Sugar, and Donald E Herring. “Adjustable Robotic Tendon using a “Jack Spring””. In: *Rehabilitation Robotics, 2005. ICORR 2005. 9th International Conference on*. IEEE. 2005, pp. 113–118. ISBN: 0780390032.
- [29] Chand T. John, Ajay Seth, Michael H. Schwartz, and Scott L. Delp. “Contributions of muscles to mediolateral ground reaction force over a range of walking speeds”. In: *Journal of Biomechanics* 45.14 (2012), pp. 2438–2443. ISSN: 0021-9290. DOI: [10.1016/j.jbiomech.2012.06.037](https://doi.org/10.1016/j.jbiomech.2012.06.037).
- [30] Takahiro Kagawa and Yoji Uno. “A human interface for stride control on a wearable robot”. In: 1. IEEE. 2009, pp. 4067–4072. ISBN: 9781424438044.
- [31] H. Kazerooni. “Hybrid Control of the Berkeley Lower Extremity Exoskeleton (BLEEX)”. In: *The International Journal of Robotics Research* 25.5-6 (May 2006), pp. 561–573. ISSN: 0278-3649. DOI: [10.1177/0278364906065505](https://doi.org/10.1177/0278364906065505).
- [32] K. Kong, H. Moon, B. Hwang, D. Jeon, and M. Tomizuka. “Impedance compensation of SUBAR for back-drivable force-mode actuation”. In: *Robotics, IEEE Transactions on* 25.3 (2009), pp. 512–521.
- [33] Roy Kornbluh, Ron Pelrine, Qibing Pei, Marcus Rosenthal, Scott Stanford, Neville Bonwit, Richard Heydt, Harsha Prahlad, and Subramanian V Shastri. “Application of dielectric elastomer EAP actuators”. In: *Artificial Muscles Reality, Potential and Challenges* (2001). Ed. by Eds. Bar-Cohen, pp. 457–503.
- [34] A.C. Lo et al. “Robot-assisted therapy for long-term upper-limb impairment after stroke”. In: *New England Journal of Medicine* 362.19 (May 2010), pp. 1772–1783. ISSN: 1533-4406. DOI: [10.1056/NEJMoa0911341](https://doi.org/10.1056/NEJMoa0911341).
- [35] Ho Shing Lo and Sheng Quan Xie. “Exoskeleton robots for upper-limb rehabilitation: State of the art and future prospects”. In: *Medical Engineering & Physics* 34.3 (2012), pp. 261–268. ISSN: 13504533. DOI: [10.1016/j.medengphy.2011.10.004](https://doi.org/10.1016/j.medengphy.2011.10.004).

- [36] Tad McGeer. “Passive dynamic walking”. In: *The International Journal of Robotics research* 9.2 (1990), pp. 62–82.
- [37] Luke M Mooney, Elliott J Rouse, and Hugh M Herr. “Autonomous exoskeleton reduces metabolic cost of human walking”. In: *Journal of Neuro-Engineering and Rehabilitation* 11.1 (2014), p. 151. ISSN: 1743-0003. DOI: [10.1186/1743-0003-11-151](https://doi.org/10.1186/1743-0003-11-151).
- [38] A Mulgaonkar, Roy Kornbluh, and Hugh Herr. “A new frontier for orthotics and prosthetics: application of dielectric elastomer actuators to bionics”. In: *Dielectric Elastomers as Electromechanical Transducers: Fundamentals, Materials, Devices, Models and Applications of an Emerging Electroactive Polymer Technology* (2011), p. 193.
- [39] Breno Gontijo do Nascimento, Claysson Bruno Santos Vimieiro, Danilo Alves Pinto Nagem, and Marcos Pinotti. “Hip Orthosis Powered by Pneumatic Artificial Muscle: Voluntary Activation in Absence of Myoelectrical Signal”. In: *Artificial Organs* 32.4 (2008), pp. 317–322. ISSN: 0160-564X. DOI: [10.1111/j.1525-1594.2008.00549.x](https://doi.org/10.1111/j.1525-1594.2008.00549.x).
- [40] Nicola Piccinelli. “Controllo di locomozione a dinamica quasi passiva basato su principi energetici (Almost passive dynamic locomotion control based on energy principles)”. Master’s Degree Thesis. University of Verona, 2014.
- [41] José Luis Pons. *Wearable Robots : Biomechatronic Exoskeletons*. Ed. by José Luis Pons. Wiley Online Library, 2008, p. 338. ISBN: 9780470512944. DOI: [10.1002/9780470987667](https://doi.org/10.1002/9780470987667).
- [42] G.a. Pratt and M.M. Williamson. “Series elastic actuators”. PhD thesis. 1995, pp. 399–406. ISBN: 0-8186-7108-4. DOI: [10.1109/IRDS.1995.525827](https://doi.org/10.1109/IRDS.1995.525827).
- [43] Gill A Pratt, Matthew M Williamson, Peter Dillworth, Jerry Pratt, and Anne Wright. “Stiffness isn’t everything”. In: *Experimental Robotics* 4 (1997), pp. 253–262.
- [44] ReWalk Robotics. URL: <http://rewalk.com/>.
- [45] R J Sanchez, J Y Liu, S Rao, P Shah, R Smith, T Rahman, S C Cramer, J E Bobrow, and D J Reinkensmeyer. “University of California Postprints Automating arm movement training following severe stroke : Functional exercises with quantitative feedback in a gravity-reduced environment”. In: *Rehabilitation* (2006).
- [46] G.S. Sawicki, K.E. Gordon, and Daniel P Ferris. “Powered Lower Limb Orthoses: Applications in Motor Adaptation and Rehabilitation”. In: *9th International Conference on Rehabilitation Robotics, 2005. ICORR 2005*. (2005), pp. 206–211. DOI: [10.1109/ICORR.2005.1501086](https://doi.org/10.1109/ICORR.2005.1501086).
- [47] Robert A Scheidt, Jonathan B Dingwell, Ferdinando A Mussa-ivaldi, Timothy Verstynen, Philip N Sabes, Erin V L Vasudevan, Gelsy Torres-oviedo, Susanne M Morton, Jaynie F Yang, and J Amy. “Learning to Move Amid Uncertainty Learning to Move Amid Uncertainty”. In: *Journal of Neurophysiology* (2011), pp. 971–985.
- [48] J. Surentu, GJM Tuijthof, and JL Herder. “Optimized artificial muscles for an inherently safe robotic arm”. In: *IEEE 10th International Conference on Rehabilitation Robotics, 2007. ICORR 2007*. 2007, pp. 1070–1076.

- [49] Kenta Suzuki, Gouji Mito, Hiroaki Kawamoto, Yasuhisa Hasegawa, and Yoshiyuki Sankai. "Intention-Based Walking Support for Paraplegia Patients with Robot Suit HAL". In: *Advanced Robotics* 21.12 (2007), pp. 1441–1469. ISSN: 0169-1864. DOI: [10.1163/156855307781746061](https://doi.org/10.1163/156855307781746061).
- [50] Darryl G. Thelen and Frank C. Anderson. "Using computed muscle control to generate forward dynamic simulations of human walking from experimental data". In: *Journal of Biomechanics* 39.6 (2006), pp. 1107–1115. ISSN: 0021-9290. DOI: [10.1016/j.jbiomech.2005.02.010](https://doi.org/10.1016/j.jbiomech.2005.02.010).
- [51] K Thoroughman and R Shadmehr. "Learning of action through adaptive combination of motor primitives." In: *Nature* 407.6805 (Oct. 2000). ISSN: 0028-0836. DOI: [10.1038/35037588](https://doi.org/10.1038/35037588).
- [52] Annick AA Timmermans, Henk AM Seelen, Richard D Willmann, and Herman Kingma. "Technology-assisted training of arm-hand skills in stroke: concepts on reacquisition of motor control and therapist guidelines for rehabilitation technology design". In: *Journal of NeuroEngineering and Rehabilitation* 6 (2009).
- [53] N. Tsagarakis and Darwin G. Caldwell. "Improved modelling and assessment of pneumatic muscle actuators". In: *Robotics and Automation, 2000. Proceedings. ICRA'00. IEEE International Conference on*. Vol. 4. IEEE, 2000, pp. 3641–3646.
- [54] Heike Vallery, Edwin H F van Asseldonk, Martin Buss, and Herman van der Kooij. "Reference trajectory generation for rehabilitation robots: complementary limb motion estimation." In: *IEEE transactions on neural systems and rehabilitation engineering : a publication of the IEEE Engineering in Medicine and Biology Society* 17.1 (Feb. 2009), pp. 23–30. ISSN: 1558-0210. DOI: [10.1109/TNSRE.2008.2008278](https://doi.org/10.1109/TNSRE.2008.2008278).
- [55] Heike Vallery, Alexander Duschau-Wicke, and Robert Riener. "Hiding robot inertia using resonance". In: *Conference proceedings : Annual International Conference of the IEEE Engineering in Medicine and Biology Society. IEEE Engineering in Medicine and Biology Society. Conference 2010* (Jan. 2010), pp. 1271–4. ISSN: 1557-170X. DOI: [10.1109/IEMBS.2010.5626416](https://doi.org/10.1109/IEMBS.2010.5626416).
- [56] A.J. Van Den Bogert. "Exotendons for assistance of human locomotion". In: *Biomedical engineering online* 2.1 (2003), pp. 17–24.
- [57] Ronald Van Ham, Thomas G Sugar, Bram Vanderborght, Kevin W Hollander, and D Lefeber. "Review of Actuators with Passive Adjustable Compliance/Controllable Stiffness for Robotic Applications". In: September (2009), pp. 81–94.
- [58] J. F. Veneman, R. Ekkelenkamp, R. Kruidhof, F.C.T. van der Helm, and H. van der Kooij. "A Series Elastic- and Bowden-Cable-Based Actuation System for Use as Torque Actuator in Exoskeleton-Type Robots". In: *The International Journal of Robotics Research* 25.3 (2006), pp. 261–281. ISSN: 0278-3649. DOI: [10.1177/0278364906063829](https://doi.org/10.1177/0278364906063829).

- [59] Kevin Warwick, Mark Gasson, Benjamin Hutt, Iain Goodhew, Peter Kyberd, Brian Andrews, Peter Teddy, and Amjad Shad. “The application of implant technology for cybernetic systems.” In: *Archives of neurology* 60.10 (Oct. 2003), pp. 1369–73. ISSN: 0003-9942. DOI: [10.1001/archneur.60.10.1369](https://doi.org/10.1001/archneur.60.10.1369).
- [60] Michael Wehner, Brendan Quinlivan, Patrick M. Aubin, Ernesto Martinez-Villalpando, Michael Baumann, Leia Stirling, Kenneth Holt, Robert Wood, and Conor Walsh. “A lightweight soft exosuit for gait assistance”. In: *Proceedings - IEEE International Conference on Robotics and Automation* (2013), pp. 3362–3369. ISSN: 10504729. DOI: [10.1109/ICRA.2013.6631046](https://doi.org/10.1109/ICRA.2013.6631046).
- [61] B. Weinberg, J. Nikitczuk, S. Patel, B. Patrilli, C. Mavroidis, P. Bonato, and P. Canavan. “Design, Control and Human Testing of an Active Knee Rehabilitation Orthotic Device”. In: *Proceedings 2007 IEEE International Conference on Robotics and Automation* (Apr. 2007), pp. 4126–4133. ISSN: 1050-4729. DOI: [10.1109/ROBOT.2007.364113](https://doi.org/10.1109/ROBOT.2007.364113).
- [62] Sung H You, Sung Ho Jang, Yun-Hee Kim, Mark Hallett, Sang Ho Ahn, Yong-Hyun Kwon, Joong Hwi Kim, and Mi Young Lee. “Virtual reality-induced cortical reorganization and associated locomotor recovery in chronic stroke: an experimenter-blind randomized study.” In: *Stroke: A Journal of Cerebral Circulation* 36.6 (2005), pp. 1166–1171.
- [63] A.B. Zoss, H. Kazerooni, and A. Chu. “Biomechanical design of the Berkeley lower extremity exoskeleton (BLEEX)”. In: *Mechatronics, IEEE/ASME Transactions on* 11.2 (Apr. 2006), pp. 128–138. ISSN: 1083-4435. DOI: [10.1109/TMECH.2006.871087](https://doi.org/10.1109/TMECH.2006.871087).
- [64] European Commission. *HORIZON 2020: Health, Demographic Change and Wellbeing*. URL: <http://ec.europa.eu/programmes/horizon2020/en/h2020-section/health-demographic-change-and-wellbeing>.
- [65] National Center for Simulation in Rehabilitation Research (NCSRR) Stanford University. *OpenSim Documentation*. Version 3.x. URL: <http://simtk-confluence.stanford.edu:8080/display/OpenSim/OpenSim+Support>.
- [66] Stanford University. *OpenSim Project*. Version 3.2. URL: <https://simtk.org/home/opensim>.